Development of a scanning force microscope for *in-vivo*, minimally invasive inspection of human knee cartilage.

Thèse présentée à la Faculté des Sciences
Institut de Microtechnique
Université de Neuchâtel

Pour l'obtention du grade de *"Docteur ès Sciences"*

par

Raphaël Imer

Diplômé en électronique-physique
de l'Université de Neuchâtel

Acceptée sur proposition du jury:

Prof. assoc. Dr. Urs Staufer, directeur de thèse
Prof. Dr. Nico F. de Rooij, rapporteur
Prof. Dr. Ueli Aebi, rapporteur
Prof. MD. Niklaus Friederich, rapporteur

Soutenue le 21 février 2008

Université de Neuchâtel

FACULTE DES SCIENCES
Secrétariat-Décanat de la faculté
- Rue Emile-Argand 11
- CP 158
- CH-2009 Neuchâtel

IMPRIMATUR POUR LA THESE

Development of a scanning force microscope for in-vivo, minimally invasive inspection of human knee cartilage

Raphaël IMER

UNIVERSITE DE NEUCHATEL

FACULTE DES SCIENCES

La Faculté des sciences de l'Université de Neuchâtel,
sur le rapport des membres du jury

MM. U. Staufer (directeur de thèse),
N. de Rooij, U. Aebi (Université de Bâle)
et N. Friederich (Klinik für Orthopädie, Bruderholz)

autorise l'impression de la présente thèse.

Neuchâtel, le 14 mars 2008

Le doyen :
F. Kessler

UNIVERSITE DE NEUCHATEL
FACULTE DES SCIENCES
Secrétariat - décanat de la faculté
Rue Emile-Argand 11 - CP 158
CH-2009 Neuchâtel
félix Kessler

■ Téléphone : +41 32 718 21 00 ■ E-mail : secretariat.sciences@unine.ch ■ www.unine.ch/sciences

« Ce n'est qu'en essayant continuellement que l'on finit par réussir. Donc: plus ça rate, plus on a de chances que ça marche. »

Proverbe Shadok

To Ling, Sophie and Alexandre
With Love

Abstract

Osteoarthritis (OA) is a painful and disabling joint disease that is characterized by degradation of articular cartilage. It affects, most often, middle-aged and older people. However, young and sportive people can also develop osteoarthritis (OA), often as a result of severe knee injuries like ligament rupture, meniscus lesion or joint dislocation. For an early diagnosis of this disease and optimized treatment, surgeons need a quantitative measurement of the quality of cartilage.

Recent *ex-vivo* measurements on healthy, diseased, and enzymatically altered cartilage demonstrated that the scanning force microscope (SFM) used as nanoindenter is a sensitive tool for detecting the small changes such as those occurring in early OA. Therefore, the SFM may allow diagnosing the early stages of OA long before the first symptoms (pain) arise. To be used by clinicians, a diagnostic tool needs to provide a fast and reliable diagnosis of cartilage degeneration, at best directly during the intervention. Moreover, it should also allow for post operative monitoring of the treated areas. Based on these requirements, we developed the scanning force arthroscope (SFA). This clinical instrument integrates an SFM into a standard arthroscopic sleeve and was used for direct, quantitative, *in-situ* inspection of articular cartilage. The stabilization and the positioning of the instrument relative to the surface under investigation was performed by means of eight inflatable balloons

(stabilization stage). An integrated three-dimensional (3D) scanner allowed raster scanning and probing of a small area of cartilage around the point of insertion (scanning stage). A SFM probe with an integrated deflection sensor was mounted at the distal end of the instrument (indentation stage).

After some preliminary tests, measurements by the arthroscopic SFM were recorded inside a cadaver knee. The insertion, positioning and stabilization of the instrument were guided by a regular optical arthroscope. During this phase a cannula protected the cantilever. After removal of this protection, load-displacement curves were successfully recorded under wet (Ringer's solution) and dry (CO_2) conditions. Finally the dynamic elastic modulus $|E^*|$ of agarose gel and pig's cartilage were calculated, using experimental values obtained with the latest version of the instrument.

KEYWORDS
Scanning force microscope, articular cartilage, arthroscopy, biomechanics, degradation, indentation, minimally invasive instrument, stiffness, osteoarthritis, clinical diagnostics, nanotechnology, nanomedicine, IT SFM.

Résumé

L'arthrose est une maladie articulaire douloureuse et invalidante caractérisée par la dégénérescence du cartilage. Elle affecte, le plus souvent, des personnes d'âge moyen ou avancé. Cependant, des personnes jeunes et sportives peuvent également développer de l'arthrose, souvent en raison de graves blessures au genou, comme la rupture d'un ligament, de lésions au ménisque ou d'une dislocation de l'articulation. Afin de permettre un diagnostic précoce et un traitement optimisé de cette maladie, les chirurgiens ont besoin d'une mesure quantitative de la qualité du cartilage.

Des mesures ex-vivo réalisées sur du cartilage en bonne santé, malades, et enzymatiquement altéré ont démontré que le microscope à force atomique (AFM) utilisé comme indenteur nanométrique est un outil suffisamment sensible pour détecter les changements survenant dans le cartilage au début de l'artrose. Par conséquent, l'AFM permet de diagnostiquer l'arthrose bien avant que les premiers symptômes (douleur) apparaissent. Pour être utilisé par les chirurgiens, un tel outil de diagnostique doit pouvoir fournir une information rapide et fiable sur la dégénérescence du cartilage, au mieux directement pendant l'intervention. Il doit également permettre un suivi post opératoire des zones traitées.

Sur la base de ces exigences, nous avons développé le scanning force arthroscope (SFA). Cet instrument utilisé pour une inspection quantitative directe du cartilage articulaire intègre un AFM à l'intérieur d'une gaine arthroscopique. La stabilisation et le positionnement de l'instrument par rapport à la surface mesurée sont réalisés à l'aide de huit ballons gonflables (étage de stabilisation). Un scanner tridimentionnel intégré permet de scanner et de mesurer une petite zone de cartilage autour du point d'insertion (étage de balayage). Une sonde AFM intégrant un capteur de déflection est installée à l'extrémité de l'instrument (étage d'indentation).

Après quelques essais préliminaires, des mesures arthroscopic ont été réalisés dans un genou de cadavre à l'aide de cet outil. L'insertion, le positionnement et la stabilisation de l'instrument sont guidés par un arthroscope. Durant ces phases, une canule protégé le levier. Après la suppression de cette protection, des courbes de force ont pu être enregistrées dans des conditions humides (solution de Ringer) et sèches (CO_2). Finalement, le module d'élasticité dynamique $|E^*|$ de gel agarose et de cartilage de porcs ont été calculés en utilisant la dernière version de l'instrument.

MOTS CLÉS
Microscope à balayage, cartilage articulaire, arthroscopie, biomécanique, dégradation, indentation, instrument faiblement invasif, élasticité, arthrose, diagnostique clinique, nanotechnologie, nanomedicine, IT SFM.

Contents

Chapter 1

Introduction

1.1 The knee joint

During daily activities, human knee joints are subject to forces that can range from several times the body weight for people with relative sedentary activities to ten times the body weight for professional athletes [1]. During flexion, the knee must allow for free rotations to guarantee the 3D mobility required for walking, running and jumping, but in full extension, when it undergoes considerable efforts caused by small moment arms, the knee must be very stable. The ability to fulfill these conflicting requirements and to support millions of loading cycles before showing significant degradation results from the complex configuration of the various components forming the human knee joint.

This section, mainly based on the anatomy textbook written by Henry Gray [2] in 1918, will present some physiologic and kinematic aspects of this complex but fascinating articulation, in order to understand how knee problems occur.

1.1.1 Physiology

The bony structure of the knee joint is relatively unstable. The stability is assumed by the surrounding components like ligaments, menisci, muscles or tendons. Their function are described as follows:

Bones

The femur, the tibia and the patella are the three bones that form the knee joint. A fourth one, the fibula, is placed on the lateral side of the tibia, but doesn't participate in the articulation. The femur, characterized by two prominent extremities at the end of a long quasi cylindric body, is the longest and the strongest bone of the human body. The two round eminences found at its lower end are called lateral and medial femoral condyle. These two condyles are separated by an interval called the intercondylar fossa. The tibia, characterized by a quasi triangular horizontal section is the second longest bone of the skeleton. Its upper extremity, called the tibial plateau, is large and relatively flat. The tibial plateau is divided by the intercondylar eminence into two condyles: the lateral and the medial tibial condyle. The intercondylar eminence of the tibia fits into the intercondylar fossa of the femur. The patella, also called the knee cap, is a flat, triangular and moveable bone wrapped inside the quadriceps tendon. The patella protects the front of the joint, and transmits the force to the tibia by increasing the lever arm of the quadriceps muscles. The patella gives more stability to the femur under load. The bony structure of the knee joint is shown in figure 1.1.

Articular capsule

The articulation is surrounded by the articular capsule, which consists of a strong, thin and fibrous membrane. The inner surface of the capsule is covered by the synovial membrane which secrets the synovial fluid. This clear or slightly yellowish highly viscous fluid lubricates the

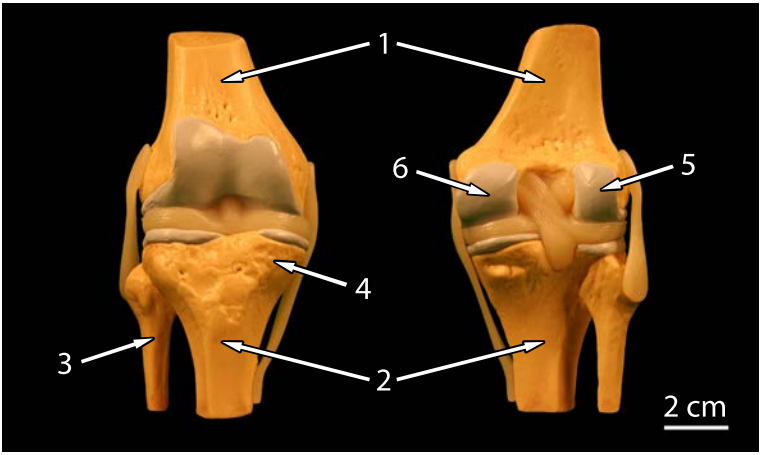

Figure 1.1. Picture of the front side and the back side of a human knee joint. The bony structure of the knee is formed by the femur (1), the tibia (2) and the fibula (3). The upper extremity of the tibia is called tibial plateau (4). The lower end of the femur is divided in two condyles, the lateral femoral condyle (5) and the medial femoral condyle (6).

joint, provides nutrients to cartilage and protects it against enzymatic degradation. The synovial fluid is composed of a dialyzate of blood plasma, filtered through semipermeable walls of blood vessels. It contains proteins, glucose in low concentration, some cellular component and the hyaluronic acid mucopolysaccharide produced by synovial cells. At rest, due to the high molecular weight of hyaluronate, synovial fluid is highly viscous, but during motion, the joint surface creates fluid shear. The hyaluronate molecules align parallel to the direction of the shear force which drastically decreases the viscosity. Consequently, the viscosity of synovial fluid can vary from 0.5 to 150 N/m^2s.

Ligaments

The articular capsule is strengthened on each side by the collateral ligaments. The medial collateral ligament (MCL) and the lateral collateral ligament (LCL) laterally stabilize the knee and avoid yawn movements. In the center of the knee, the anterior cruciate ligament (ACL) in the front, and the posterior cruciate ligament (PCL) in the back control the back-and-forth motion and limit inner rotation of the knee. Ligaments are highly vascularized short bands of fibrous connective tissue that connect bones to bones. Ligaments are shown in figure 1.2.

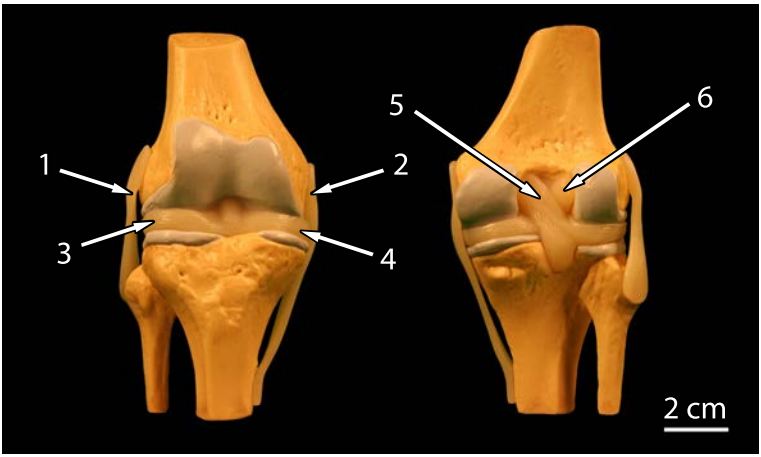

Figure 1.2. The ligamentous structure of the knee is formed by the lateral collateral ligament (LCL) (1), the medial collateral ligament (MCL) (2), posterior cruciate ligament (PCL) (5), and the anterior cruciate ligament (ACL) (6). The tibia and the femur are separated by the lateral (3) and the medial menisci (4).

Tendons

The structure of tendons is similar to those of ligaments. Tendons are longer than ligaments and connect bones to muscles. The largest tendon in the knee is called the patellar tendon. This strong, flat, ligamentous strip connects the tibia to the quadriceps muscle in the front of the thigh. It completely covers the patella.

Meniscus

The femur and the tibia are separated by the menisci. These two fibrocartilaginous, relatively avascular, C-shaped disks increase conformity, stability and shock absorption in the knee joint. During knee movements, the menisci move a bit. These small displacements increase the contact surface and improve the pressure distribution inside the knee. Due to the presence of nerve endings in their structure, menisci serve as proprioceptive structures, providing a feedback mechanism for joint position sense.

Muscles

The muscles surrounding the knee joint are responsible for the extension and the flexion of the lower leg. In the front of the thigh, the quadriceps form the extensor mechanism of the knee. It is subdivided into four different muscles, the rectus femoris, the vastus lateralis, the vastus medialis and the vastus intermedius. This is the most voluminous muscle of the human body. On the back, the hamstrings form the flexor mechanism. It consists of five muscles, the semimembranosus, the semitendinosus, the gracilis, the sartorius and the biceps femoris.

1.1.2 Kinematics

Despite most of the motion occurring in the sagittal plane, the knee joint is not a simple hinge joint, but a complex articulation with six degrees of freedom: three translational planes and three rotational planes. Flexion and extension are the principal movements. When the knee is passively flexed, the flexion angle can go up to 160˚. The degree of rotation depends of the flexion angle, but is limited to 10˚ for medial rotation and to 30˚ for lateral rotation. During flexion-extension, automatic rotation also occurs. These small rotations, mainly induced by the asymmetry of the two femoral condyles, add stability to the knee joint. The relative motion of the femur and the tibia is a combination of rolling, sliding and rotation. As shown in figure 1.3, the contact point between these bones is not fixed, but changes during the movement.

In two dimensions, the kinematic of the knee can be described as a rotation around a moving center. The method of Rouleaux was applied for determining the instant center of rotation (ICR) point on the femur. This is the point where at any instant of time, the velocity is equal to zero. The two dimensional analysis is a simplification of the three dimensional anatomic reality, where the knee motion must be described as a combination of rotation and translation along the same moving axis [3, 4, 5, 6, 7].

The knee joint is continuously under load. The magnitude, the type and the duration of this load dependent on the type of activity. For example, the tibia-femoral joint reaction force for a person slowly climbing a step can be estimated to 3.5 times the body weight [1]. During a jump, this force is higher, up to 20 times the body weight. Loads are transmitted across the joint when bone surfaces enter in contact. Shock absorption and load transmission functions are essentially assumed by the articular cartilage.

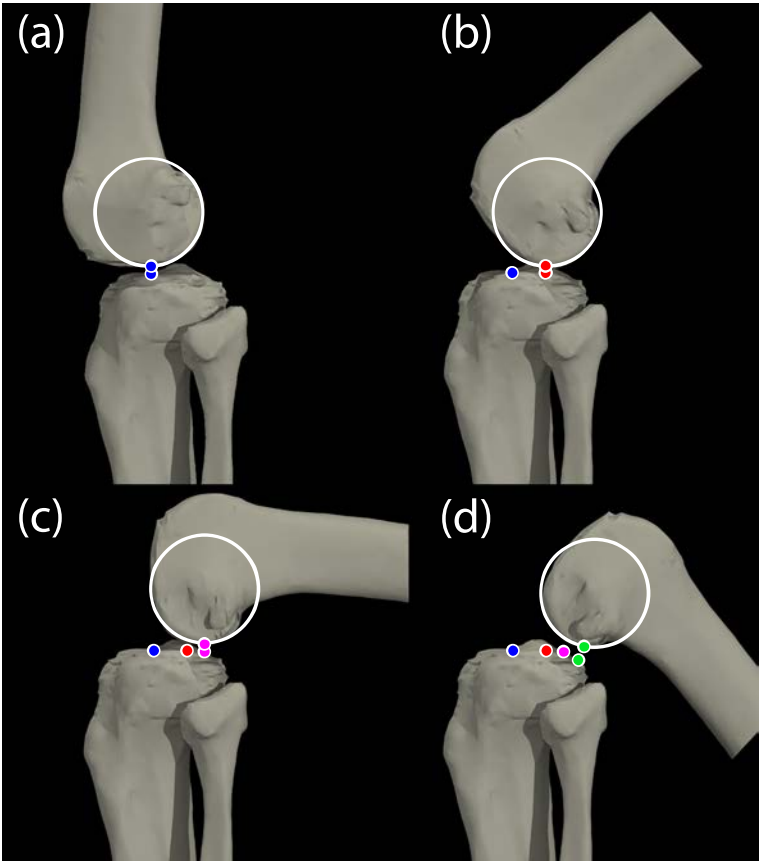

Figure 1.3. During flexion, the relative motion of the femur and the tibia is a combination of rolling, sliding and rotation. The contact point between these bones is not fixed, but depend of the flexion angle. **(a)** Contact point for a flexion angle of 0˚. **(b)** Contact point for a flexion angle of 45˚. **(c)** Contact point for a flexion angle of 90˚. **(d)** Contact point for a flexion angle of 135˚.

1.2 Articular cartilage

The hyaline cartilage is a thin layer of soft tissue that cover the end of bones in a synovial joint. Cartilage thickness varies through the joint between 0.5 to 3 mm. The mechanical properties of this tissue directly depends on its structure. This section will describe the composition and the properties of articular cartilage.

1.2.1 Composition and structure

Articular cartilage is composed of isolated cells, the chondrocytes, embedded in a large extracellular matrix (ECM). The main components of the ECM are water, collagen fibrils and proteoglycans. Other quantitatively minor components like proteins, hyaluronates, fibronectins and lipids are also present. The figure 1.4 shows the molecular organization of articular cartilage.

Chondrocytes

The chondrocytes are the only type of cells found in cartilage. They are responsible for the formation and the maintenance of articular cartilage. These highly differentiated cells control the production of collagen fibrils, proteoglycans and enzymes. In mature tissue, chondrocytes represent about 10% of the total volume of the ECM.

Interstitial water

Representing 65% to 80% of the total weight of normal articular cartilage, water is the main constituent of the ECM. Inorganic salts, such as sodium, calcium, chloride and potassium, are dissolved in it. Interstitial water promotes the transport of nutrients for articular cartilage and provides a source of lubricant for the joint.

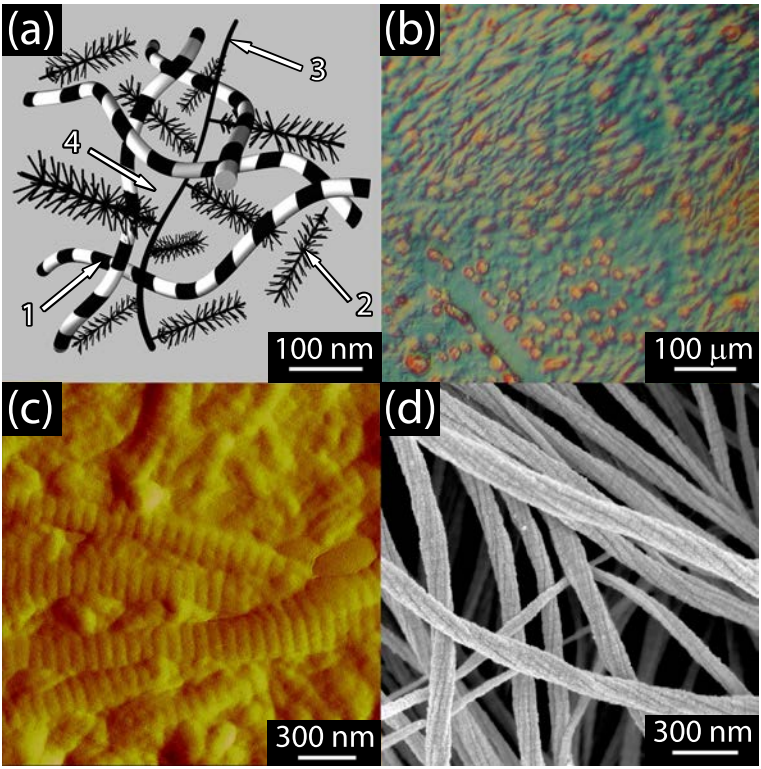

Figure 1.4. **(a)** Schematic view of the organization of the different components constituting articular cartilage. (1) Collagen fibril, (2) Monomer, (3) Hyaluronic acid, (4) Interstitial fluid. **(b)** Picture of cartilage under optical microscope. **(c)** Topographic AFM image of articular cartilage recorded with a sharp silicon tip in contact mode. **(d)** SEM picture of collagen fibers taken by R. Gottardi and M. Stolz.

Collagen

Collagen molecules are made of three polypeptide chains (α-chains). These three left-handed helix are twisted together into a right-handed triple helix. These macromolecules are packed into an organized overlapping bundle to form the collagen fibrils. Collagen fibers are bundle of fibrils. Collagen fibers form a fibrilar meshwork that provide the tensile strength and the shear properties to hyaline cartilage.

Depending on the region, the diameter of articular cartilage fibers vary between 10 to 100 nm. At least 15 of the 28 types of collagen described in scientific literature are present in articular cartilage, but more than 90% is collagen type II.

Proteoglycans

Proteoglycans (PGs) are complex macromolecules formed by a protein core onto which glycosaminoglycan (GAG) chains are covalently bound. The most common GAG are chondroitin sulfate (CS), keratan sulfate (KS) and hyaluronan (HA). In articular cartilage, PG can be found in a simple or aggregating form. The most common form, aggrecans, consist of an extended protein core on which KS and CS chains are attached. A link protein attaches aggrecans to HA to form PG aggregate. Another aggregating, versican, and two nonaggregating PG, bigglycan and decorin, can be found in articular cartilage at a lower level.

The CS and KS chains contain a large number of sulfate (SO_4) and carboxyl ($COOH$) groups, which become electrically charged in solution. These negative charges create a strong electrostatic repulsion force that require positives charges to maintain the charge balance: Ca^+ and Na^+ ions dissolved in the interstitial fluid are attracted into

the collagen structure and create a swelling pressure called Donnan osmotic pressure π (c.f. Equ. 1.1). This pressure plays an important role in the load support ability of cartilage. It is also the major cause for maintaining cartilage hydration. The Donnan osmotic pressure can be written as:

$$\pi = RT\Delta c \tag{1.1}$$

where R is the universal gas constant, T the absolute temperature and Δc the difference of ion concentration between the interstitial fluid and the surrounding solution.

The structure and composition of articular cartilage varies zonally. As shown in figure 1.5, four zones can be identified:

- **The superficial tangential zone:** This zone forms the gliding surface of articular cartilage. The chondrocytes are elongated and parallel to the surface, the water content is maximal, the collagen fibrils are parallel to the surface and the proteoglycan concentration is minimal.

- **The middle zone:** This zone is the largest one. The chondrocytes are spherical and the collagen fibrils randomly orientated.

- **The deep zone:** This zone is the opposite of the superficial tangential zone. The chondrocytes are arranged in columns, the collagen fibrils are perpendicular to the surface, the water content is minimum and the proteoglycans concentration is maximum.

- **The calcified zone:** This is a transitional zone which separates the hyaline cartilage from the subchondral bone.

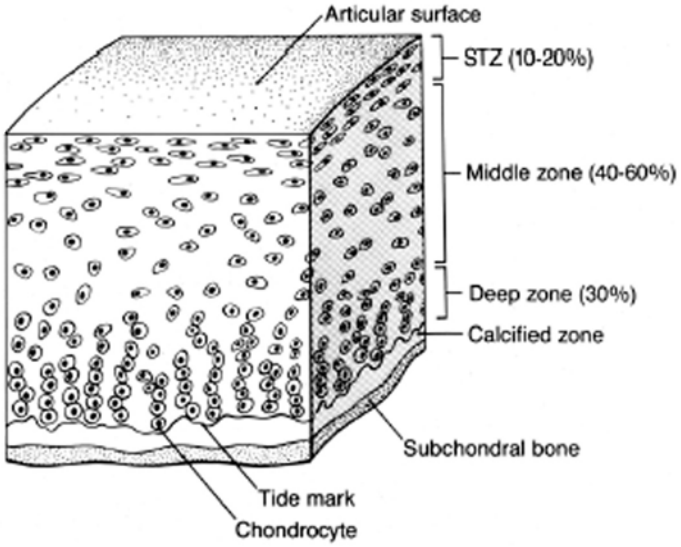

Figure 1.5. Schematic view of the organization of cartilage in function of the thickness. Four zones with different structure and composition can be identify; the superficial tangential zone, the middle zone, the deep zone and the calcified zone. (Reproduced from Mow VC, Proctor CS, Kelly MA: Biomechanics of articular cartilage, in Nordin M, Frankel VH (eds): Basic Biomechanics of the Musculoskeletal System, ed 2. Philadelphia, PA, Lea % Febiger, 1989, pp 3157.)

1.2.2 Biomechanics

Articular cartilage is subjected, daily, to large range of constraints. Its stress and strain response varies in function to the loading mode. In order to understand the biomechanical properties of articular cartilage, the tissue must be considered as a biphasic material. The solid phase is formed by collagens fibers and the fluid phase by the rest of the ECM. Depending on the rate and the duration of the applied load, cartilage exhibits two distinct types of stiffness:

- **A flow-dependent mechanism:** occurs when a constant load is applied to cartilage. The tissue's deformation increase slowly with time, until reaching an equilibrium position. Due to the very low permeability of articular cartilage, the water trapped into the microscopic pores of the matrix cannot rapidly move out and causes high frictional drag forces. This huge interstitial fluid pressure minimizes the stress acting on the solid matrix. The load supported by the fluid is approximately 20 times greater than those supported by the solid matrix. For normal articular cartilage, the equilibrium elastic modulus E ranges typically from 0.5 to 1.0 MPa [8].

- **A flow-independent mechanism:** occurs when short and cyclic loads are applied to cartilage. During loading, the pressure gradient is too small to induce a fluid flow into the solid matrix. The stress-strain response to a dynamic load can be described by the complex compressive modulus (E^*). E^* can be decomposed into storage modulus ($E^{'}$) and loss modulus ($E^{''}$). The storage modulus is directly proportional to the energy stored in a cycle of deformation and the loss modulus is proportional to the average dissipation of energy. For normal articular cartilage, the complex compressive modulus E^*, depends of the loading frequency, but typically ranges from 15 MPa (at 0.1 Hz) to 60 MPa (at 40 Hz) [9].

1.2.3 Mathematical model

In order to create a predictive model of the tissue's mechanical behavior, cartilage can be modeled by combining two types of mathematical elements:

- **The spring,** usually used to model the solid phase of cartilage. It is considered as a perfectly elastic element with instantaneous reaction. This element is able to store energy. The extension of a linear spring (ΔL) is directly proportional to the load (tensile stress, F_S) applied on it. The slope of the strain stress curve (spring constant, k) defines the stiffness of the linear spring.

$$F_S = k \cdot \Delta L \tag{1.2}$$

- **The dashpot,** usually used to model the liquid phase of cartilage. It is considered as a perfectly viscous element with gradual reaction. This element dissipates energy. The resistance (shear stress, F_D) of a linear dashpot is given by the multiplication of the strain rate ($\Delta L / \Delta t$) and the coefficient of viscosity (η).

$$F_D = \eta \cdot \frac{\Delta L}{\Delta t} \tag{1.3}$$

Numerous elements with various k or η can be combined to create different mathematical models describing cartilage stress and strain behavior. The standard viscoelastic model, which is generally a good realistic model for cartilage consist of a spring (k_1) in series with a spring (k_2) and a dashpot (η_3) in parallel.

1.3 Osteoarthritis

Articular cartilage distribute load and provide lubrication in joints with an extraordinary longevity. However, a variety of factors can lead to a complete degeneration of this tissues with age. Due to its avascular, aneural and alymphatic nature, articular cartilage has a very poor ability to self-repair lesions. After the age of 50, almost the totality of people show clinical symptoms of OA. However, its expression and its gravity are very different from one person to another. With the increase of life expectancy, millions of people are suffering from this degenerative disease. The American Academy of Orthopedic Surgeons (AAOS) identify OA as one of the leading cause of physical disability worldwide. This section will describe different aspects of the disease.

1.3.1 Etiology

OA is a painful and progressive joint disease characterized by degradation of the articular surface, hypertrophy of the bone and thickening of the articular capsule [10, 11, 12]. OA is the most common form of arthritis. Its main symptoms are chronical pains, restriction of mobility, crepitus during motion and in the severest cases, the joint can be filled by fluid and a bone deformity can appear. For a long time, OA was only considered as a degenerative disorder and a natural consequence of aging. Recently, several studies have demonstrated that OA is an active disease process, with a high variety of factors that can induced or facilitate its development. These factors differ across population [13] but generally includes:

- **Aging:** With age, the bio-mechanical properties of cartilage are reduced. This loss of efficiency leads to the destruction of the tissue. Generally 90% of the population over 65 years of age show significant signs of OA [14].

- **Obesity:** Overweight causes greater pressure on the articulation; the degradation of articular surface is consequently accelerated [15].

- **Trauma:** Severe knee injuries commonly found in young and sportive people, like ligament rupture, meniscus lesions or fracture of the joint surface are a high risk factor for developing OA at old age. Neyret et al. [10] established that the incidence of radiographic OA is about 65% at 27 years in patients with ruptured ligament. This incidence actually increases, if the patient has combined lesions of multiple ligaments or of other structures such as the meniscus.

- **Repetitive stress injuries:** Some occupations like line work, dock work, mining and carpet or floor laying have shown higher incidence of OA in the knee [16, 17].

- **Gender:** A 1999 AAOS unpublished study shows that women outnumber men by a ratio of 2 to 1 for nearly all age groups. Maillefert et al. [18], found that hip OA in women is more frequent, have greater structural severity, and require total hip arthroplasty more often than OA in men.

- **Race:** A study by Anderson et al. [19], based on 5,193 black and white participants aged between 35 and 74 years reveals significant association between race and OA. A higher prevalence of OA was found in blacks than whites. This difference is even greater for black women.

- **Genetic predisposition:** Some studies have shown a relationship between gene mutation and OA [20, 21]. Further work is needed to isolate the responsible genes.

1.3.2 Structural changes

OA causes structural and biochemical changes in cartilage, including alterations in the microstructure and composition of collagen and PG networks [22]. Early OA is characterized by a regenerative phase during which the synthesis of ECM and the proliferation of chondrocyte (hyperplasia) is stimulated. This attempt to repair cartilage defects is quickly followed be a degenerative phase characterized by an insufficient synthesis of ECM and chondrocyte death (chondroptosis). During the progression of OA, the first detectable change in the ECM microstructure is an increase of the water content. This structural change causes a decrease of interstitial fluid pressure which leads to cartilage matrix erosion. At an advanced stage of OA, some variations in the size and in the arrangement of collagen fibers can be observed. In contrast to the normal cartilage that exhibits a random orientation of the collagen network, diseased cartilage exhibits a preferred orientation [23]. As shown in figure 1.6, this orientation follows the movement within the joint. Finally, the PG content in cartilage decrease proportionally to the severity of the disease.

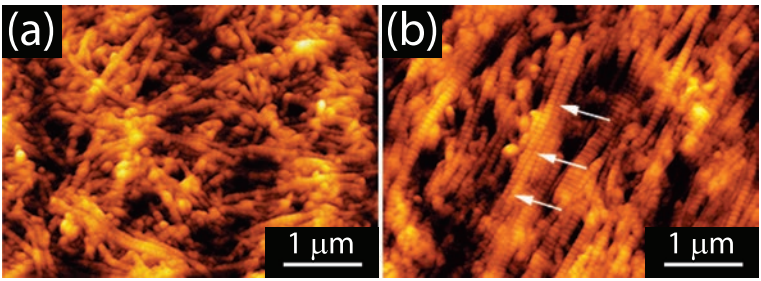

Figure 1.6. Surface topography of normal (A) and osteoarthritic (B) articular cartilage. (Reproduced from Stolz et al. [23]

1.3.3 Diagnosis

Early diagnosis of OA is a challenge for doctors. The disease often starts long before middle age, but the first symptoms are only noticed decades later, when the structural and biomechanical changes in cartilage are already irreversible. Different methods are available for detecting, evaluating or excluding OA. Some of these techniques are illustrated in figure 1.7.

X-ray radiography

X-ray radiography consists of exposing a part of the body to a small dose of ionizing radiation to produce an image. This is the oldest and most frequently used method to asses damage in OA including loss of joint space, subchondral sclerosis, bony cysts and osteophytes. Kellgren and Lawrence [24] first describe a classification system for radiological evaluation of knee OA. Radiography evidence accompanied by pain symptoms are often the first clinical criteria used for diagnosing OA.

Magnetic resonance imaging

Magnetic resonance imaging (MRI) is a tomographic image technique that uses the magnetic properties of hydrogen and its interaction with a large external magnetic field to produce highly detailed images of the human body [25]. MRI can generate three dimensional volumetric images or two-dimensional cross-sectional images at any orientation, including oblique planes. Due to its high spatial resolution and superior soft tissue contrast MRI has the potential for evaluating the severity of cartilage changes in OA. The recent developments in cartilage imaging follow two main directions :

1. Optimization of quantitative techniques such as T1-rho, T2-mapping or delayed Gadolinium-Enhanced MRI of Cartilage (dGEMRIC) imaging. These techniques aim to quantify PG and water content of the ECM.

2. Development of morphologic techniques based on high magnetic field. These promising techniques aim to directly visualize cartilage structure and defects.

MRI is a very powerful tool to evaluate the cartilage state of health but before becoming a routine clinical practice, this techniques requires further development.

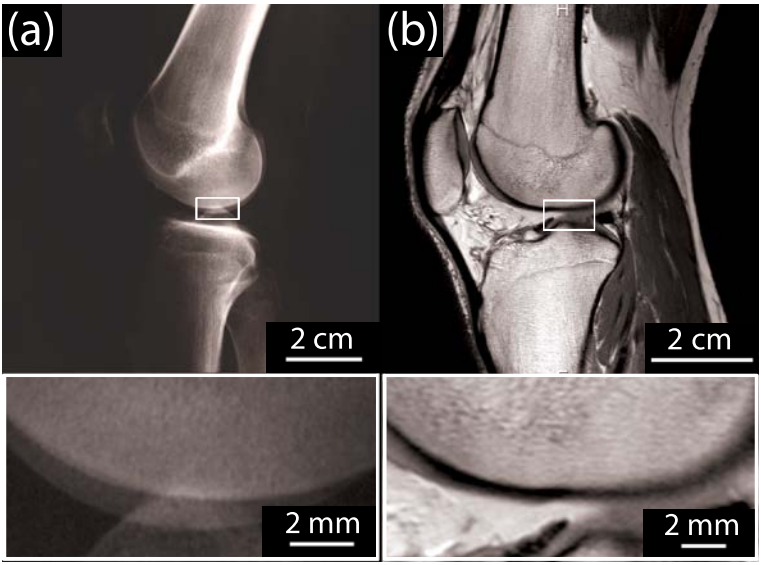

Figure 1.7. Picture of a left knee taken by **(a)** X-ray radiography and by **(b)** MRI. The insets exhibit the articular cartilage surface imaged with the two same technics.

Ultrasound

Ultrasound is a diagnostic imaging technique used to visualize the human body. Ultrasound is particulary suited to observe soft tissues like eyes, heart, ligament or tendons. In contrast to other imaging techniques like X-ray or MRI, high-frequency ultrasound do not only provide an image of the cartilage, but can also provide quantitative information on its biomechanical properties. Unfortunately, due to the configuration of the knee joint, only a small part of the articular surface can be explored with an external source. New ultrasonic probes [26, 27, 28] have been developed to analyzed the surface of articular cartilage inside the knee joint under arthroscopy. This kind of instrument enables the assessment of cartilage at the millimeter to upper micrometer scale. However, this is still not sufficient to detect the early degenerative changes due to OA.

Arthroscopy

Arthroscopy is a minimally invasive surgery performed in an operating room under local, regional or general anesthesia. During this procedure, the surgeon performs only two or three very small incisions in the skin. Through the first one, a long, thin, viewing scope, called an arthroscope, is inserted in the knee. This instrument contains an optical lens system and a illumating system which allow surgeon to inspected the inner structure of the joint. For better visualization, a camera is connected to the eye piece of the scope and the image is transferred to a video monitor. Through other incisions, a variety of cutting, shaving or grabbing instruments are used to diagnose and treat injuries. During an arthroscopy, the joint is constantly flushed with liters of physiological liquid (Ringer' solution). This saline fluid is used to expand the tissues, flush out debris and reduce the possibility of infection. At the end of the surgery, the incisions are closed with stripes or stitches. Compared to

other techniques, arthroscopy is less painful and allows a quicker recovery. Most patients with knee arthroscopy can leave the hospital the same day.

The Japanese physicians Kenji Takagi and Masaki Watanabe were the first pioneers in arthroscopy. At the beginning of the 20th century, they highly contributed to the development of this techniques by designing the first arthroscope [29]. Between 1921 and 1926, Eugen Bircher published several papers describing 60 arthroscopic knee procedures that preceded an open meniscectomy. It was the first time that arthroscopy was used in a large scale for clinical procedures [30]. Knee arthroscopy was initially used as a diagnostic technique for evaluating articular cartilage disease.

Multiple grading systems have been developed to classify cartilage injury. In 2000, the International Cartilage Repair Society (ICRS) created the ICRS Cartilage Injury Evaluation Package [31] which combines patient questionnaires with subjective knee evaluation forms. Figure 1.8 describes this grading system in more detail. Arthroscopy, which allows direct visualization and palpation of articular cartilage, is certainly more sensitive for identifying small lesions than all other imaging methods. But arthroscopy is also more invasive and for that reason this technique is currently only rarely used for knee investigation.

Indentation

Stiffness is a key parameter for measuring cartilage's state of health because it expresses how well the forces acting in the joint are absorbed and transduced by the articulation. Well-establish indentation procedures originally developed in materials science for testing the hardness of metals, ceramics or polymers have been adapted to the studies of biological tissues. Current material testing systems or clinical indentation

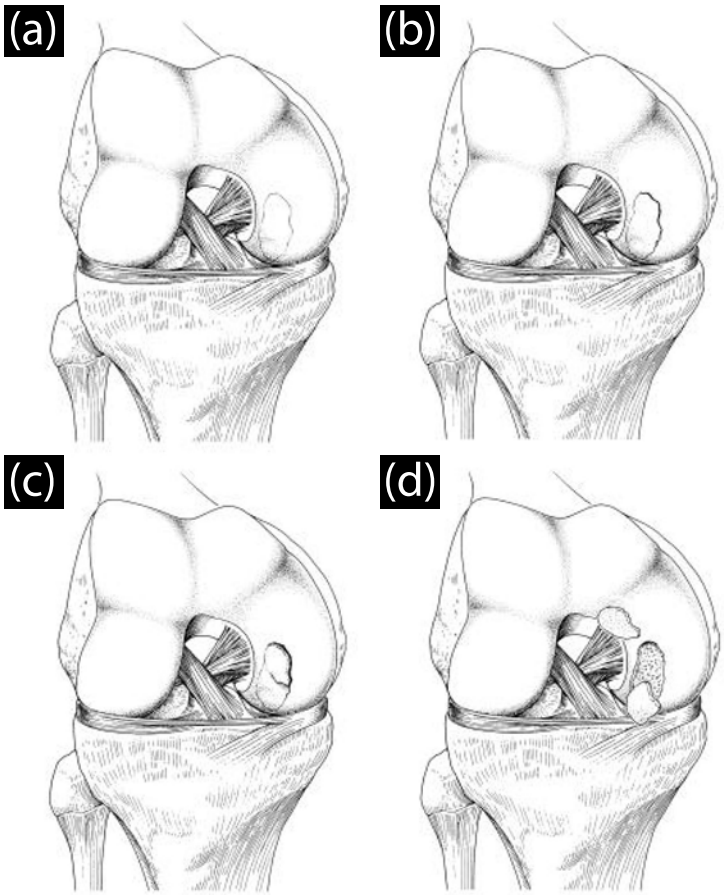

Figure 1.8. ICRS classification of cartilage lesions. **(a)** ICRS Grade I: Stable, continuity: Softened area covered by intact cartilage. **(b)** ICRS Grade II: Partial discontinuity, stable on probing. **(c)** ICRS Grade III: Complete discontinuity, "dead in situ", not dislocated. **(d)** ICRS Grade IV: Dislocated fragment, loose within the bed or empty defect > 10mm in depth. Reproduced from ICRS Classification of OCD-Lesions (Osteochondritis-Dissecans) [31].

devices perform average measurements over several square micrometers. The lateral size of these probes is too large to discriminate the stiffness of the collagen network from those of the rest of the ECM. Therefore, the detection of early OA, characterized by an increase of the water content of the ECM without significant structural change in the collagen network, is not possible by classical indentation.

Ex-vivo unconfined compression testing of normal, diseased, and altered cartilage, performed by Stolz et al. [32], revealed that an SFM used as nanoindenter is sensitive enough to detected early alterations in the biomechanical properties of cartilage. Measurements performed, with such probes, on porcine articular cartilage showed a radical improvement in the sensitivity of the measurements when the lateral size of the indenter was below one micrometer. The SFM invented in 1986 by Binnig, Quate and Gerber [33] is able to image, measure and manipulate matter at the level of a single cell and bellow. This nanotool consists of a very sharp tip mounted at the end of a soft silicon cantilever which bends in response to the force acting between the tip and the sample. Usually, an optical read-out system composed by a laser and a photodiode is used to detected the deflection of the cantilever while the tip is moving over the sample surface in a raster scan. A detailed description of an SFM setup is given in figure 1.9.

1.3.4 Treatment

A wide range of treatment options are available for treating OA and its symptoms. Depending on the age of the patient and the stage of the disease, the clinician in accordance with the patient decides the course of treatment. Generally, these options can be categorized onto five major groups. Based on a review published by the AAOS in January 2004, this section briefly describes the most current techniques [34, 35, 36].

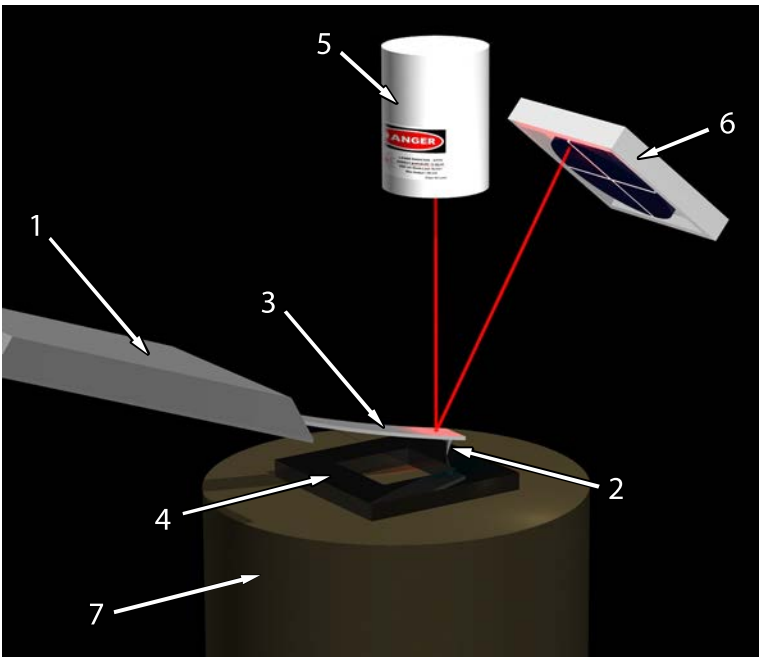

Figure 1.9. Description of SFM principle. The SFM (1) consists of a very sharp tip (2) mounted at the end of a soft silicon cantilever (3) which bends in response to the force acting between the tip and the sample (4). An optical read-out system composed by a laser (5) and a photodiode (6) is used to detected the deflection of the cantilever. A piezo-electric tube (7) is used to performed the scanning.

Health and behavior modifications

The first and perhaps easiest step against OA consists of health and behavior modifications. This treatment concerns all stages of the disease and includes:

- **Patient education:** The more the patient understands about his condition, the better prepared he is to make decisions about his treatment. Patient education focuses on understanding the disease and learning about treatment options.

- **Physical therapy and exercise:** The impact of the disease can be significantly reduce by developing individualized exercise and pain management programs [37].

- **Weight loss:** Loss of weight reduces the stress on the articulation, that can result in a reduction of pain and extension of the mechanical function of the knee joint [38].

- **Knee brace:** When OA is centered on one side of the knee, the use of a knee brace is especially helpful. The brace can assist with stability and function.

Drug therapy

Generally, doctors prescribe drugs for the treatment of OA. Medications are only used to reduce or eliminate pains. At this time, no drugs are available to cure OA.

- **Simple pain relievers:** Analgesics, often available without prescription, are very effective in reducing pain at an early stage of OA. However, like all drugs, they have potential side effects. Additionally, the human body can build up tolerance, reducing with time the desired effects.

- **Nonsteroidal anti-inflammatory drug (NSAID):** NSAID are a stronger type of pain relievers. Like analgesics, they reduce pain and inflammation, but do not stop the degradation of the articular surface. These kind of drugs often cause strong side effects affecting kidney or liver functions.

- **Glucosamine and/or chondroitin sulfate:** Glucosamine and chondroitin sulfate are natural compounds in the body that help making human cartilage strong and rigid. They are also sold as a nutritional supplement in many drugstores and health food stores. It is thought that glucosamine or chondroitin sulfate supplements may be able to help the body repair damaged cartilage, but this has not yet been proven.

Intra-articular treatment

Intra-articular treatments consist of injecting medications directly into the joint space of a painful, inflamed arthritic joint. There are two types of treatment:

- **Corticosteroid injections:** If analgesics or NSAIDs treatment don't show significant improvement of joint function, an injection of corticosteroid directly into the knee can sometimes be helpful for short-term pain relief. Corticosteroids or cortison are natural hormones produced by the adrenal glands in the human body. Generally, steroid injections are prescribed only 3 or 4 times per year and per joint.

- **Viscosupplementation with hyaluronic acid:** This widely used treatment consist of a series of intra-articular injections of hyaluronic acid. The exact mechanism of action is unclear, but beneficial effects with minimal adverse reactions have been observed in a significant number of patients [39].

Surgery

The first treatment of OA is nonsurgical, but when conservative treatment is not sufficient to relieve pain and improve joint function, surgery can be recommended.

- **Arthroscopy:** During arthroscopy, the surgeon uses small instruments to treat damaged cartilage. The surgeon can remove any debris from the joint (debridement procedure) or clean the knee (lavage or irrigation procedure). During the same surgery, he can also correct other problems like torn meniscus or damaged ligament. For people under 55 years old, arthroscopy can be a good solution to delay more serious surgery like joint replacement.

- **Osteotomy:** Osteotomy consists of reshaping bones in order to improve the knee alignment. This procedure can temporarily reduce pain and improve knee function. It may even stimulate the growth of new cartilage, but in the long term, people with osteotomy will often need a total knee replacement.

- **Cartilage transfer:** A cartilage transfer procedure consists of moving healthy cartilage from a normal area to a damaged area of the knee. The cartilage plugs come from non-weight-bearing areas of the knee. Mosaicplasty and osteochondral autograft transfer system (OATS) are the usual applied procedures. These two techniques are very similar, and differ only in the number of plugs and their size.

- **Cartilage Implantation:** Autologous chondrocyte implantation (ACI) is a relatively new technique which consists in taking several cartilage cells from the knee and culturing them in vitro. Once millions of cells have been grown they are re-implanted into the area of damaged cartilage. The goal of this treatment is to

replace deep defects in cartilage of relatively young people (typically from 15 to 55 years of age). After cartilage implantation, a planned rehabilitation programme is necessary to stimulate cells to produce the right kind of cartilage.

- **Arthroplasty:** Arthroplasty consists of a partial or total knee joint replacement. This procedure is recommended when pain is severe and movements are significantly limited. Generally, the results of joint replacement are excellent. Prothesis are made of cobalt-chrome or titanium metals and smooth, wear-resistant plastic like polyethylene. The lifetime for a prothesis is estimated to be 10 years. The first attempts to replace a knee joint were made in the 1860's [40]. The success rate of these early attempts was poor because of infections and limitations in the materials used.

Bibliography

[1] Van C. Mow and Wilson C. Hayes. *Basic Orthopaedic Biomechanics*. Lippincott-Raven, second edition, 1997.

[2] Henry Gray. *Anatomy of the Human Body*. Philadelphia: Lea & Febiger, 20th ed. edition, 1918.

[3] M.A.R. Freeman and V. Pinskerova. The movement of the normal tibio-femoral joint. *J Biomech*, 38(2):197–208, February 2005.

[4] Andrew H. Hansen, Dudley S. Childress, and Erick H. Knox. Roll-over shapes of human locomotor systems: effects of walking speed. *Clin Biomech (Bristol, Avon)*, 19(4):407–414, May 2004.

[5] Vikas V. Patel, Katherine Hall, Michael Ries, Jeff Lotz, Eugene Ozhinsky, Colleen Lindsey, Ying Lu, and Sharmila Majumdar. A

three-dimensional mri analysis of knee kinematics. *Journal of Orthopaedic Research*, 22(2):283–292, 2004.

[6] Jennifer M. Scarvell, Paul N. Smith, Kathryn M. Refshauge, Howard R. Galloway, and Kevin R. Woods. Comparison of kinematic analysis by mapping tibiofemoral contact with movement of the femoral condylar centres in healthy and anterior cruciate ligament injured knees. *Journal of Orthopaedic Research*, 22(5):955–962, 2004.

[7] C. Owen Lovejoy. The natural history of human gait and posture: Part 3. the knee. *Gait Posture*, 25(3):325–341, March 2007.

[8] R. K. Korhonen, M. S. Laasanen, J. Töyräs, J. Rieppo, J. Hirvonen, H. J. Helminen, and J. S. Jurvelin. Comparison of the equilibrium response of articular cartilage in unconfined compression, confined compression and indentation. *J Biomech*, 35(7):903–909, Jul 2002.

[9] S. Park, C. T. Hung, and G. A. Ateshian. Mechanical response of bovine articular cartilage under dynamic unconfined compression loading at physiological stress levels. *Osteoarthritis and Cartilage*, 12(1):65–73, January 2004.

[10] P. Neyret, S. T. Donell, and H. Dejour. Results of partial meniscectomy related to the state of the anterior cruciate ligamentreview at 20 to 35 years. *Journal of Bone and Joint Surgery-British Volume*, 75(1):36–40, January 1993.

[11] Hiroshi Asano, Takeshi Muneta, Hiroo Ikeda, Kazuyoshi Yagishita, Yoshiaki Kurihara, and Ichiro Sekiya. Arthroscopic evaluation of the articular cartilage after anterior cruciate ligament reconstruction: A short-term prospective study of 105 patients. *Arthroscopy*, 20(5):474–481, May 2004.

[12] Anna I Vasara, Jukka S Jurvelin, Lars Peterson, and Ilkka Kiviranta. Arthroscopic cartilage indentation and cartilage lesions of anterior cruciate ligament-deficient knees. *Am J Sports Med*, 33(3):408–414, Mar 2005.

[13] Michael Doherty. Risk factors for progression of knee osteoarthritis. *The Lancet*, 358(9284):775–776, September 2001.

[14] J. Cushnaghan and P. Dieppe. Study of 500 patients with limb joint osteoarthritis. I. Analysis by age, sex, and distribution of symptomatic joint sites. *British Medical Journal*, 50(1):8, 1991.

[15] P Pottie, N Presle, B Terlain, P Netter, D Mainard, and F Berenbaum. Obesity and osteoarthritis: more complex than predicted! *Ann Rheum Dis*, 65(11):1403–1405, 2006.

[16] David Coggon, Peter Croft, Samantha Kellingray, David Barrett, Magnus McLaren, and Cyrus Cooper. Occupational physical activities and osteoarthritis of the knee. *Arthritis & Rheumatism*, 43(7):1443–1449, 2000.

[17] C Coopera and D Coggona. Physical activity and knee osteoarthritis. *The Lancet*, 353(9171):2177–2178, June 1999.

[18] J F Maillefert, A Gueguen, M Monreal, M Nguyen, L Berdah, M Lequesne, B Mazieres, E Vignon, and M Dougados. Sex differences in hip osteoarthritis: results of a longitudinal study in 508 patients. *Ann Rheum Dis*, 62(10):931–934, October 2003.

[19] Jennifer J. Anderson and David T. Felson. Factors associated with osteoarthritis of the knee in the first national health and nutrition examination survey (hanes i): evidence for an association with overweight, race, and physical demands of work. *Am. J. Epidemiol.*, 128(1):179–189, July 1988.

[20] F M Cicuttini and T D Spector. Genetics of osteoarthritis. *Ann Rheum Dis*, 55(9):665–667, September 1996.

[21] T Lapvetelainen, M M Hyttinen, A-M Saamanen, T Langsjo, J Sahlman, S Felszeghy, E Vuorio, and H J Helminen. Lifelong voluntary joint loading increases osteoarthritis in mice housing a deletion mutation in type ii procollagen gene, and slightly also in non-transgenic mice. *Ann Rheum Dis*, 61(9):810–817, September 2002.

[22] H A Alhadlaq, Y Xia, J B Moody, and J R Matyas. Detecting structural changes in early experimental osteoarthritis of tibial cartilage by microscopic magnetic resonance imaging and polarised light microscopy. *Ann Rheum Dis*, 63(6):709–717, 2004.

[23] P. Hunziker, M. Stolz, and U. Aebi. Nanotechnology in medicine: Moving from the bench to the bedside. *Chimia*, 56(10):520–526, 2002.

[24] J. H. Kellgren and J. S. Lawrence. Radiological assessment of osteo-arthrosis. *Ann Rheum Dis*, 16(4):494–502, December 1957.

[25] Z.-P. Liang and P. C. Lauterbur. *Principles of Magnetic Resonance Imaging: A Signal Processing Perspective*. Wiley-IEEE Press, 1999.

[26] Koji Hattori, Yoshinori Takakura, Masao Ishimura, Takashi Habata, Kota Uematsu, and Ken Ikeuch. Quantitative arthroscopic ultrasound evaluation of living human cartilage. *Clin Biomech (Bristol, Avon)*, 19(2):213–216, Feb 2004.

[27] S. Saarakkala, M. S. Laasanen, J. S. Jurvelin, K. Torronen, M. J. Lammi, R. Lappalainen, and J. Toyras. Ultrasound indentation of normal and spontaneously degenerated bovine articular cartilage. *Osteoarthritis and Cartilage*, 11(9):697–705, September 2003.

[28] Mikko S Laasanen, Simo Saarakkala, Juha Töyräs, Jani Hirvonen, Jarno Rieppo, Rami K Korhonen, and Jukka S Jurvelin. Ultrasound indentation of bovine knee articular cartilage in situ. *J Biomech*, 36(9):1259–1267, Sep 2003.

[29] Watanabe. Memories of the early days of arthroscopy. *Arthroscopy*, 2(4):209–214, December 1986.

[30] Christopher W Kieser and Robert W Jackson. Eugen bircher (1882-1956) the first knee surgeon to use diagnostic arthroscopy. *Arthroscopy*, 19(7):771–776, September 2003.

[31] M. Brittberg, P. Aglietti, R. Gambardella, L. Hangody, H. J. Hauselmann, R. P. Jakob, D. Levine, S. Lohmander, B. R. Mandelbaum, L. Peterson, and H.-U. Staubli. International cartilage repair society cartilage injury evaluation package. Developed during ICRS 2000 Standards Workshop, April 2000.

[32] M. Stolz, R. Raiteri, A. U. Daniels, M. R. VanLandingham, W. Baschong, and U. Aebi. Dynamic elastic modulus of porcine articular cartilage determined at two different levels of tissue organization by indentation-type atomic force microscopy. *Biophysical Journal*, 86(5):3269–3283, May 2004.

[33] G. Binnig, C. F. Quate, and Ch. Gerber. Atomic force microscope. *Phys. Rev. Lett.*, 56(9):930–933, March 1986.

[34] AAOS. Osteoarthritis of the knee: Treatment options. American Academy of Orthopedic Surgeons, 2004.

[35] AAOS. Osteoarthritis of the knee: Joint replacement. American Academy of Orthopedic Surgeons, 2004.

[36] A Pendleton, N Arden, M Dougados, M Doherty, B Bannwarth, J W J Bijlsma, F Cluzeau, C Cooper, P A Dieppe, K-P Gunther, H J Hauselmann, G Herrero-Beaumont, P M Kaklamanis, B Leeb, M Lequesne, S Lohmander, B Mazieres, E-M Mola, K Pavelka, U Serni, B Swoboda, A A Verbruggen, G Weseloh, and I Zimmermann-Gorska. Eular recommendations for the management of knee osteoarthritis: report of a task force of the standing committee for international clinical studies including therapeutic trials (escisit). *Ann Rheum Dis*, 59(12):936–944, December 2000.

[37] Sheila C O'Reilly, Ken R Muir, and Michael Doherty. Effectiveness of home exercise on pain and disability from osteoarthritis of the knee: a randomised controlled trial. *Ann Rheum Dis*, 58(1):15–19, January 1999.

[38] Robin Christensen, Else Marie Bartels, Arne Astrup, and Henning Bliddal. Effect of weight reduction in obese patients diagnosed with knee osteoarthritis: a systematic review and meta-analysis. *Ann Rheum Dis*, 66(4):433–439, April 2007.

[39] DY. Wen. Intra-articular hyaluronic acid injections for knee osteoarthritis. *Am Fam Physician*, 62:565–570, 2000.

[40] AA Shetty, A. Tindall, P. Ting, and FW Heatley. The evolution of total knee arthroplasty. Part 1: introduction and first steps. *Current Orthopaedics*, 17(4):322–325, 2003.

Chapter 2

Instrument realization

2.1 Introduction

The clinical instruments available on the market for evaluating cartilage state of health can only diagnose structural changes at an advanced stage of the disease, when it's usually too late for a treatment. Towards an early diagnosis of OA, but also for the development of drugs and effective therapies, we have designed a more sensitive diagnostic tool, called SFA [1, 2]. This arthroscopic instrument allow to measure *in-vivo* the biomechanical properties of articular cartilage at the submicrometer scale by indentation testing with an SFM probe.

As shown in figure 2.1, the SFA is comprised of a handle, a shaft and a complete SFM setup. To be used during standard surgery, it must have dimensions comparable to those of classical arthroscopic instruments (typical outer diameter about 5 mm). To fit this important requirement, the SFM setup which includes a stabilization stage, a scanning stage and an indentation stage, had to be miniaturized. Another big limitation concerns the materials. Actually, the SFA like any other medical instrument must be sterilized before entering in the operating room. The

preferred method for sterilization is through hot steam in an autoclave. For at least 15 minutes, the instrument is maintained at a pressure of 103 kPa (15 psi) and a temperature of 121˚C. The materials employed must not only be able to resist this sterilization procedure, but additionally, they must be biocompatible or at least non-toxic. This chapter will describe in more detail the different parts forming the tool itself, as well as the elements required for its operation.

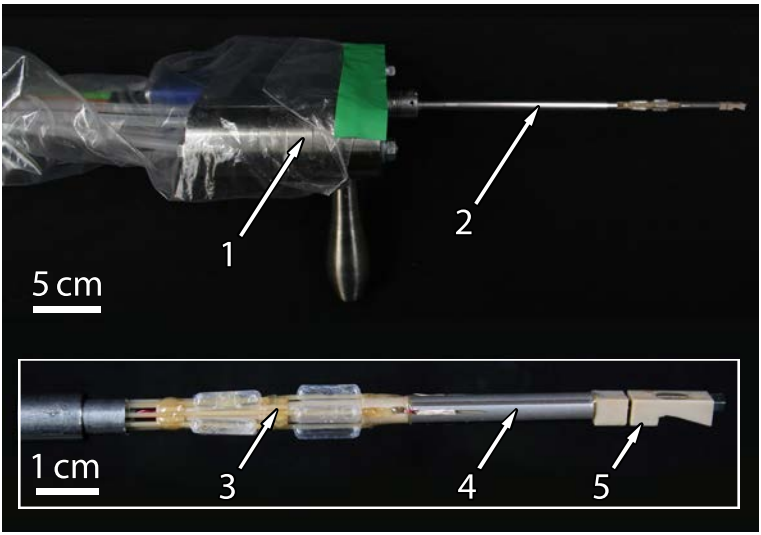

Figure 2.1. Picture of the SFA v.2. The handle (1) facilitates the manipulation of the instrument. The electrical and pneumatic connections are embedded into a rigid shaft (2). The inset exhibits a magnified image of the distal end of the instrument containing from left to right, the stabilization stage (3), the scanning stage (4) and the indentation stage (5).

2.2 Stabilization stage

Considering the desired resolution of the measurements and the special environment of an operating room, the major challenges for recording SFM measurements inside a human body were the stabilization of the instrument and the dampening of vibrations. The stabilization stage was specially designed for that purpose.

2.2.1 Inflatable balloons

The stabilization stage consisted of eight inflatable angioplasty balloons arranged on a polyetheretherketone (PEEK) holder in two sets of four (cf. Fig. 2.2). To increase the stabilization, the first set is rotated against the second by an angle of 45˚. To ensure well-controlled unidirectional inflation, polyethylene terephthalate (PET) square end offset balloons (Advanced Polymers, Inc.,Salem, NH, USA) with 5 mm in length and 3 mm in diameter were customized.

During an arthroscopy, the joint was continually flushed with a physiological salt solution (Ringer's solution). The balloons used the same liquid to wedge the SFA into the joint cavity by filling the gap between the instrument and the bones (cf. Fig. 2.3 (a)). The use of Ringer's solution for inflating the balloons allowed to increase the dampening of outside vibrations and prevent damage in case of leakage. This pneumatic system was not only responsible for the stabilization of the instrument, but was also effective for carrying out the coarse approach. As shown in figure 2.3 (b), the distal end of the instrument could be moved towards the cartilage's surface by adjusting the differential pressure between opposite balloons. This patented system [3] allowed to displace the tool tip in a plane perpendicular to the cartilage surface.

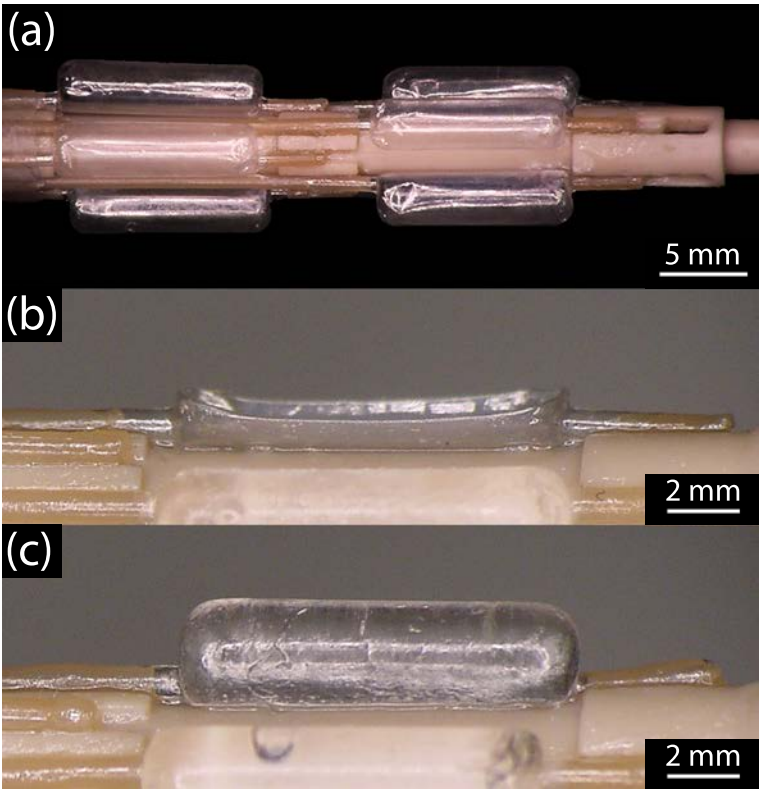

Figure 2.2. Picture of the stabilization stage. **(a)** The stabilization stage consists of eight angioplasty balloons. These balloons are inflated with Ringer's solution. The difference in height between deflated **(b)** and inflated balloon **(c)** is around 2 mm.

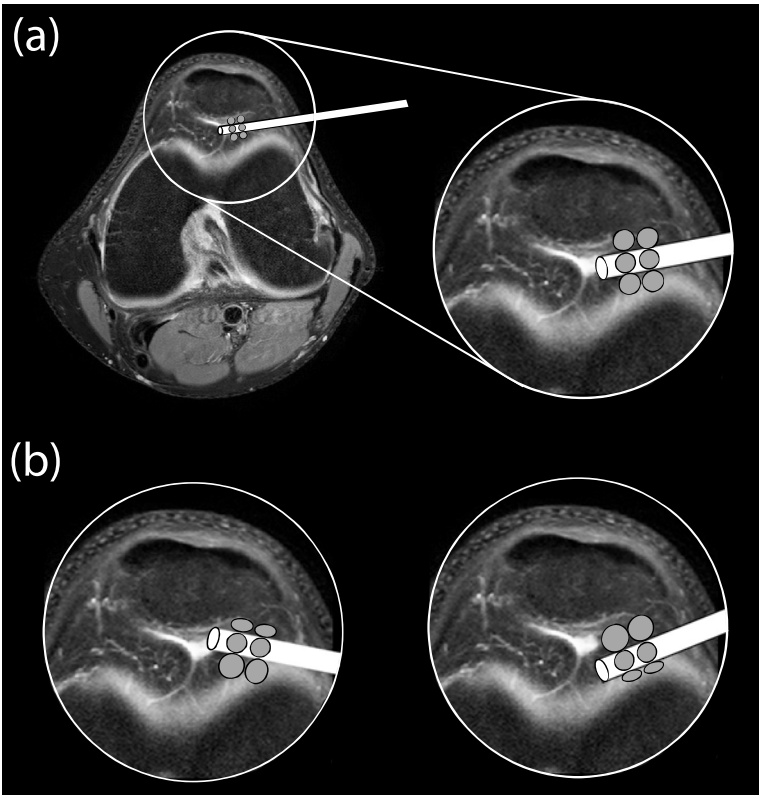

Figure 2.3. Schematic view of the pneumatic system. **(a)** Eight inflatable balloons wedge the SFA inside the knee by filling the gap between the instrument and the cavity. **(b)** The instrument can be positioned inside the knee by adjusting the differential pressure in opposite balloons.

2.2.2 Syringe pushers

Each balloon was inflated and deflated with physiological liquid through a capillary tube (outer diameter = $512\ \mu m$, inner diameter = $256\ \mu m$, PEEK material) by a syringe-pusher (cf. Fig. 2.4). This device used a carriage and an endless screw actuated by a stepper motor to move the piston of a syringe forwards and backwards. An open linear ball bearing system (Sferrax, CH) prevented rotation of the carriage. The stepper motor (Sonceboz, CH) was connected to the endless screw by a flexible shaft coupling. A 4-port cross manifold (Legris, CH) was connected at the output of each syringe for distributing the liquid through several circuits. During the whole intervention, the pressure in the balloons was monitored by a pressure sensor (UNIMEC, CH). In order to purge the residual air in the system, a low vacuum system was connected to the top port of the manifold.

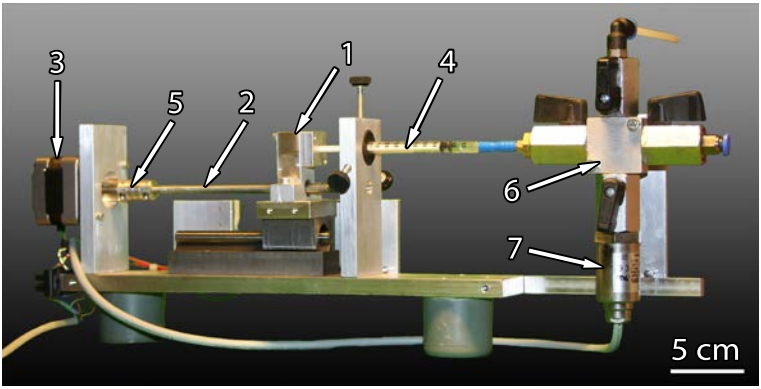

Figure 2.4. Picture showing the different parts forming of a syringe-pusher: carriage (1), endless screw (2), stepper motor (3), syringe's piston (4), flexible shaft coupling (5), 4-port cross manifold (6) and pressure sensor (7).

2.2.3 Electronics and software

The syringe pushers were connected to an electronic box which contains the drivers for the stepper motor and the alimentation circuits for the pressure sensors. A DAQCard-1200 acquisition card from National Instrument was used to interface the electronic box with a dedicated computer. A LabVIEW program was developed to automatically control the movements of the syringe-pushers. A joystick, which allowed to access all these features, has been integrated to the software. As shown in figure 2.5, the interface of the software was divided in three parts:

- **The control panel** allowed to select the number of steps, the direction of rotation and the number of trips executed by the stepper motors.
- **The balloons panel** allowed to visualize the instant pressure of each balloon, to activate or deactivate the syringe-pushers one by one, and to select or deselect a full stack of balloons.
- **The program panel** allowed you to define standard procedures, such as balloons initialization, tool stabilization or instrument withdraw.

2.3 Scanning stage

The scanning stage was essential to apply a controlled load on the cartilage surface during indentation measurements. A 3D scanner effective to establish a two-dimensional (2D) map of cartilage stiffness and not only to record a one point measurement was highly desirable. A grid of data was achieved by combining a raster scan in the XY plan with an indentation movement in the z-direction. For each point of the grid, a set of 5 load-displacement curves was recorded and the stiffness was calculated (cf. Fig. 2.6).

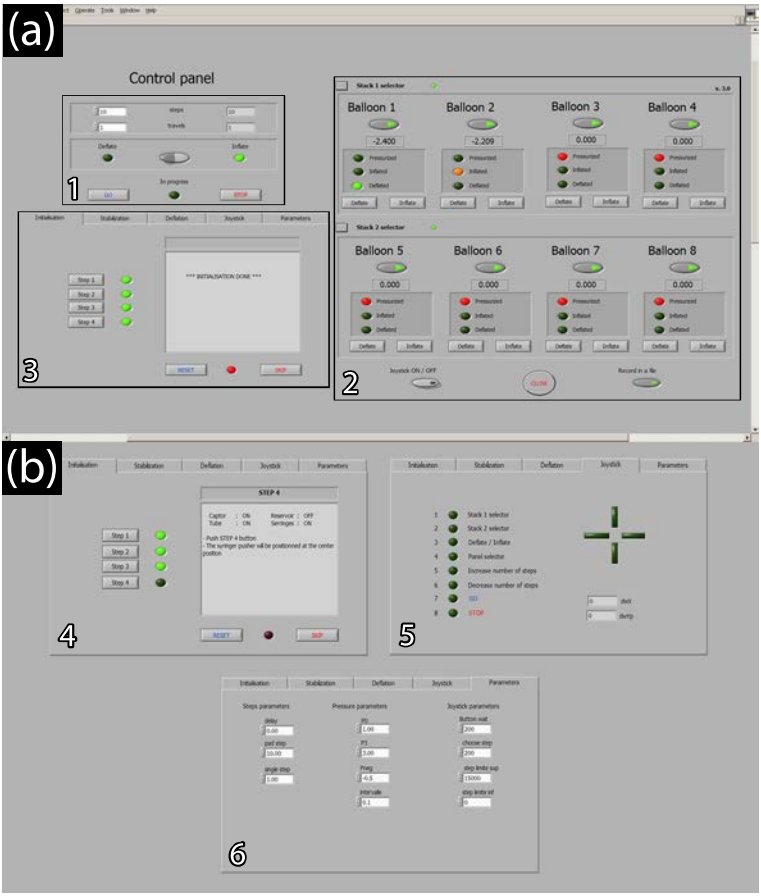

Figure 2.5. **(a)** Picture of the software interface which is divided into three zones: the control panel (1), the balloons panel (2) and the programme panel (3). **(b)** The programme panel allows to: define different automatic procedures like initialization of the balloons (4), monitor the movements of the joystick (5), or define the programme's constants.

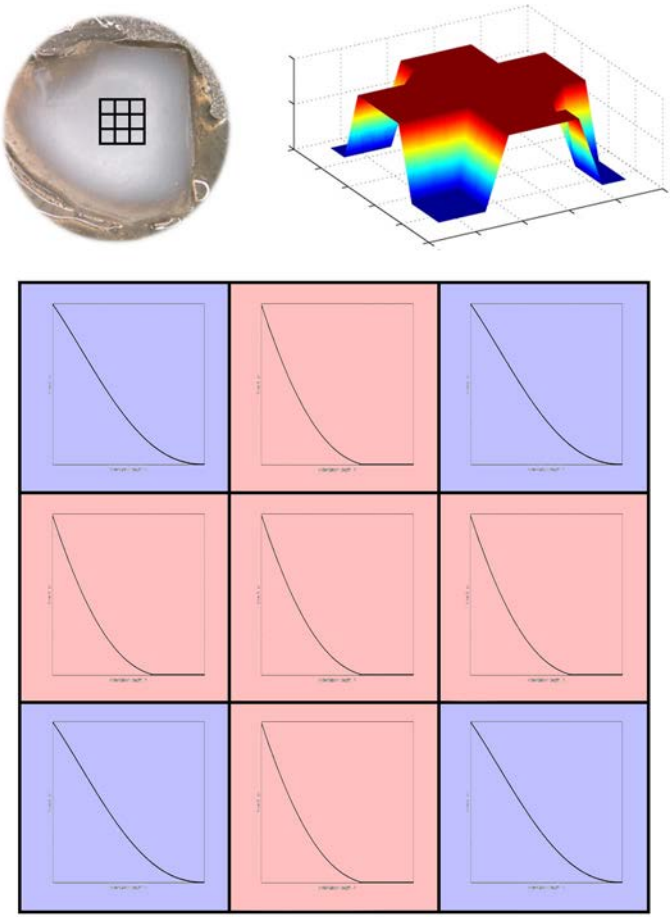

Figure 2.6. The 3D scanner implemented in the instrument allows to define a grid of measurements. For each point of the grid, a indentation is performed and a load-displacement curve is recorded. For each curve, the dynamic elastic modulus $|E^*|$ is computed (cf. Chapter 3). Thus, a 2D map of cartilage stiffness is created

2.3.1 Tube scanner

Almost all SFM scanners are based on the inverse piezoelectric effect. In a piezoelectric crystal, the positive and negative charges are arranged in dipoles. These dipoles, locally aligned, form small areas called Weiss domains. The domains are randomly oriented but can be aligned during the fabrication process by applying, at high temperatures, a strong electric field across the material. This process is called poling. Later, if an external electric field is applied in the opposite direction, the dipoles are displaced by electrostatic forces, and a mechanical deformation appears in the crystal [4, 5]. Depending on the voltage applied between the inner and outer electrodes, the tube scanner contracts laterally or longitudinally (cf. Fig. 2.7), thereby providing, an XYZ motion.
The axial contraction Δx of the tube can be estimated by the following equation [6, 7]:

$$\Delta x \approx d_{31} \cdot \frac{L}{(D_o - D_i)} \cdot U \tag{2.1}$$

where d_{31} is the strain coefficient (displacement normal to polarization direction), L is the tube length, D_o, and D_i are respectively the outer, and the inner diameter of the tube and U is the applied voltage.

The quartered electrodes make lateral scanning possible. The radial displacements $\Delta y \; or \; \Delta z$ of the tube can be estimated by the following equation:

$$\Delta y \; or \; \Delta z \approx \frac{2\sqrt{2}}{\pi} \cdot \frac{2 d_{31} L^2}{(D_o - D_i)(D_o + D_i)} \cdot U \tag{2.2}$$

The scanner implemented into the scanning stage consisted of a four-segmented piezoelectric tube made of lead zirconate titanate (PZT) ceramic (PIC 151, PI ceramic, Germany). Table 2.1 gives the detailed

characteristics of this material. The tube length was 30 mm, the outer and inner diameter were respectively 3.2 and 2.2 mm. Theoretically, the tube implemented into the SFA allowed to address a volume of $1 \times 6 \times\ 6\ \mu m^3$, when operated at a maximum voltage of $\pm\ 100\ V$. However, to enable a good interpretation of the measurements, a fine calibration of the scanner was essential. This calibration is presented in Chapter 3.

Parameter	Symbol	Units	Value
Density	ρ	g/cm^3	7.8
Dielectric constant	ε_{33}		2400
Quality factor	Q		100
Curie Temperature	T_c	$^{\circ}C$	250
Strain coefficients	d_{31}	pm/V	-210
	d_{33}	pm/V	500

Table 2.1: Detailed characteristics of PIC 151.

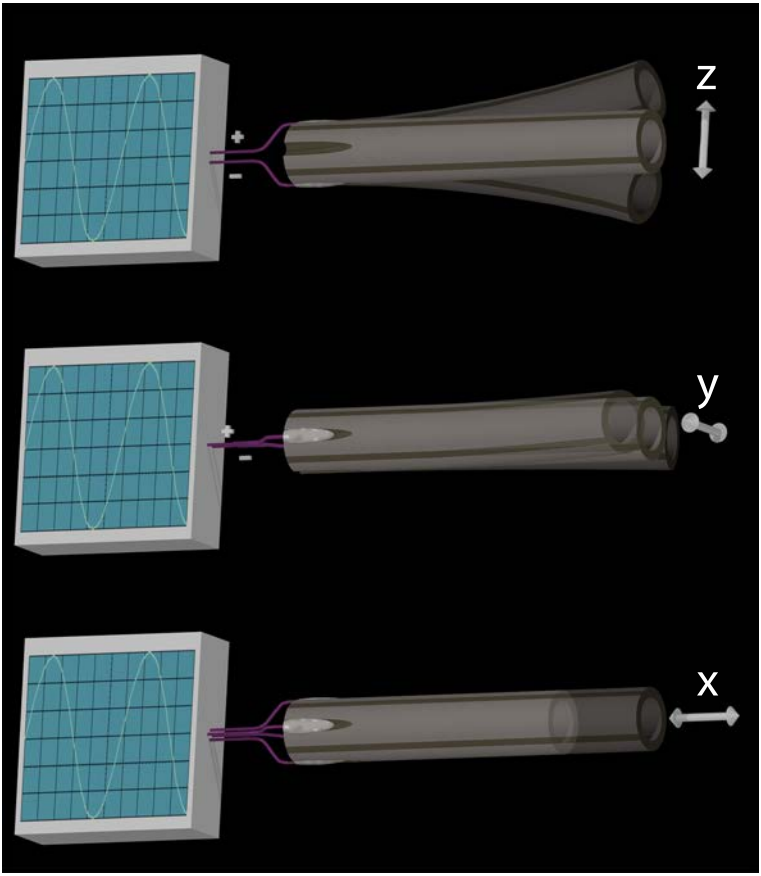

Figure 2.7. Schematic representation of the piezoelectric tube deflection. Depending on the voltage applied between the inner and outer electrodes, the tube scanner contracts laterally (z-axis and y-axis) or longitudinally (y-axis). This tube is able to provide a full XYZ motion.

2.3.2 Encapsulation

The lead contained in PZT posed some concerns of biocompatibility. Due to its high toxicity for cells, lead is generally banished from the human body. Therefore, we conducted a preliminary test where we grown up Buffalo rat liver (BRL) cells on PZT and as reference on glass. After 24 hours of incubation, the size, the shape and the number of cells were compared under fluorescence microscope. No significant differences between the cells on the two different substrates were observed (cf. Fig. 2.8). Even if PZT was non toxic, an encapsulation of the tube scanner was still necessary to protect the tissues from the relatively high voltages ($\pm$ 100 V) used during indentation testing. This encapsulation was performed by the deposition under vacuum of a thin film of parylene obtained by polymerization of di-paraxylylene. Parylene coating formed an homogenous, uniform, and clear film with excellent electrical insulation.

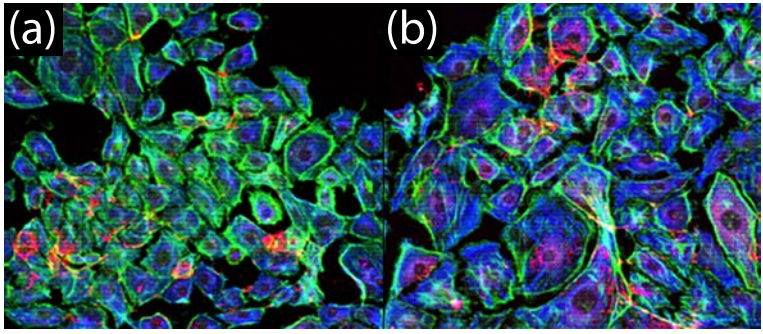

Figure 2.8. The non toxicity of PZT was tested by comparing under fluorescence microscope the number, the size and the shape of BRL cells grown on **(a)** PZT and **(b)** glass as reference.

2.4 Indentation stage

The indentation stage contained the SFM cantilever required to measure the biomechanical properties of cartilage. This was the most delicate part of the instrument.

2.4.1 Tip connector

An important feature of this stage was the ability to quickly exchange the probe in case of cantilever failure. For that purpose, a small PEEK connector that could be easily detached from the rest of the instrument was designed. The female part was directly fixed at the end of the scanning stage. The male part contained the SFM chip. To facilitate the approach, the sensor was tilted by an angle of 15˚. A stainless steel screw-bolt system ensured the connection during operation. This three-contact connector is shown in figure 2.9.

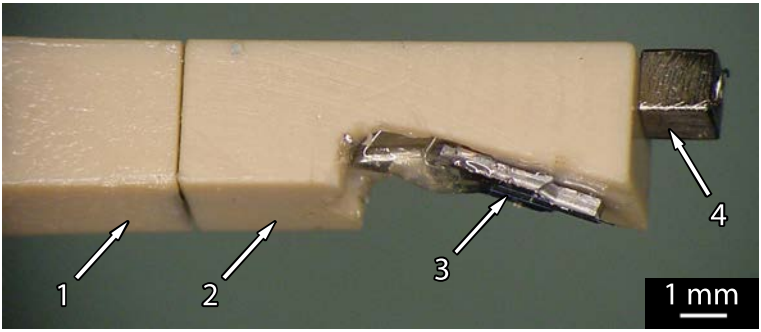

Figure 2.9. The tip connector which consists of a female part (1) and a male part (2). The SFM probe (3) is glued on the male part. A locking system (4) forms by a microscrew and a microbolt (ISO M 0.7).

2.4.2 SFM probe

The SFM probe mounted on the connector consisted of a rectangular silicon cantilever on which a 10 μm high pyramidal tip was integrated. The cantilever was 500 μm long, 80 μm wide and 3 μm thick. The chips used during measurements with SFA were designed and fabricated, by T. Akyiama, S. Gautsch and D. Parrat, as part of another project. The fabrication process for such probes required eight depositions or growths, eight photolithographies, seven wet etchings and six dry etchings [8, 9]. These probes are shown in figure 2.10. A resonance frequency f_c of 40 kHz and a spring constant k_c of 5.5 N/m were calculated for these probes by using the following equations:

$$f_c = \frac{t}{\sqrt{6}\pi L^2}\sqrt{\frac{E}{\rho}}, \tag{2.3}$$

$$k_c = \frac{Ewt^3}{4L^3}, \tag{2.4}$$

where L is the length of the cantilever, w the width, t the thickness, E is the Young's modulus, ρ is material density.

2.4.3 Deflection sensor

Due to the very limited space available in the knee joint, a piesoresisitve stress sensor was directly implemented on the cantilever, replacing the classic laser and photodiode based detection. The piezoresistive effect describes the change of electrical resistance of a material under mechanical deformation. This change of resistance can be expressed by the following equation:

$$\frac{\Delta R}{R} = (\Pi_L + \frac{1+2\nu}{E})\sigma_L, \tag{2.5}$$

where Π_L is the longitudinal piezoresistive coefficient, ν the Poisson's ratio, E the Young's modulus and σ_L the applied longitudinal stress. The piezoresistor implemented at the base of the cantilever was defined by diffusing p-type boron atoms into a n-doped silicon substrate. On each SFM chip, a reference piezoresistor was implemented right next to the main cantilever. This short lever allows to compensate thermal drifts which may occur during measurements. Aluminium lines were defined along the sensor to connect the piezoresistors to the chip's bonding pads. To insulate the piezoresistors and the metal lines, the sensor was passivated by a silicon nitride layer.

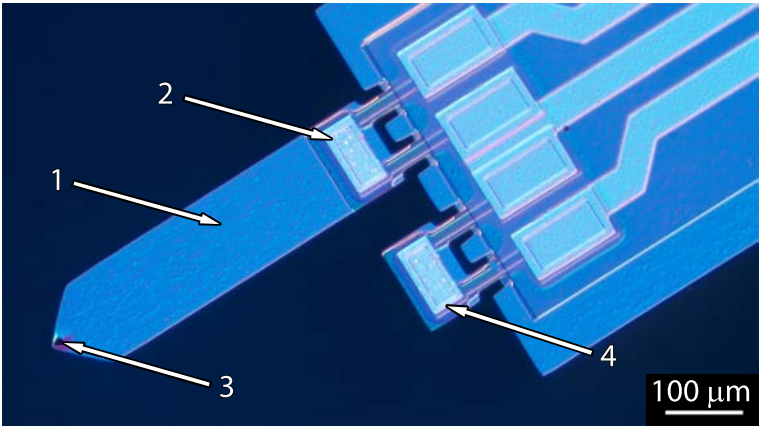

Figure 2.10. The piezopiezoresistive probes used to perform *in-vivo* indentation testing of articular cartilage consist of a very sharp tip (3) at the end of a thin cantilever (1). A piesoresisitve stress sensor (2) is implemented at the base of the cantilever. A second piesoresisitve stress sensor (4) is implemented on a shorter cantilever. This sensor is used as reference (4) to compensate the thermal drifts. (Photo: H.R. Bramaz).

2.5 Handle

The SFM setup implemented into the instrument required a large number of electric and pneumatic connections. Due to the restricted dimensions of the tool's shaft (outer diameter about 5 mm), these connections were implemented in the handle. During measurements, the part of the instrument which stayed outside the body was simply stabilized by the hand of the surgeon. For this reason, the design of the handle directly influenced the accuracy of the positioning and the quality of the stabilization.

2.5.1 Handle design

In order to reduce electronic noise during measurements, the distance between the deflection sensor and the amplifier was minimized. The electronic was inserted into the handle. For this reason its size was larger than those of a classical arthroscopic instrument. Despite the fact that the SFA handle was made of stainless steel, the instrument was not fully sterilizable. Repeated exposure to hot steam in autoclave could quickly damage the electronic components. This problem was solved by making the electronic part of the handle detachable from the rest of the tool. Thus, only the tip of the tool was sterilized. During the surgery, the non-sterile part of the instrument was placed in a sterile protective socket just before being reconnected to the rest of the instrument. The biggest challenge was to design a handle which contained simultaneously 16 electrical connections and 8 individual pneumatic connections. The design of the SFA handle is shown in figure. 2.11.

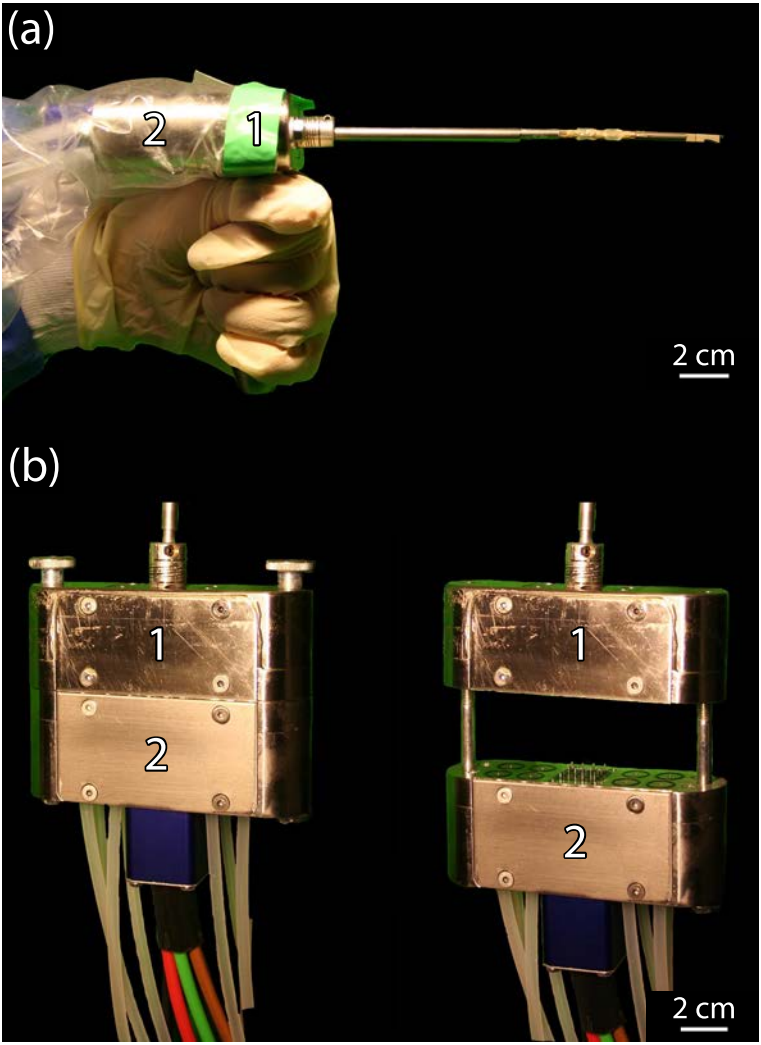

Figure 2.11. **(a)** Side view of the SFA handle. **b)** and **c)** The part of the handle which contain the electronic components (2) is detachable from the rest of the tool (1).

2.5.2 Embedded electronic

The circuit inserted into the instrument handle for measuring the deflection of the cantilever consisted of a Wheatstone bridge coupled to a current buffer amplifier (cf. Fig. 2.12). The change of resistance generated in the piezoresistor was converted into an output voltage V_{out} by the Wheatstone bridge. At equilibrium (i.e. without cantilever deflection) the two legs of the bridge are balanced. When the resistance changes, i.e. with cantilever deflection, the bridge became unbalanced and a voltage was produced at the output of the circuit. A current buffer amplifier was used to transfer the output signal of the Wheatstone bridge, having a low output impedance level, to a voltage amplifier with high input impedance level. This amplifier, implemented outside of the instrument, had an amplification factor of 1000.

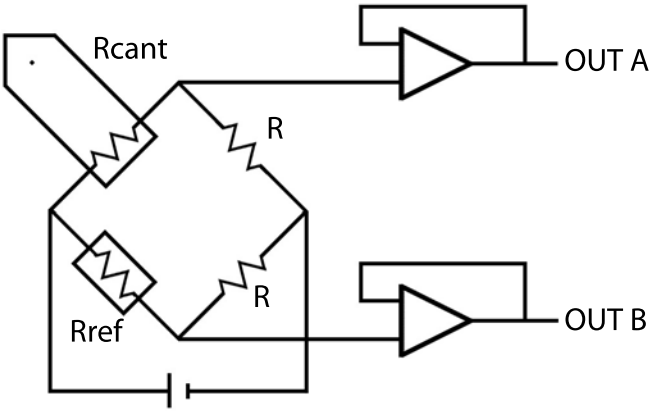

Figure 2.12. Schematic view of the electronics implemented in the handle.

2.6 Nanoscope Electronic

The standard hardware of a commercially available SFM (Multimode SFM equipped with a Nanoscope III controller, Veeco, Santa Barbara, CA) was employed for generating the indentation, and recording the cantilever deflection signal. A schematic view of the full set-up necessary to probe, *in-vivo*, the biomechanical properties of articular cartilage is shown in figure 2.13.

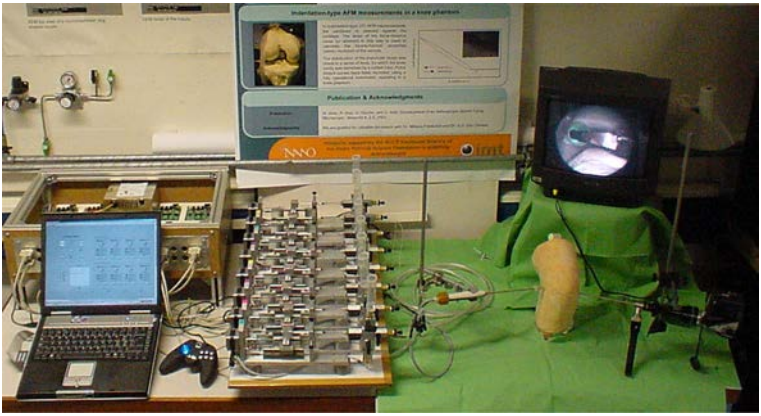

Figure 2.13. Picture of the full SFA setup. During the surgery, an arthroscope allows the surgeon to visualize the inner knee on a TV screen. A computer, eight syringe-pushers with its own electronics are used to control the inflation of the stabilization stage. The Nanoscope III controler is used for generating the indentation, and recording the cantilever deflection signal.

Bibliography

[1] R. Imer, T. Akiyama, N.F. de Rooij, M. Stolz, U. Aebi, N.F. Friederich, U. Koenig, D. Wirz, AU Daniels, and U. Staufer. Development of Atomic Force Microscope for Arthroscopic Knee Cartilage Inspection. *Japanese Journal of Applied Physics*, 45(3B):2319–2323, 2006.

[2] R. Imer, T. Akiyama, N.F. de Rooij, M. Stolz, U. Aebi, R. Kilger, N.F. Friederich, D. Wirz, AU Daniels, and U. Staufer. In situ measurements of human articular cartilage stiffness by means of a scanning force microscope. *Journal of Physics: Conference Series*, 61(1):467–471, 2007.

[3] U. Staufer and R. Imer. US 20060111739 A1 - Device for stabilising and/or positioning a medical tool in a body cavity. Technical report, Institut of Microtechnology, University of Neuchâtel, 2006.

[4] C. J. Chen. Electromechanical deflections of piezoelectric tubes with quartered electrodes. *Applied Physics Letters*, 60(1):132–134, January 1992.

[5] M. M. Pfeffer. *Conception and realization of a compact scanning near-field optical microscope.* PhD thesis, Ecole polytechnique fédérale de Lausanne (EPFL), 1998.

[6] PI Ceramic GmbH. PT120-PT140 - Piezoceramic Tubes. Product information (2008).

[7] DW Pohl. Some thoughts about scanning probe microscopy, micromechanics, and storage. *IBM J. Res. Dev*, 39:701–711, 1995.

[8] S. Gautsch. *Development of An Atomic Force Microscope and Measurement Concepts for Characterizing Martian Dust and Soil Particles.* PhD thesis, University of Neuchâtel, 2002.

[9] D. Parrat. *Atomic Force Microscopy for Characterizing Dust Particles of the Martian Arctic Soils*. PhD thesis, University of Neuchâtel, 2007.

Chapter 3

Instrument calibration

3.1 Scanner calibration

3.1.1 Setup

Open-loop piezoelectric actuators exhibit hysteresis. This phenomena is based on crystalline polarization effects of the material. When an external electrical field is created, the atomic dipoles are aligned with the field. But when the field is removed, the dipoles stay partially aligned and a gap in the voltage-displacement curve appears. Hysteresis is totally compensated in a closed-loop [1, 2].

A dedicated set-up (cf. Fig. 3.1) was build to calibrate the scanner. The instrument was fixed onto a 3-axis tilt platform stage which allowed to align the instrument relatively to a reference surface placed on a 3-axis translation stage. A reflective surface was added on the top of the indentation stage (cf.figure 3.2). This set-up was placed under a Wyko NT1100 optical profiler (Veeco Instruments Inc., USA).

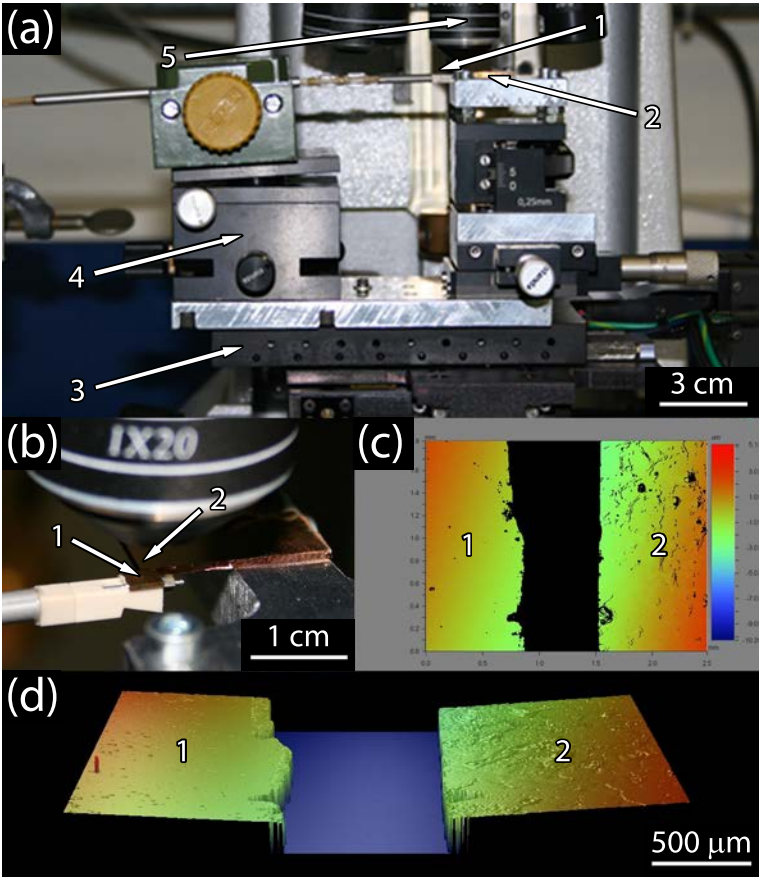

Figure 3.1. Picture of the setup used for calibrating the scanner. **(a)** The back of the SFA (1) is placed under the objective of a Wyko NT1100 optical profiler (5). A 3-axis tilt platform stage (4) and a translation stage (3) allow to align the instrument with a reference platform (2). **(b)** The back of the instrument (1) is aligned with the reference platform (2) under the optical profiler. **(c)** and **(d)** Voltages from -100 to +100 were applied to the electrodes of the scanner. For each value, a height profile was recorded.

3.1.2 Results

Voltages from -100 to +100 were applied to the electrodes of the scanner. For each value of voltage, a three-dimensional surface profile measurement was recorded. The z-displacement of the tube in function of the applied voltage was constructed using these data. (cf. figure 3.2). This curve was necessary to calibrated the data recorded with the Nanoscope software. The range of the scanner could be also determined by this way. For the scanner implemented in the SFA, the scan in the z-direction correspond to a displacement of the tip of about $44\ \mu m$.

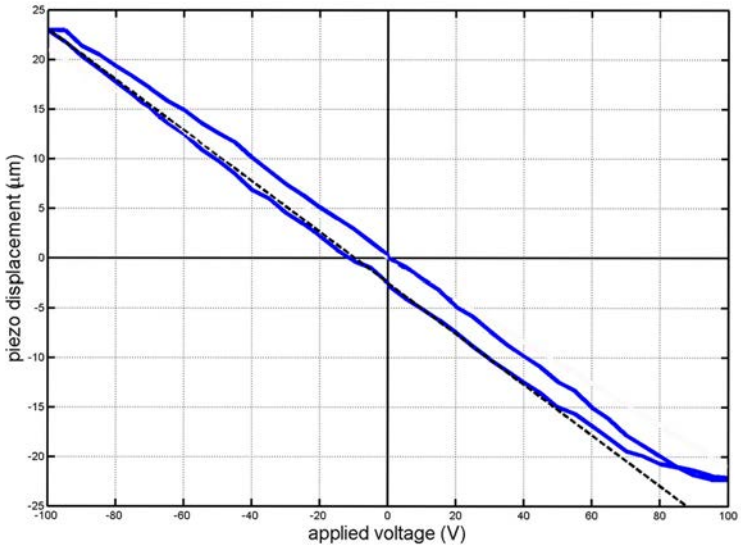

Figure 3.2. Calibration curve for the z-axis of the scanner is created.

3.2 Sensor calibration

3.2.1 Setup

Like the tube scanner, the piezoresitive cantilever had to be calibrated. No special set-up was required for that purpose. The SFA cantilever was placed into a commercial SFM (Multimode SFM with a Nanoscope III controller, Veeco, Santa Barbara, CA).

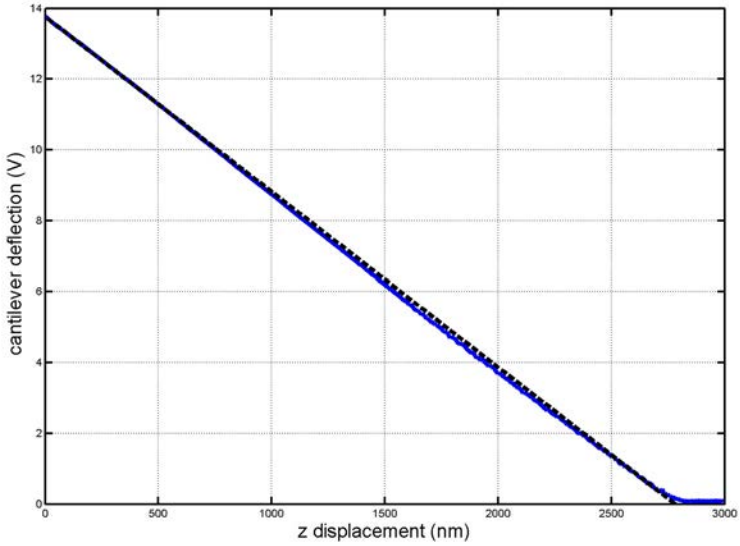

Figure 3.3. The piezoresitive cantilever was calibrated by recording a approach curve on a stainless steel disk. During this measurement, the scanning stage of the SFA was disabled and the indentation was performed by means of a calibrated piezoelectric tube. The load-displacement curve obtained was used for calibration.

3.2.2 Results

An approach curve (cf. Fig. 3.3) performed on a stainless steel sample was recorded using the SFA piezoresistive sensor combined with the piezoelectric tube of the Veeco Nanoscope. During this measurement, the scanning stage of the SFM was disabled. The slope of this curves was used to calibrated the data recorded with the Nanoscope software.

3.3 SFM tips

Stolz et al. [3] measured the biomechanical properties of articular cartilage at two different scales with an SFM. The dynamic elastic modulus obtained with a sharp pyramidal tip (radius $\sim$ 20 nm) was 100 times lower than those obtained with a spherical tip (radius $\sim$ 2.5 μm). This huge difference can be explain by the biphasic structure of cartilage. Collagen fibers have a diameter of about 50 nm and are spaced by several hundred of nanometers. At the nanometer scale, the sharp tip can penetrate between the fibers and then measure the stiffness of the ECM gel (fluid phase). At the micrometer scale, the spherical tip can't penetrate between the fibers and then measure their own stiffness (solid phase). Additional measurements performed on normal, diseased and enzymatically altered porcine cartilage demonstrated that early degradation of articular cartilage was only detectable at the nanometer scale while passed unnoticed at the micrometer scale.

To date, the interpretation of SFM indentation testing on biological samples are based on the Hertz model. This model was originally developed in 1881 by the German physicist Heinrich Rudolf Hertz [4, 5, 6]. The value of Young's modulus of the sample is given by

$$F = \frac{4}{3}\sqrt{R}Eh_f, \tag{3.1}$$

Where F is the total applied load, R the radius of the indenter, E the young's modulus and h_f the penetration depth.

The Hertz model which is often used to analyze indentation experiments under the assumption that the sample is large, homogeneous and isotropic, is not well appropriate in case of a nanometer scale pyramidal SFM tip. We have explore two different ways for microfabricating nanometer scale spherical tips.

3.3.1 Cantilevers with glued bead-tips

The first approach consisted of fabricating a cantilever having a hole in place of the tip and then to glue a small silicate bead inside. The fabrication steps of this kind of cantilevers (c.f. 3.4 and 3.5) consisted first to grown a 2 μm thick layer of thermal oxide on both sides of a quartz wafer. Then, the backside of the wafer was patterned by photolithography. 1.8 μm of oxide was removed by wet chemical etching in buffered hydrofluoric (BHF) acid. In the next step, the cantilever shape and a hole of 5 μm in diameter were patterned in the front of the wafer by a second photolithography. These structures were transferred into silicon oxide by wet etching in BHF. During this step, the remaining oxide on the backside was completely removed. In order to form a 5 μm silicon membrane, the wafer was anisotropically etched in potassium hydroxide (KOH) for 26 hours. During this etching, the remaining oxide layer on the top of the wafer was partially etched. A short wet etching in BHF was needed to completely removed this layer. A second KOH etching was needed to open the hole through the silicon membrane and to release the cantilever. A last BHF etching was performed to removed the remaining silicon oxide.

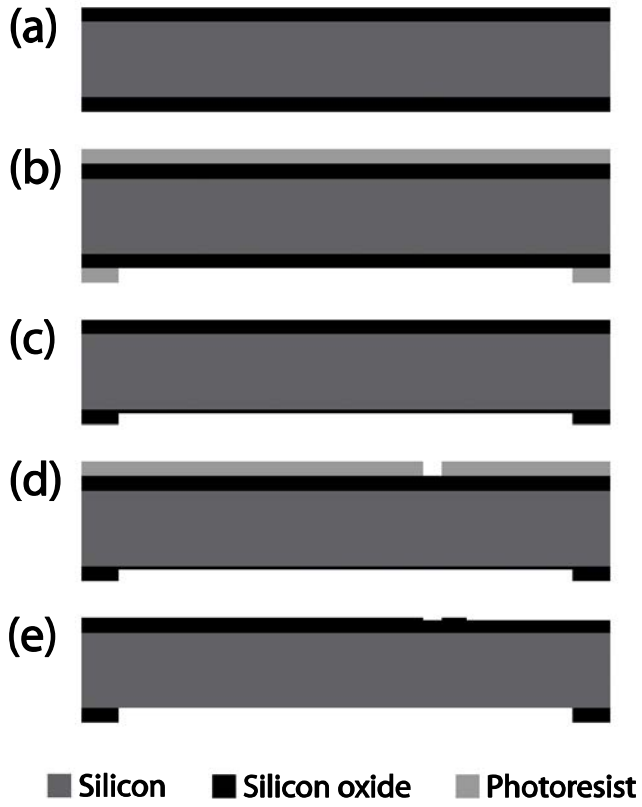

Figure 3.4. Cantilever with hole: fabrication process part I: **(a)** Thermal oxidation $(2\ \mu m)$ of a silicon wafer, **(b)** backside structuring with a photolithography, **(c)** $1.8\ \mu m$ of oxide removing by wet chemical etching in BHF, **(d)** Front side photolithography (cantilever and hole definition), **(e)** Oxide removing by wet chemical etching in BHF.

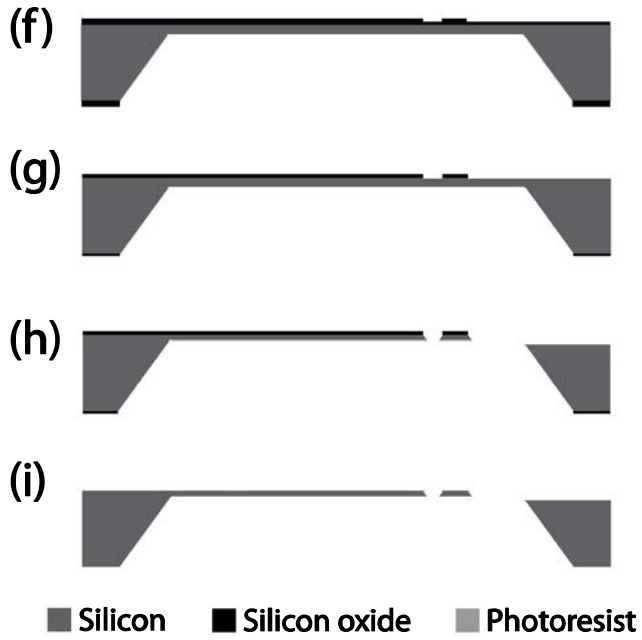

Figure 3.5. Cantilever with hole: fabrication process part II: **(f)** Membrane formation through anisotropic wet etching of the silicon in KOH, **(g)** Patterning of the cantilever and hole structure in BHF, **(h)** KOH etching of the silicon for cantilever release and hole opening, **(i)** Silicon oxide removing in BHF.

Once the cantilever fabricated, the next step was to glue a silicate bead into the hole. For that purpose, a home-made 3D micromanipulator allowed us to manipulate a glass micro pipette. The end of the micro pipette was dipped into a droplet of ultraviolet (UV) glue. Beads of 10 μm in diameter were placed on a silicon wafer. One of them was trapped at the end of the pipette and carefully placed into the cantilever hole. The small amount of glue transferred into the hole during this step was polymerized under UV light. The excess of glue was removed by placing the cantilever into an oxide plasma for several minutes. The exact duration of this step depends on the amount of glue in excess and must be defined for each cantilever. The procedure describes above was performed under a light microscope. Figure 3.6 shows SEM pictures of the final probes.

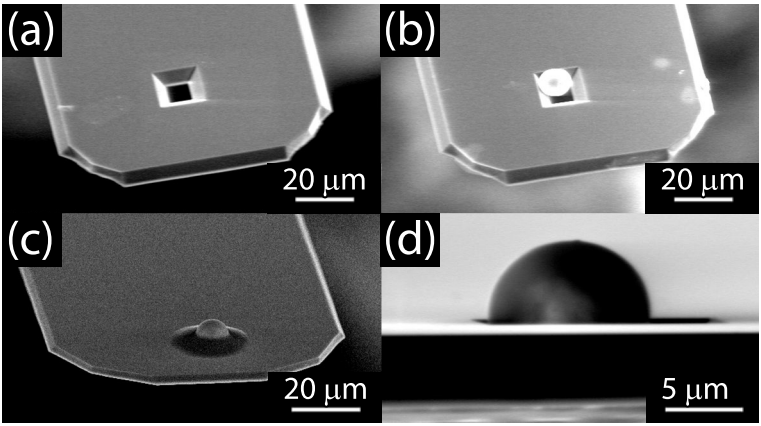

Figure 3.6. SEM pictures of SFM cantilevers with hole. **(a)** Cantilevers without bead. **(b)** cantilever with a bead in the hole, **(c)** cantilever with a bead glued into the hole, **(d)** side view of the cantilever and the bead.

3.3.2 Cantilevers with microfabricated bead-tips

The second approach consisted of creating a bead directly at the top of a standard SFM tip. To produce such a probe, a thin film of silicon dioxide (SiO_2) was deposited on the front side of a commercial SFM cantilever (Pointprobe, NanoWorld AG, Neuchâtel, CH) by atmospheric pressure chemical vapor deposition (APCVD) process. The SiO_2 film was formed by reacting silane (SiH_4) and oxygen at a temperature of 450˚C. The chemical reaction was :

$$SiH_4 + O_2 \rightarrow SiO_2 + 2H_2 \tag{3.2}$$

APCVD process is susceptible to gas phase reaction and step coverage is often poor. This non-conformal step coverage produce on each edges an accumulation of SiO_2. In the case of a sharp SFM tip, a bead was formed at its top. The bead diameter could be selected by varying the thickness of the SiO_2 film. Six different oxide thickness (30, 50, 70, 300, 500 and 1000 nm) were selected and deposited on cantilevers. The resulting tips (cf. Fig 3.7) showed a bead diameter ranging from $0.5\ \mu m$ for a nominal oxide thickness of 30 nm to $11.4\ \mu m$ for a nominal value of $1\ \mu m$. The characteristics (bead diameter, spring constant, resonance frequency and Q factor) of these tips are shown in table 3.1. The deposition rate of oxide can be reduced by changing the dilution of gases. Oxide thickness smaller than 30 nm have been obtained. Figure 3.8) shows a transmission electron microscope (TEM) image of a tip. This picture clearly shows a silicon tip covered by an oxide layer.

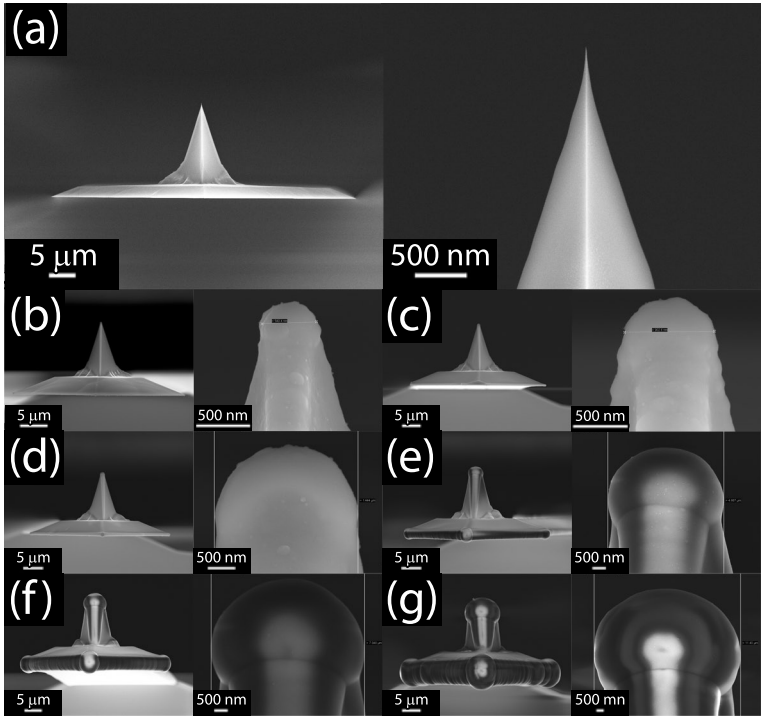

Figure 3.7. SEM pictures of cantilevers with APCVD beads. **(a)** Commercial SFM tips (Pointprobe, NanoWorld AG, Neuchâtel, CH) before oxide deposition. **(b)-(g)** Same cantilevers after oxide deposition. The diameter of the beads is proportional to the thickness of the oxide. The characteristics of these tips are detailed in table 3.1.

Tip nb	Oxide thick. (nm)	Spring constant k_{sader} (N/m)	$k_{cleveland}$ (N/m)	Res. freq. (kHz)	Q factor	Bead dia. (μm)
(b)	30	31.6	29.2	241	593	0.55
(c)	50	18.2	18.9	213	428	0.90
(d)	70	19.0	17.4	196	484	1.44
(e)	300	17.7	16.0	183	470	4.67
(f)	500	19.3	13.0	176	558	7.04
(g)	1000	14.4	24.7	212	285	11.4

Table 3.1: Comparison of the APCVD beads characteristics in function of the oxide thickness. A SEM picture for each tip was taken (cf. Fig. 3.7).

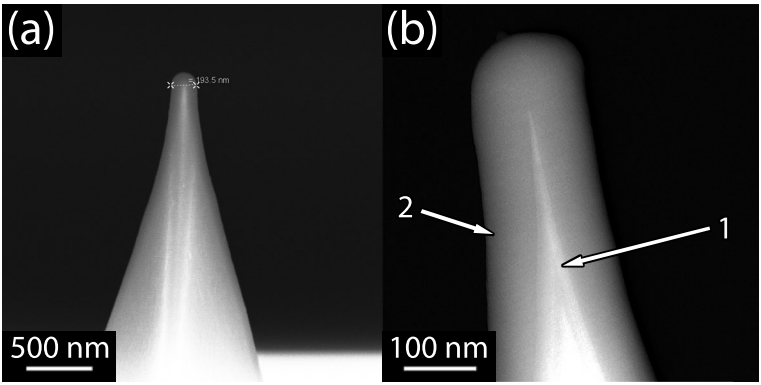

Figure 3.8. **(a)** SEM and **(b)** TEM pictures of an APCVD tip. A bead diameter of 193.5 nm was obtained by deposing an oxide layer of 100 nm. The TEM picture clearly shows the interface between the sharp silicon tip (1) and the oxide layer (2).

3.4 Data analysis

Stiffness is the mechanical parameter that describes the resistance of an elastic material to a nondestructive load. This parameter is very sensitive to the internal structure of the tested material, therefore it is the key parameter to evaluate cartilage's state of health. Stolz et al. [3] developed a method, called indentation-type atomic force microscopy (IT AFM), for measuring cartilage stiffness at the nanometer scale. In this method, an SFM cantilever was used as nanoindenter to record cyclic load-displacement curves at different sites of the sample (cf. Fig. 3.9). The dynamic elastic modulus $|E^*|$ was computed from these curves according to a modeling method proposed by Oliver and Pharr in 1992 [7]. In this approach, the upper part of unloading curves was fitted by a simple power-law equation such as

$$p = B(h - h_f)^m \tag{3.3}$$

where p is the indenter load, h is the vertical displacement of the indenter, h_f represents the final unloading depth, and B and m are fitting parameters. For pyramidal tip geometry $m = 2$ [8].

The unloading stiffness could then be determined by using

$$S = \frac{dP}{dh} = mB(h - h_f)^{m-1}, \tag{3.4}$$

Finally, it was assumed that the dynamic elastic modulus $|E^*|$ was proportional to the reduced modulus of elasticity E_r provided by the Hertz model [4, 5, 6].

$$\begin{aligned} |E^*| &\approx E_r \\ |E^*| &= \frac{\sqrt{\pi}}{2}(1 - \nu^2)\frac{S}{\sqrt{A}} \end{aligned} \tag{3.5}$$

where ν is Poisson's ratio, S the contact stiffness, and A an area function related to the effective cross section of the indenter.

As shown in Chapter 1, articular cartilage exhibits different types of stiffness depending on the rate and the duration of the applied load. In case of short and cyclic loads, the elastic modulus depends of the loading frequency. For that reason, the cyclic rate employed during measurement should reflect the loading rate of normal ambulation. For articular cartilage this rate corresponds to a vertical displacement frequency of 3 Hz [9].

In IT AFM measurements of soft biological materials, the lower part of load-displacement curves are often subject to interactions between the tip and the sample such as electrostatic interactions or adhesion forces. In order to minimize these effects, only the upper 75% of the unloading curves were considered during the calculation of the dynamic elastic modulus $|E^*|$.

During data analysis, the precise localization of the initial point of contact between the tip and the sample is certainly the most difficult problem. The irregular surface and the low stiffness of the samples explain the lack of abrupt increase in load that usually marks the point of contact between the tip and the sample. This problem can be solved by calibrating the instrument on a reference material like Agarose gel just before measuring. The disadvantage of this technique is that the calibration curve obtained is valid only for exactly the same set of parameters. Every time a parameter changes, a new calibration curve must be determined.

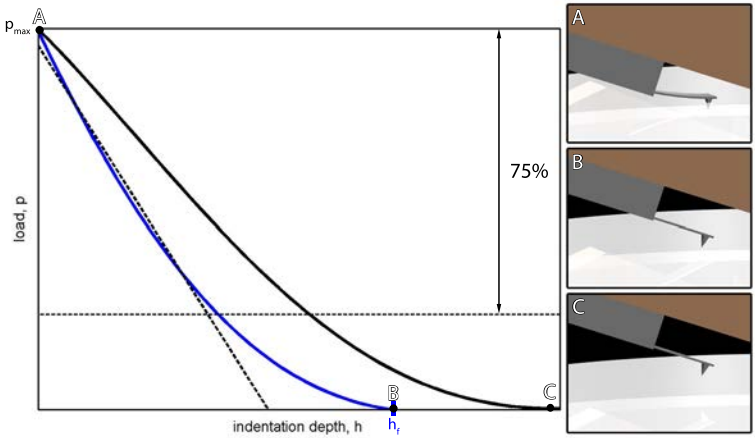

Figure 3.9. Schematic load-indentation curve representing a complete cycle of loading (black curve) and unloading (blue curve). During the loading phase, the cantilever is slowly approached to the surface. Close to the surface, the tip is suddenly attracted by the sample (van der Waals interactions) and enter in contact with it. Then the cantilever is bent upwards. During the unloading phase, the cantilever is gradually withdraw from the surface (A). Due to adhesion forces, the cantilever bend in the opposite direction (B) until it suddenly loses the contact (C). p_{max} is the maximum applied load at the maximal indentation depth, h_{max}. In IT AFM measurements with a sharp pyramidal tip, only the upper 75% of the unloading curve is used for calculating of the stiffness S.

Bibliography

[1] Rostislav V. Lapshin. Analytical model for the approximation of hysteresis loop and its application to the scanning tunneling microscope. *Rev. Sci. Instrum.*, 66(9):4718–4730, September 1995.

[2] M. M. Pfeffer. *Conception and realization of a compact scanning near-field optical microscope.* PhD thesis, Ecole polytechnique fédérale de Lausanne (EPFL), 1998.

[3] M. Stolz, R. Raiteri, A. U. Daniels, M. R. VanLandingham, W. Baschong, and U. Aebi. Dynamic elastic modulus of porcine articular cartilage determined at two different levels of tissue organization by indentation-type atomic force microscopy. *Biophysical Journal*, 86(5):3269–3283, May 2004.

[4] H. Hertz. Uber die Beruhrung fester elastischer Korper. *Journal fur die reine und angewandte Mathematik*, 92:156–171, 1882.

[5] Atsushi Ikai. *The World of Nano-Biomechanics: Mechanical Imaging and Measurement by Atomic Force Microscopy*. Elsevier Science, Nov. 2007.

[6] JJ Vlassak, M. Ciavarella, JR Barber, and X. Wang. The indentation modulus of elastically anisotropic materials for indenters of arbitrary shape. *Journal of the Mechanics and Physics of Solids*, 51(9):1701–1721, 2003.

[7] WC Oliver and GM Pharr. An Improved Technique for Determining Hardness and Elastic Modulus Using Load and Displacement Sensing Indentation Experiments. *Journal of Materials Research*, 7(6):1564–1583, 1992.

[8] MR Vanlandingham, SH McKnight, GR Palmese, RF Eduljee, JW Gillespie, and J.R.R.L. McCulough. Relating elastic modulus to indentation response using atomic force microscopy. *Journal of Materials Science Letters*, 16(2):117–119, 1997.

[9] D.E.T. Shepherd and B.B. Seedhom. A technique for measuring the compressive modulus of articular cartilage under physiological loading rates with preliminary results. *Proceedings of the Institution of Mechanical Engineers, Part H: Journal of Engineering in Medicine*, 211(2):155–165, 1997.

Chapter 4

Instrumental experimentation

4.1 Preliminary tests

4.1.1 Knee model

A to-scale breadboard model of the instrument, slightly different from those described in Chapter 2, was used to perform indentation testing inside a flexible, anatomic knee model. The main goal of this first experiment was to assess, *in-situ*, the quality of the stabilization and the accuracy of the positioning. As shown in figure 4.1, the SFM chip, was glued on a PCB which was soldered at the end of the scanning stage. A simple sleeve of stainless steel was used as handle. The electronic components used to measure the deflection of the cantilever were located in a separated box, connected to the instrument by several meters of cables. Finally, the eight syringe-pushers required to inflate the balloons were actuated by hand.

The plastic knee model (cf. Fig. 4.2) used for this experiment included the femur, the tibia, the fibula, and some ligaments. However, several elements, like muscles, patella, fat pad or even skin were missing.

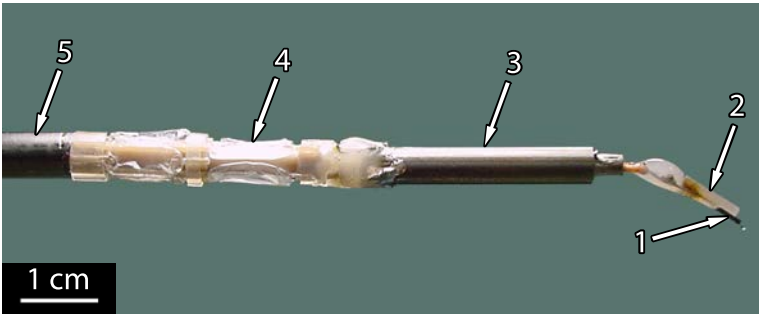

Figure 4.1. Side view of the bread-board model used during preliminary tests. The indentation stage consisted of an SFM chip (1) glued on a PCB (2) and soldered at the end of the scanning stage (3). The stabilization stage was formed by eight angioplasty balloons (4). A sleeve of stainless steel was used as handle (5).

These elements were essential during the stabilization of the instrument. Thus, in order to mimic the cavity naturally formed by these elements, a polyvinyl chloride (PVC) tube was added between the lateral femoral condyle and the tibial plateau on the left side of the model (cf. Fig. 4.3). Before inserting the instrument into the knee model, the surfaces of the bones were visually inspected and a zone for the measurements was selected. Considering the relative accessibility of this zone, the use of protection for the tool tip during the insertion was not required. The instrument was directly inserted into the PVC tube from the lateral side of the knee. The eight balloons were simultaneously inflated to wedge the SFA. Then, the SFM cantilever was slowly moved towards to the knee surface by changing the pressure in the balloons. Finally, a 1 Hz sine wave with an amplitude of 125 V was applied to the z-axis of the piezoelectric tube to perform the indentation testing.

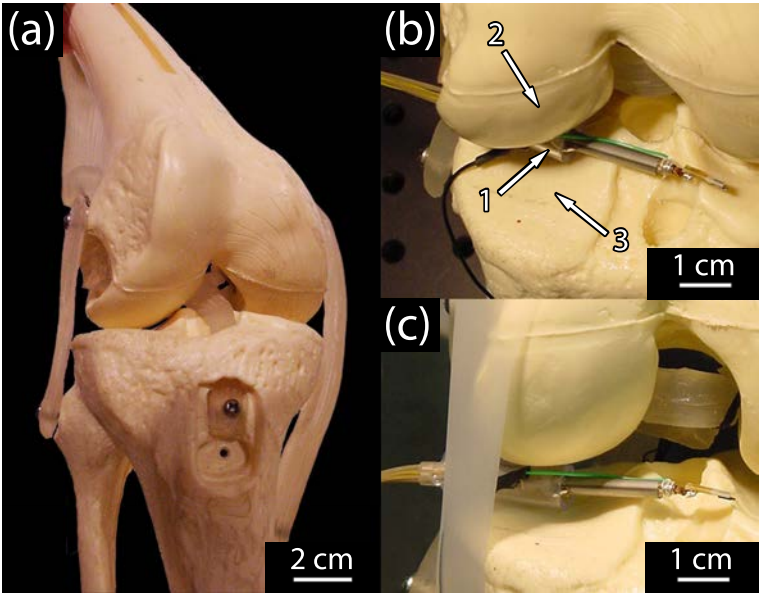

Figure 4.2. Description of the setup used during preliminary tests. **(a)** A plastic knee model including the tibia, the femur, the fibula, the collateral and the cruciate ligaments was used as test sample. **(b)** During measurements, the instrument was stabilized in a PVC tube (1) placed between the femoral condyle (2) and the tibia plateau (3). This tube simulated the knee cavity naturally formed by the bones, the muscles and the skin. **(c)** Side view of the instrument after performing the coarse approach by means of the stabilization stage.

Several load-displacement curves were recorded on the tibial plateau of the knee model. Each one consisted of an average over 5 consecutive indentation cycles. Figure 4.3 shows an example of measurements obtained in this way.

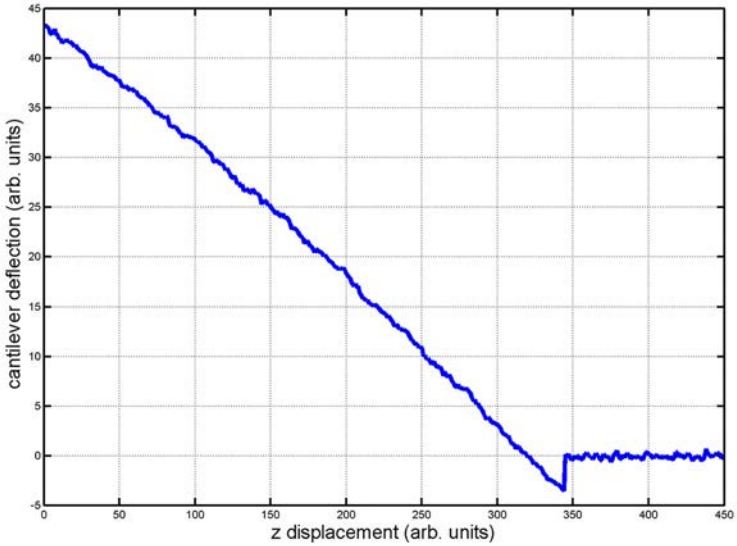

Figure 4.3. Averaged load-displacement curve based on 5 loading/unloading cycles taken at a frequency of 1 Hz during indentation testing inside a plastic knee model.

4.1.2 Pig's ankle

Due to their availability and proximity in size to humans, pigs articulations are widely used for modeling human joints. Therefore, and in order to validate the instrument under conditions similar to those found during surgery, a series of measurements were performed inside a pig's ankle.

The instrument used for this experiment was comparable to the one used before. The major improvement concerned the indentation stage, where the SFM probe was mounted on a tip connector. This connector improved the reliability of the instrument and allowed a quick exchange of the cantilever in case of failure.

The lower leg of a sacrificed pig was obtained from a slaughter house (cf. Fig. 4.4 (a)). A large opening was performed on the top of the ankle. The joint was optically inspected and a measurement area was selected. The instrument was delicately inserted, positioned and wedged into the joint cavity. The space available for stabilizing the instrument is considerably smaller in a pig's ankle that in a human knee joint; consequently only the first stack of balloons could be used for stabilization during these measurements (cf. Fig. 4.4 (b)). The coarse approach was performed by means of the pneumatic system, and a 10 Hz sine wave with an amplitude of 125 V was applied to the z-axis of the piezoelectric tube to perform the indentation testing.

Several load-displacement curves were recorded from the top of the pig's ankle. Each one consisted of an average over 5 consecutive indentation cycles. Figure 4.5 shows an example of the results obtained during these experiments.

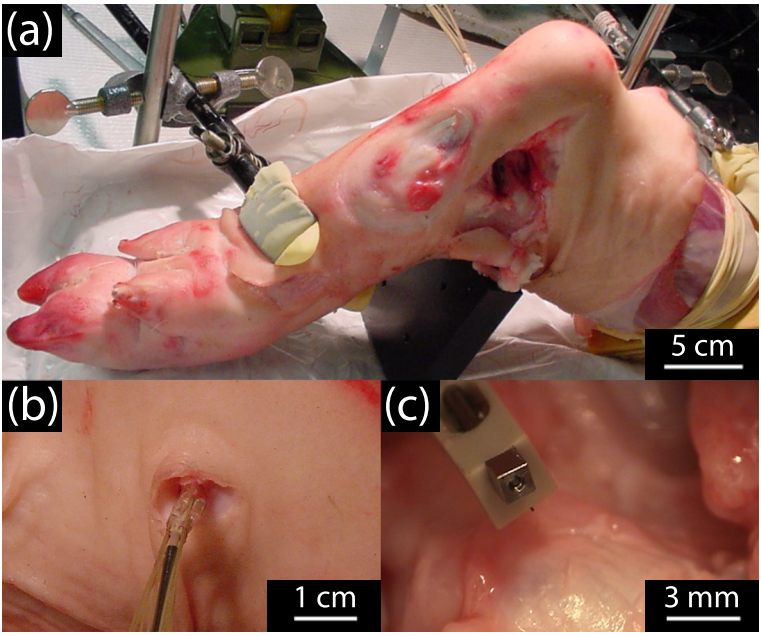

Figure 4.4. Description of the setup used during measurements inside the pig's ankle. **(a)** The lower leg of a pig was fixed by two clamps on the measuring table. **(b)** Due to the small dimensions of the pig's ankle, only the first set of balloons could be used for the stabilization of the instrument. The second one was outside of the knee during all the measurements. **(c)** A large opening performed on the top of the ankle allowed to have a good visualization of the instrument during the measurements.

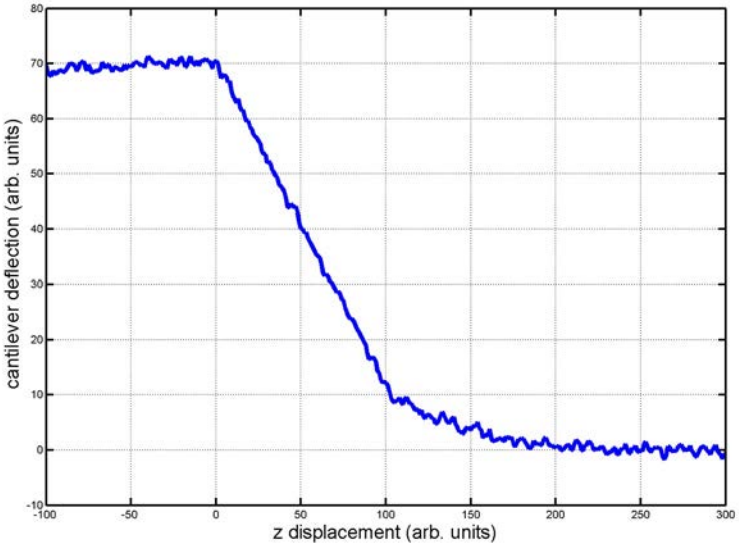

Figure 4.5. Averaged load-displacement curve based on 5 loading/unloading cycles taken at a frequency of 2 Hz during indentation testing in a pig's ankle.

4.2 In-situ measurements

4.2.1 Open knee surgery

The first measurements inside a human knee joint were recorded with the SFA inside the knee of a cadaver during a simulated open knee surgery. The main goal of this experiment was to determine which part of an injured knee could be probed by our instrument.

A new version of SFA (SFA v.1) was specially design for this experiment (cf. Fig. 4.6). This first fully functional prototype of the instrument comprised five different components: a handle to which a shaft was fixed. At the end of this shaft, the stabilization stage, the scanning stage and the indentation stage were used to produce the indentation.

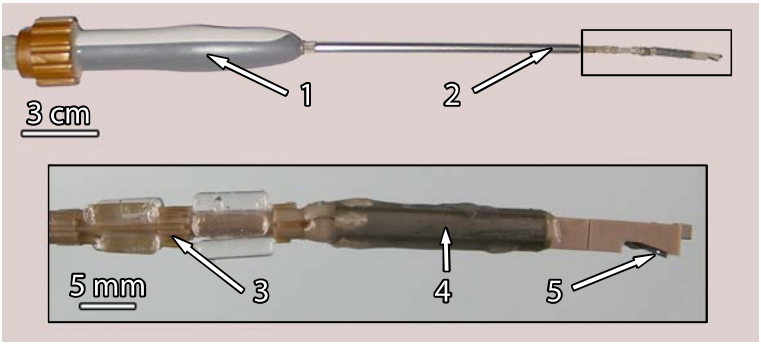

Figure 4.6. Picture of the SFA v.1. The handle (1) facilitated the manipulation of the instrument. The electrical and pneumatic connections were embedded in the rigid shaft (2). The inset exhibits a magnified image of the distal end of the instrument containing from left to right, the stabilization stage (3), the tube scanner (4) and the SFM sensor (5).

The pneumatic system was automated. An electronic box and a dedicated computer program controlled the inflation and the deflation of the balloons.

These measurements were carried out in the left knee of a human cadaver (cf. Fig. 4.7). A small opening was created into the knee in order to grant access for the instrument. A larger opening performed on the opposite side allowed visualizing the inside of the joint. The knee was first optically inspected and a measurement area was selected. Then, the SFA was inserted, positioned, and stabilized. During this phase, a stainless steel sleeve protected the distal end of the instrument. Finally, the sleeve was pulled back and a 2 Hz sine wave with an amplitude of 125 V was applied to the z-axis of the piezoelectric tube to perform the indentation testing.

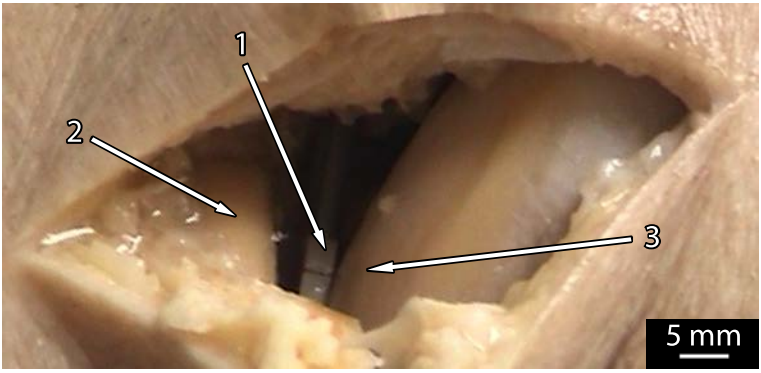

Figure 4.7. Picture of the SFA during an open knee surgery in a human cadaver. The large opening performed along the knee, simplify the positioning the instrument (1). During the measurements, the distal end of the SFA was wedged between the tibial plateau (2) and the femoral condyle (3).

Several load-displacement curves were recorded inside this human knee cadaver. Each one consisted of an average over 5 consecutive indentation cycles. Figure 4.8 shows an example of the measurements obtained during the open knee surgery. This experiment constituted the first step towards *in-situ* cartilage stiffness measurement.

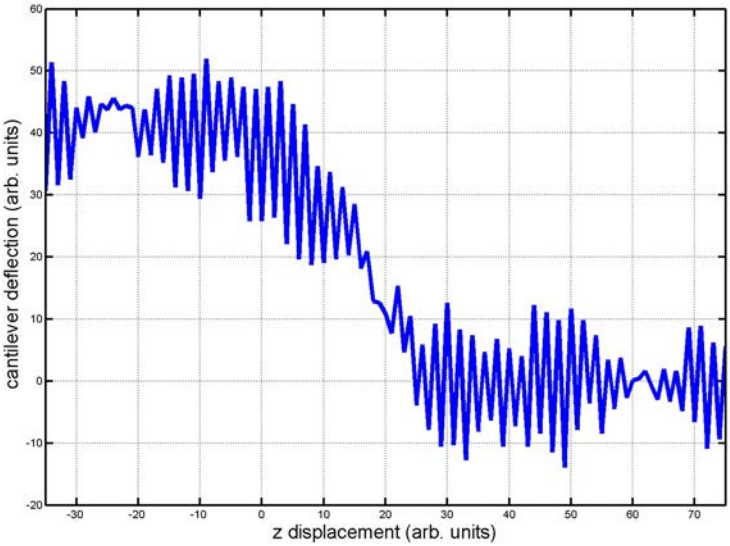

Figure 4.8. Averaged load-displacement curve based on 5 loading/unloading cycles taken during an open knee surgery of a human knee cadaver at a frequency of 2 Hz.

4.2.2 Arthroscopic surgery

The next step after having successfully recorded load-displacement curves during an open knee surgery, was to record load-displacement curves during a standard arthroscopy. New measurements were carried out in the right knee of a human cadaver with the same SFA v.1 (cf. Fig. 4.6).

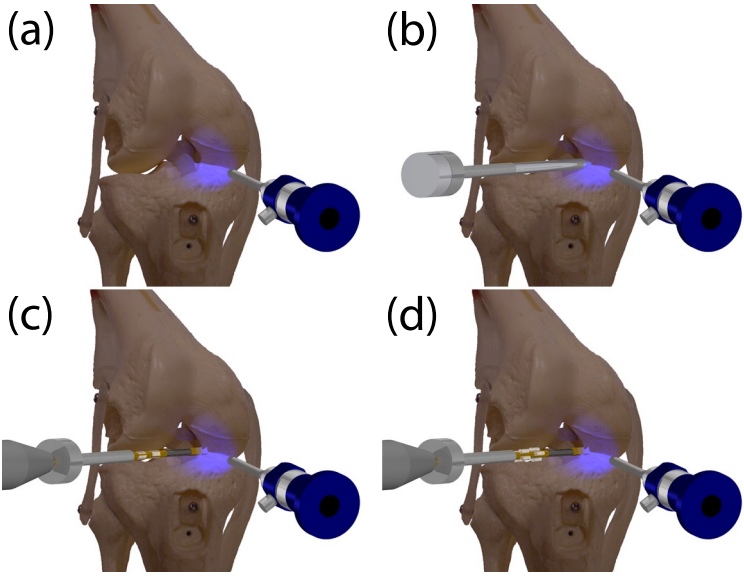

Figure 4.9. Description of the procedure employed for safely positioning and stabilizing the SFA in a joint: **(a)** Visual inspection of the knee by means of an optical arthroscope. **(b)** Creation of an entry access for the instrument. **(c)** Insertion of the SFA. **(d)** Positioning and stabilization of the instrument by inflating the balloons.

Due to the very limited dimension of the knee cavity and the constant flow of liquid commonly used to wash the knee during arthroscopy, a special procedure was defined to protect the instrument during its insertion. First, the knee was visually inspected by means of an optical arthroscope for identifying potential defects in the cartilage (cf. Fig. 4.9 (a)). Then, an access for the instrument was created at a classic arthroscopy entrance by inserting a cannula sealed by a trocar. The optical arthroscope was used to guide the final positioning of this cannula near an area of interest (cf. Fig. 4.9 (b)). The trocar inside the cannula was replaced by the SFA (cf. Fig. 4.9 (c)). Once positioned, the instrument was stabilized by means of the balloons and the coarse approach was performed (cf. Fig. 4.9 (d)).

During the whole procedure, the surgeon maintained the optical control with its instrument by means of the arthroscope (cf. Fig. 4.10). Finally, a 1 Hz sine wave with an amplitude of 125 V was applied to the z-axis of the piezoelectric tube to perform the indentation testing. During these measurements, the knee joint was continually flushed with Ringer's solution (wet conditions) or inflated with CO_2 (dry conditions).

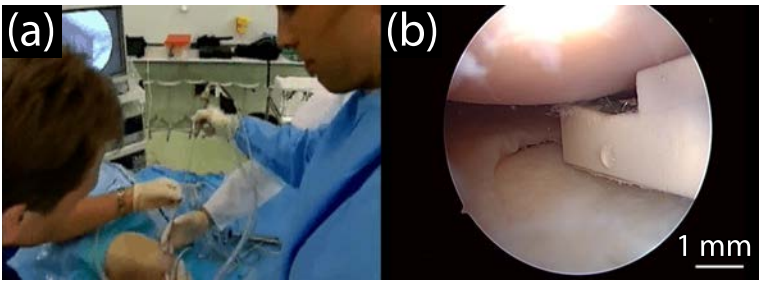

Figure 4.10. **(a)** Insertion of the SFA inside the knee joint. During the whole procedure, the surgeon had a optical view **(b)** of the inner knee by means of the arthroscope.

Load-displacements curves were recorded under both conditions. Each curve consisted of an average over 5 consecutive indentation cycles. Figure 4.11 shows an example of the results obtained during these experiments.

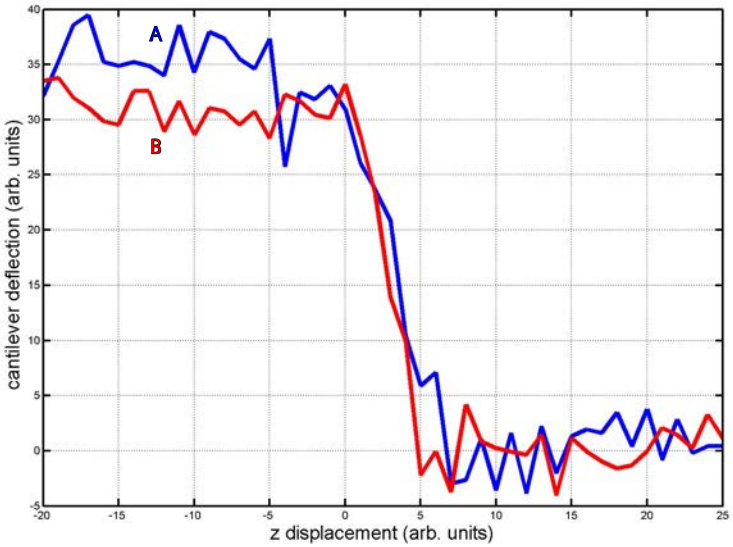

Figure 4.11. Averaged unloading curves based on 5 loading/unloading cycles taken during an arthroscopy procedure at a frequency of 1 Hz. During the measurements, the joint was flushed by a physiological solution (A) and by CO_2 (B).

4.3 Calibrated measurements

4.3.1 Introduction

A new prototype for the SFA, the SFA v.2 (cf. Fig 2.1), was designed based on the unique experience obtained during non-calibrated measurements. The purpose of this instrument was performing also quantitative analysis. The distance between the deflection sensor and the amplifier was reduced by implementing the electronics directly inside a new handle. The distal end of the instrument was cover by a thin layer of parylene to provide a high quality electrical insulation of the tube scanner. The cantilever and the tube scanner were calibrated following the procedure describe in Chapter 3. The figure 4.12 shows the setup used during measurements with the SFA v.2. The handel of the instrument was maintained during the whole experiment by a clamp. The distal end of the SFA was fixed in a PVC tube which simulate the body cavity. In order to facilitate the fine positioning of the instrument, this tube was mounted on a 3-axis stage.The sample was was placed inside a vat which allowed to keeping it wet.

4.3.2 Knee model

The first experiment was performed on the plastic femoral condyle of the previously used knee model. The model was placed upside down into the vat. The SFA was inserted and stabilized in the PVC tube. The approach was performed by means of the pneumatic system and the 3-axis scanning-stage. Finally, a 3 Hz sine wave with an amplitude of 125 V was applied to the z-axis of the piezoelectric tube to perform the indentation testing. Several load-displacement curves were recorded on that model femoral condyle. Each one consisted of an average of 5 consecutive indentation cycles. Figure 4.13 shows an example of the measurements thus obtained.

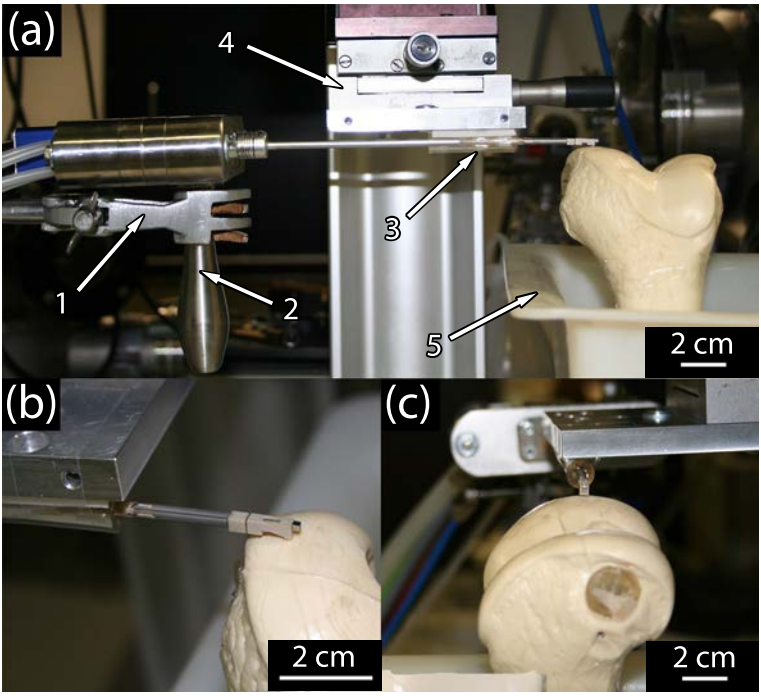

Figure 4.12. Picture of the setup used during calibrated measurements. **(a)** The handel of the instrument (2) was maintained by a clamp (1), whereas its distal end is stabilized inside a PVC tube (3). A three-axis stage (4) facilitated the fine positioning of the tool. A vat (5) allowed keeping the sample wet during the measurements. **(b)** Lateral view and **(c)** front view of the instrument. The coarse approach was performed by using the stabilization stage in combination with the 3-axis stage.

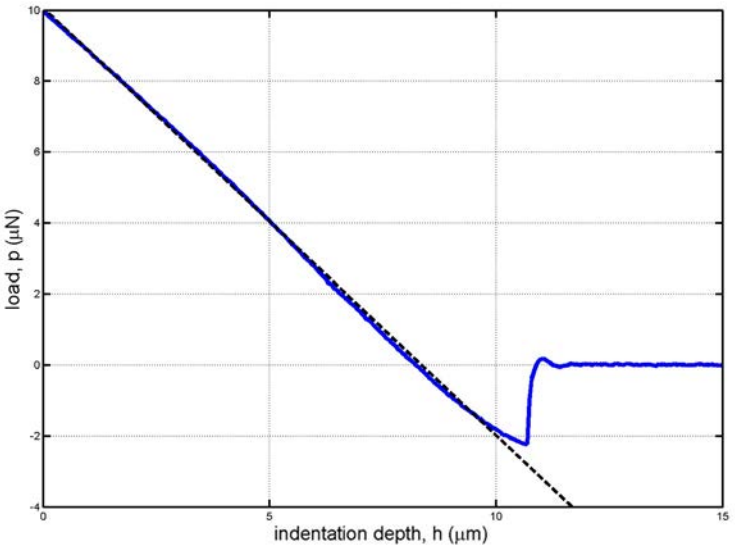

Figure 4.13. Averaged unloading curves based on 5 loading/unloading cycles taken on a plastic knee model at a frequency of 3 Hz. The resulting value of the dynamic elastic modulus was of 2 GPa.

4.3.3 Agarose gel

Due to agarose gel is widely used as a place-holder for soft material, its mechanical properties has been widely studied in the scientific literature and are now well established [1]. The main goal of this experiment was to validate SFA measurements by comparing the obtained results with the dynamic elastic modulus $|E^*|$ of agarose gel found in literature [1, 2]. Gels with 0.75%, 2.0%, 2.5% and 3.0% weight / weight agarose in deionized (DI) water were prepared. The solution was heated to 90^oC and mixed for 10 minutes by means of a magnetic stirrer. O'rings (inner ring diameter = 4 mm; outer ring diameter = 8 mm; thickness = 2 mm) were glued onto stainless steel disks (diameter = 10 mm). A droplet of the melted gel was deposited in the center of the o'ring and allowed to cool to ambient temperature. Once the gel solidified, the whole sample was immersed in DI water to avoid dehydration. The samples were fixed under the SFA using the setup previously described (cf. Fig. 4.14).

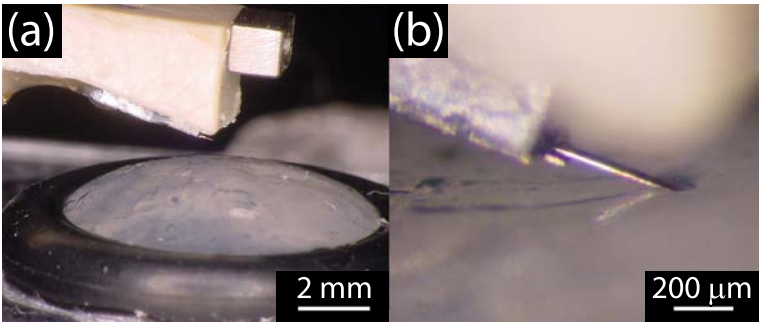

Figure 4.14. **(a)** Picture of the setup used during measurements on different agarose gel's concentrations. A droplet of melted gel was deposited in the center of a o'ring and solidified. **(b)** Zoom in on the SFM cantilever during indentation.

Finally, a 3 Hz sine wave with an amplitude of 125 V was applied to the z-axis of the piezoelectric tube to perform the indentation testing. Several load-displacement curves were recorded on agarose gel of different concentrations. Each one consisted of an average over 5 consecutive indentation cycles. Figure 4.15 shows an example of measurements obtained on gel with an agarose concentration of 0.75% (A), 2.0% (B), 2.5% (C) and 3.0% (D), respectively.

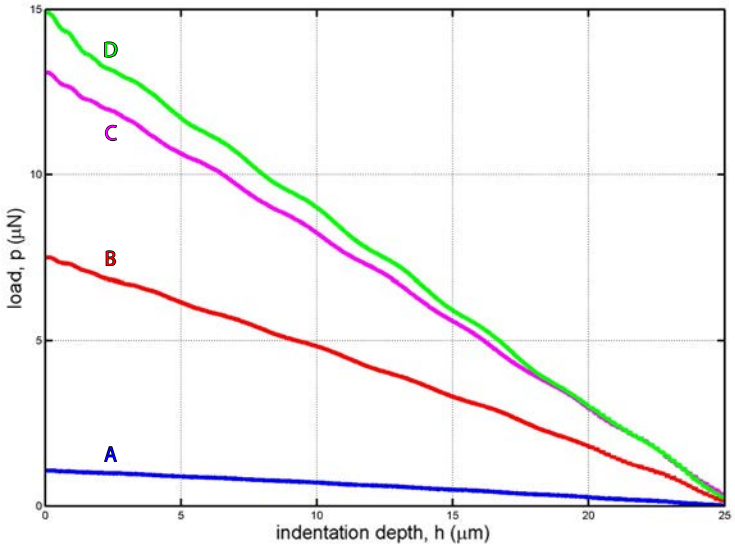

Figure 4.15. Averaged unloading curves based on 5 loading/unloading cycles taken at a frequency of 3 Hz on different concentrations of agarose gel. The resulting values of the dynamic elastic modulus were of 1 kPa for a 0.75% agarose gel (A), 10.3 kPa for a 2% (B), 28.4 kPa for a 2.5% (C) and 39.8 kPa for 3% (D).

4.3.4 Pig's knee

The last set of measurements was performed on pig's cartilage samples. The lower leg of a sacrificed pig was obtained from a slaughter house. The femur, the tibia and the patella were delicately extracted and stored in Phosphate Buffered Saline (PBS) solution until testing (2.6 mM NaH_2PO$_4$, 3 mM Na_2HPO_4, 155 mM NaCl, 0.01% NaN_3 w/v, pH 7.0).

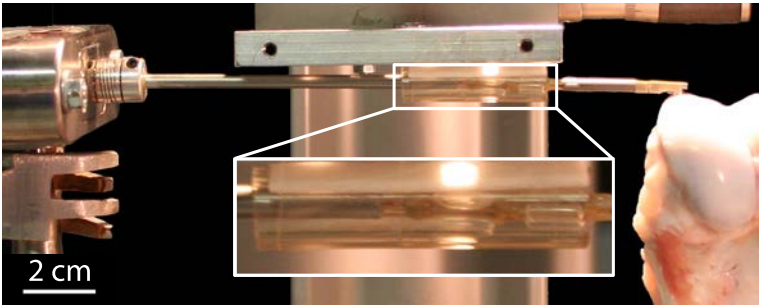

Figure 4.16. Picture of the setup used during measurements on pig's cartilage. The inset exhibits a magnified image of the stabilization stage.

During measurement DI water was regularly flushed over to the sample to keep the cartilage hydrated. A 3 Hz sine wave with an amplitude of 125 V was applied to the z-axis of the piezoelectric tube to perform the indentation testing. Several load-displacement curves were recorded on each sample. Each measurement consisted of an average over 5 consecutive indentation cycles. Figure 4.17 shows an example of measurements on the femur, figure 4.18 on the tibia and figure 4.19 on the patella.

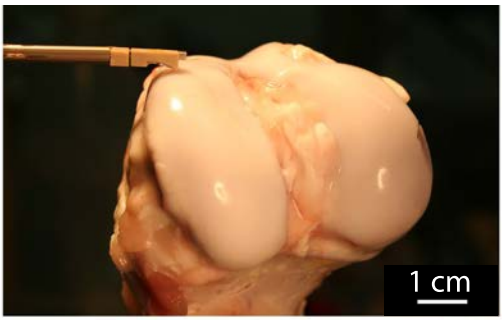

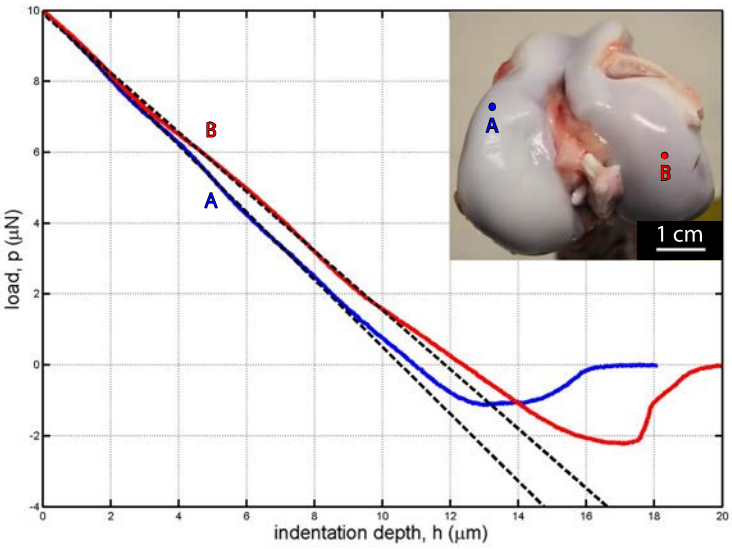

Figure 4.17. Load-displacement curves recorded on two different sites of a pig's femur. The resulting values of the dynamic elastic modulus were of 0.391 MPa (A) and 0.128 MPa (B).

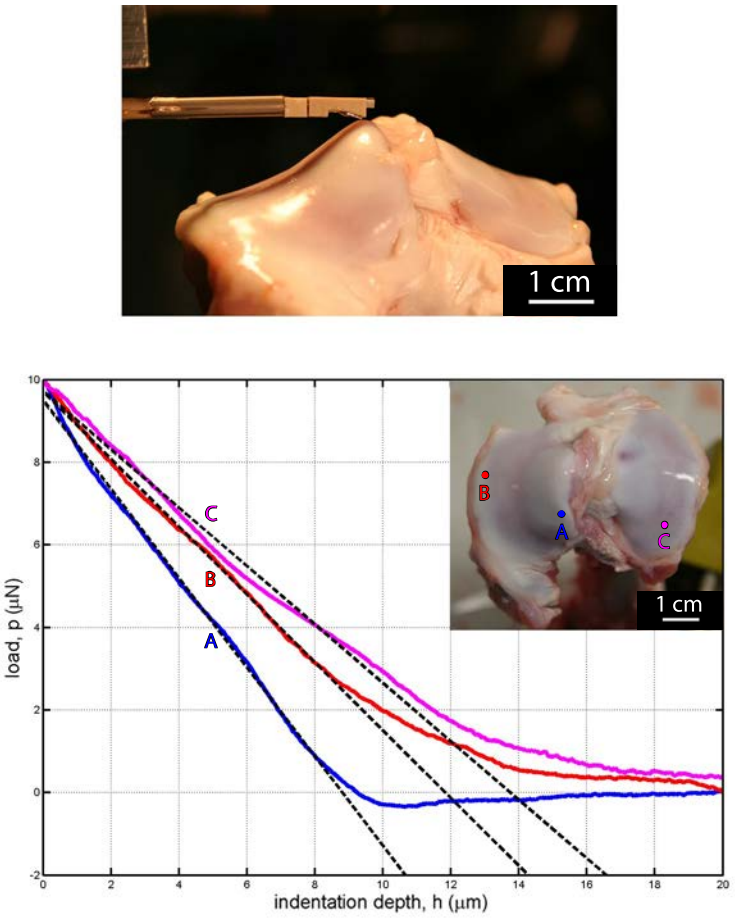

Figure 4.18. Load-displacement curves recorded on three different sites of a pig's tibia. The resulting values of the dynamic elastic modulus were of 0.289 MPa (A), 0.093 MPa (B) and 0.052 MPa (C).

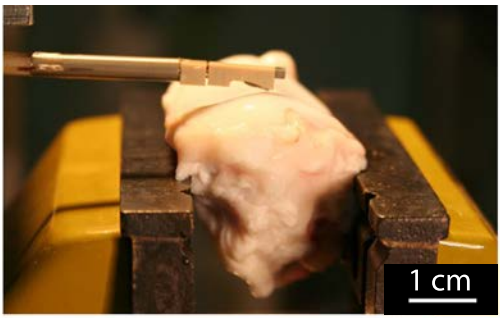

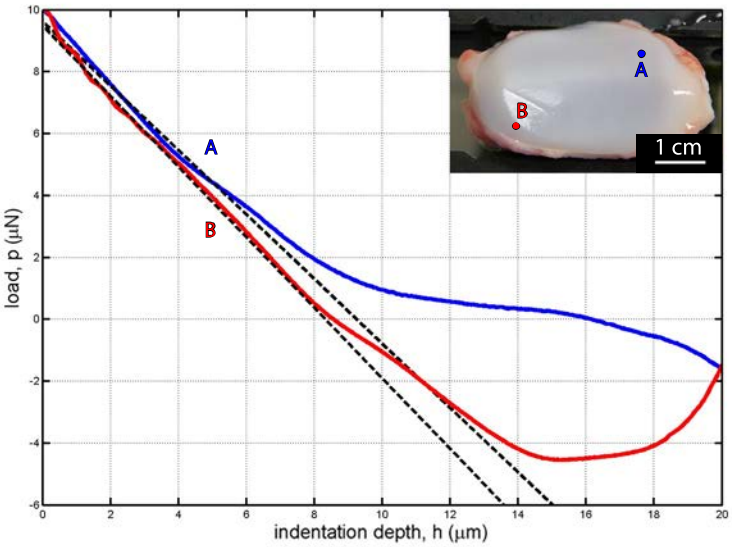

Figure 4.19. Load-displacement curves recorded on two different sites of a pig's patella. The resulting values of the dynamic elastic modulus were of 0.557 MPa (A), 0.174 MPa (B).

4.4 Data analysis

Qualitatively, the measurements recorded inside the knee phantom (figure 4.3) and the pig's leg (figure 4.5) showed the expected characteristics. The typical snap out of contact present during measurements in air could be observed in the knee phantom but not in the pig's joint because the environmental conditions were different. The main goal of these preliminary tests was to validate the concept of the tool and in particular to assess the quality of the stabilization. The signal-to-noise ratio (SNR), which refers to the quality of a signal relative to its noise, is a good indication about the quality of the instrument stabilization. The SNR is defined as

$$SNR = \frac{P_{signal}}{P_{noise}} = \left(\frac{A_{signal}}{A_{noise}}\right)^2 \tag{4.1}$$

where P_{signal} is the signal power, P_{noise} the noise power, A_{signal} is the root mean square (RMS) amplitude of the signal and A_{noise} is the RMS amplitude of the noise.

SNR is usually expressed in the logarithmic decibel scale.

$$SNR(dB) = 10log_{10}\left(\frac{P_{signal}}{P_{noise}}\right) = 20log_{10}\left(\frac{A_{signal}}{A_{noise}}\right) \tag{4.2}$$

The SNR was about 28.63 dB on the knee phantom and about 24.86 dB for the pig's ankle. As expected, a comparison between the slope of these unloading curves showed a higher values for the plastic material. However, these values must be considered with care, because the instruments used for these two measurements were different. A complete quantitative analysis would had require the calibration of the piezoelectric tube and of the piezoresistive cantilever.

The open knee surgery experiments aimed to proof the design of the instrument and more particularly to establish which area inside a human knee joint can be accessed with the SFA. In fact, not all of the knee cartilage is subjected to OA. The most often affected areas are located where bones enter in contact during loads or shock, i.e. the top of the femoral condyles, the tibial plateau, and the back of the patella. During the experiment, an arthroscopist tries to reach, one by one, all the relevant area in the knee. This has allowed to highlight some limitations of the tool. Indeed, a small number of areas, particularly near the center of the articulation, remained inaccessible. This was mainly due to the relatively long distance between the beginning of the stabilization stage and the end of the tool. The problem could be solved by reducing the size of the tube scanner. The signal recorded during the open knee surgery (cf. Fig. 4.8) was strongly compromised by 50 Hz noise, which most likely was induced by an external source. This source could not be identified, but did not reappear on further measurements. But even then, the measurements carried out with the arthroscopic SFM suffered from a high level of noise. Even though the environmental conditions could partially explain this noise, further design modifications like shortening the distance between sensor-chip and amplifier were imposed and may further improve the resolution of force measurements of the instrument.

The indentation testing recorded with the SFA during the arthroscopic procedure constituted the first measurements ever performed with an SFM inside a human knee joint. Despite the limited dimensions of the knee cavity and the constant flow of fluid used to wash the knee, the instrument was able to safely approach the cartilage surface and record load-displacement curves (cf. Fig. 4.11) under wet conditions (Ringer'solution) and under dry conditions (CO_2). During this experiment, it appeared that despite the establishment of a "safe-insertion procedure" (cf. Fig. 4.9), the positioning of the instrument inside the

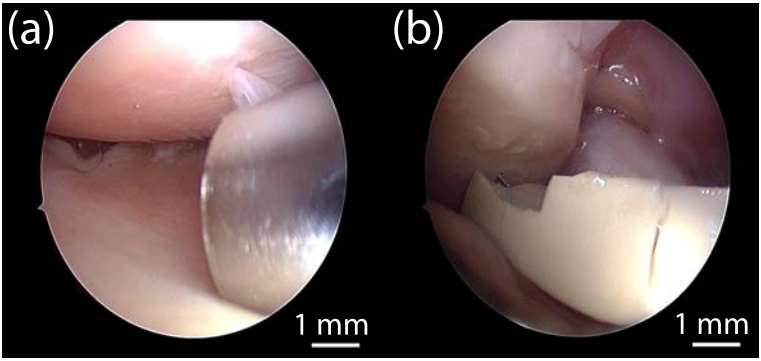

Figure 4.20. Arthroscopic views of the different damages observed during the positioning and the stabilization of the SFA (a) Lesion on the surface of cartilage due to the use of a maladapted canula. (b) Crash of the cantilever on the cartilage surface during the positioning of the instrument.

knee cavity, was delicate and time consuming. Figure 4.20 shows the different damages observed during this delicate step. The use of a transparent cannula specially designed for that purpose could be a solution to facilitate further in-vivo measurements. Unfortunately, once again, only relative data can be provided. While removing the instrument, the piezoelectric tube scanner was broken. Thus, it was impossible to calibrate the instrument and, hence, to calculate the dynamic elastic modulus $|E^*|$.

The first calibrated data were recorded on the tibial plateau of the knee model. The dynamic elastic modulus $|E^*|$ was determined from these indentation testing and the resulting value was of 2 GPa. The value found in literature for Acrylonitrile butadiene styrene (ABS) plastic $(C_8H_8 \cdot C_4H_6 \cdot C_3H_3N)_n$ was 2.4 GPa [3].

Sample	Slope	$\|E^*_{mes}\|$ in kPa	$\|E^*_{Stolz}\|$ in kPa	$\|E^*_{Chen}\|$ in kPa
Gel 0.75%	0.047	1	19	-
Gel 2%	0.329	10.3	14	15
Gel 2.5%	0.575	28.4	22	-
Gel 3%	0.654	39.8	29	35

Table 4.1: Comparison of the dynamic elastic modulus of agarose gel with concentration of 0.75%, 2.0%, 2.5% and 3.0% measured with the SFA ($|E^*_{mes}|$) and those known from scientific literature ($|E^*_{Stolz}|$ [2] and $|E^*_{Chen}|$ [1].

The second set of measurement was performed on agarose gel with different concentrations (cf. Fig. 4.15). For each concentration, the slopes of the unloading curves were directly converted into dynamic elastic modulus $|E^*_{mes}|$, using a calibration curve. This curve calculated by Stolz et al. [2] was generated by performing macroscale measurements of agarose gel stiffness in unconfined compression. A standard protocol for polymer testing, using a universal mechanical testing apparatus (Zwick Z010; Zwick GmbH, Ulm, Germany), was applied. The resulting modulus values for the different concentration of agarose gel are shown in table 4.1. The comparison of these values with those known from literature [2, 1] showed a very good correlation.

The dynamic elastic modulus $|E^*|$ was also determined for pig's articular cartilage. Some indentation measurements were recorded on the femur (cf. Fig. 4.17), the tibia (cf. Fig. 4.18) and the patella (cf. Fig. 4.19) of a sacrificed pig. For each measurements, the unloading curves were modeled using the Oliver and Pharr model as described in Chapter 3, and the calculated dynamic elastic moduli $|E^*_{cal}|$ were computed. These

values were compared with the theoretical dynamic elastic moduli $|E^*_{th}|$ obtained by using the calibration curve (cf. Table 4.2). The averaged values for the $|E^*_{cal}|$ and $|E^*_{th}|$ were 0.241 MPa and 0.235 MPa respectively. With the difficulty to precisely localized the initial point of contact between the tip and the sample mentioned in Chapter 3, the calculated value of 0.241 MPa is in good agreement to the 0.235 MPa obtained by the calibration curve.

More generally, figure 4.5, 4.8 and 4.11, show a "plateau" on the top of the load-displacement curve. Actually, the shape of the indentation connector is not well appropriate to measure unprepared samples with irregular soft surface like cartilage. During the loading, the edges of the connector touched the surface of cartilage. The cantilever bending was so limited and a "plateau" appeared on the load-displacement curve.

Sample	Figure N^o	Site N^o	Slope	$\|E^*_{cal}\|$ in MPa	$\|E^*_{th}\|$ in MPa
Femur	4.17	A	0.948	0.391	0.386
		B	0.837	0.128	0.108
Tibia	4.18	A	1.079	0.289	0.287
		B	0.821	0.093	0.096
		C	0.708	0.052	0.051
Patella	4.19	A	1.040	0.557	0.546
		B	1.140	0.174	0.171

Table 4.2: Comparison of the dynamic elastic modulus of pig's cartilage computed using the Oliver and Pharr model ($|E^*_{cal}|$) and those obtained by using the calibration curve ($|E^*_{th}|$).

Bibliography

[1] Q. Chen, B. Suki, and K.N. An. Dynamic Mechanical Properties of Agarose Gels Modeled by a Fractional Derivative Model. *Journal of Biomechanical Engineering*, 126:666, 2004.

[2] M. Stolz, R. Raiteri, A. U. Daniels, M. R. VanLandingham, W. Baschong, and U. Aebi. Dynamic elastic modulus of porcine articular cartilage determined at two different levels of tissue organization by indentation-type atomic force microscopy. *Biophysical Journal*, 86(5):3269–3283, May 2004.

[3] Commissions romandes de mathématique de physique et de chimie. *Formulaires et tables*. Commissions romandes de mathématique de physique et de chimie, 1985.

Chapter 5

Conclusion

5.1 Technical achievements

A quantitative diagnosis tool, the scanning force arthroscope (SFA), was built for probing, *in-vivo*, the biomechanical properties of human articular cartilage. A full scanning force microscope (SFM) setup was miniaturized and integrated into the shaft of a classical arthroscopic instrument. The stabilization and the positioning of the SFA inside the knee joint was realized by means of a pneumatic system. Eight balloons similar to those used for angioplasty were individually inflated with physiological salt solution (Ringer's solution). A system of syringe pushers controlled by a computer and a dedicated software were built to automatize the inflation and the deflation of the balloons. An encapsulated, four-segmented piezoelectric tube was used for scanning and probing the cartilage surface. This 3D scanner was able to probe a surface of about $1 \times 40\ \mu m^2$ with a z-range of $40\ \mu m$. The SFM sensor was based on a piezoresistive silicon cantilever with a monolithically integrated tip. This chip was mounted on a connector that could be easily exchanged. The standard electronics hardware and part of the control software of a commercially available SFM was employed

to generate the indentation and to record the cantilever deflection signal. The assessment of the tip geometry plays an important role during the analysis of the load-displacement curves. The exact geometry of a sharp silicon tip was often difficult to determine. In order to overcome this problem, we explored different ways for fabricating SFM cantilevers with spherical tips. In a first approach, we fabricated cantilevers with a hole in place of the tip. A silicate bead was manually placed and glued into this hole. However, the small tip's height of this kind of cantilever did not allow to measure soft irregular material such as articular cartilage. In a second approach, we had directly microfabricated the bead onto the SFM tip by APCVD. The size of the bead was selected by controlling the oxide thickness. These probes were used by Stolz et al. [1] to measure the mechanical stiffness on articular cartilage biopsies.

5.2 SFA Measurements

During the conception of the instrument, the SFA prototypes were tested on different samples. Uncalibrated measurements were successfully recorded during open knee surgeries on a plastic knee model, inside a pig's ankle and in a human knee cadaver. We were also able to perform, *in-vivo*, indentation testing of articular cartilage during standard arthroscopy. These preliminary tests, which constituted the first SFM measurements inside a human body, were essential to validate the concept of the instrument. Based on these results, the instrument was improved and calibrated. New measurements were performed on agarose gel, inside a plastic knee model and on pig's cartilage samples. The load-displacement curves obtained were analyzed and the dynamic elastic modulus $|E^*|$ were calculated. A very good correlation was found between these values and those published in the scientific literature.

5.3 Outlook

With the increase of life expectancy and changes in social habits, more and more people will be affected by degenerative joint disease in the next few decades. These pathologies which result for the patient in the inability to work and prevent him fully enjoying life, have also a huge economic cost impact to societies [2]. Helmick et al. [3, 4] have reported that in 2005, more than 21% of US adults (46.4 million persons) have been diagnosed with arthritis. This number is projected to increase to nearly 67 million by 2030. According to the Arthritis Foundation, the US annual cost of health caused by degenerative diseases, exceeds $120 billion.

In order to improve the understanding of musculoskeletal disorders and to develop effective treatments, more sensitive diagnostic tools, like the scanning force arthroscope, are required. The SFM is a versatile tool for imaging, measuring and manipulating soft biological tissues at the nanometer scale. The functionalization of the tip offers a wide range of new possibilities. For example, Thalhammer et al. [5] used an SFM tip as nano-scalpel and Meister et al. [6] present a nanodispenser for attoliter volume deposition using modified atomic force microscopy probes. The development of this new class of therapeutic instrument requires an interdisciplinary approach involving clinicians, biologists, physicists and engineers [7].

The SFA has proved its ability to probe the biomechanical properties of articular cartilage during a standard arthroscopy, but some aspects of the instrument have to be improved. At the present status of the instrument, the measurements are affected by technical limitations. Despite the establishment of a safe insertion procedure, the insertion and the positioning of the instrument inside the knee cavity was delicate and time consuming. A transparent cannula specially designed for that

purpose would certainly contribute to simplifying this procedure. The quality of the stabilization could be also improved by combining the pneumatic system already implemented with a microvacuum system which can fix a suck-cup on the cartilage surface through a small windows in the cannula. The load-displacement curves recorded with the SFA were obtained by using only the z-axis of the piezoelectric tube. The next step will be to repeat the same measurements for recording 2D map of elasticity using all the electrodes of the segmented piezoelectric tube. Finally, special attention must be given to the design of the SFA, because the surgeon holds the instrument in his hand during all the surgery, the weight of the SFA must be drastically reduced.

Bibliography

[1] M. Stolz, U. Aebi, and D. Stoffler. Developing scanning probe - based nanodevices - stepping out of the laboratory into the clinic. *Nanomedicine: Nanotechnology, Biology, and Medicine*, 3(1):53–62, 2007.

[2] World Health Organization. The burden of musculoskeletal conditions at the start of the new millennium. Technical Report 919, World Health Organization, 2003.

[3] Charles G. Helmick, David T. Felson, Reva C. Lawrence, Sherine Gabriel, Rosemarie Hirsch, C. Kent Kwoh, Matthew H. Liang, Hilal Maradit Kremers, Maureen D. Mayes, Peter A. Merkel, Stanley R. Pillemer, John D. Reveille, John H. Stone, and National Arthritis Data Workgroup. Estimates of the prevalence of arthritis and other rheumatic conditions in the united states: Part i. *Arthritis & Rheumatism*, 58(1):15–25, 2008.

[4] Reva C. Lawrence, David T. Felson, Charles G. Helmick, Lesley M. Arnold, Hyon Choi, Richard A. Deyo, Sherine Gabriel, Rosemarie Hirsch, Marc C. Hochberg, Gene G. Hunder, Joanne M. Jordan, Jeffrey N. Katz, Hilal Maradit Kremers, Frederick Wolfe, and National Arthritis Data Workgroup. Estimates of the prevalence of arthritis and other rheumatic conditions in the united states: Part ii. *Arthritis & Rheumatism*, 58(1):26–35, 2008.

[5] S. Thalhammer, RW Stark, S. Müller, J. Wienberg, and WM Heckl. The Atomic Force Microscope as a New Microdissecting Tool for the Generation of Genetic Probes. *Journal of Structural Biology*, 119(2):232–237, 1997.

[6] A. Meister, M. Liley, J. Brugger, R. Pugin, and H. Heinzelmann. Nanodispenser for attoliter volume deposition using atomic force microscopy probes modified by focused-ion-beam milling. *Applied Physics Letters*, 85(25):6260, 2004.

[7] P. Hunziker, M. Stolz, and U. Aebi. Nanotechnology in medicine: Moving from the bench to the bedside. *Chimia*, 56(10):520–526, 2002.

Appendix A

Stabilization stage

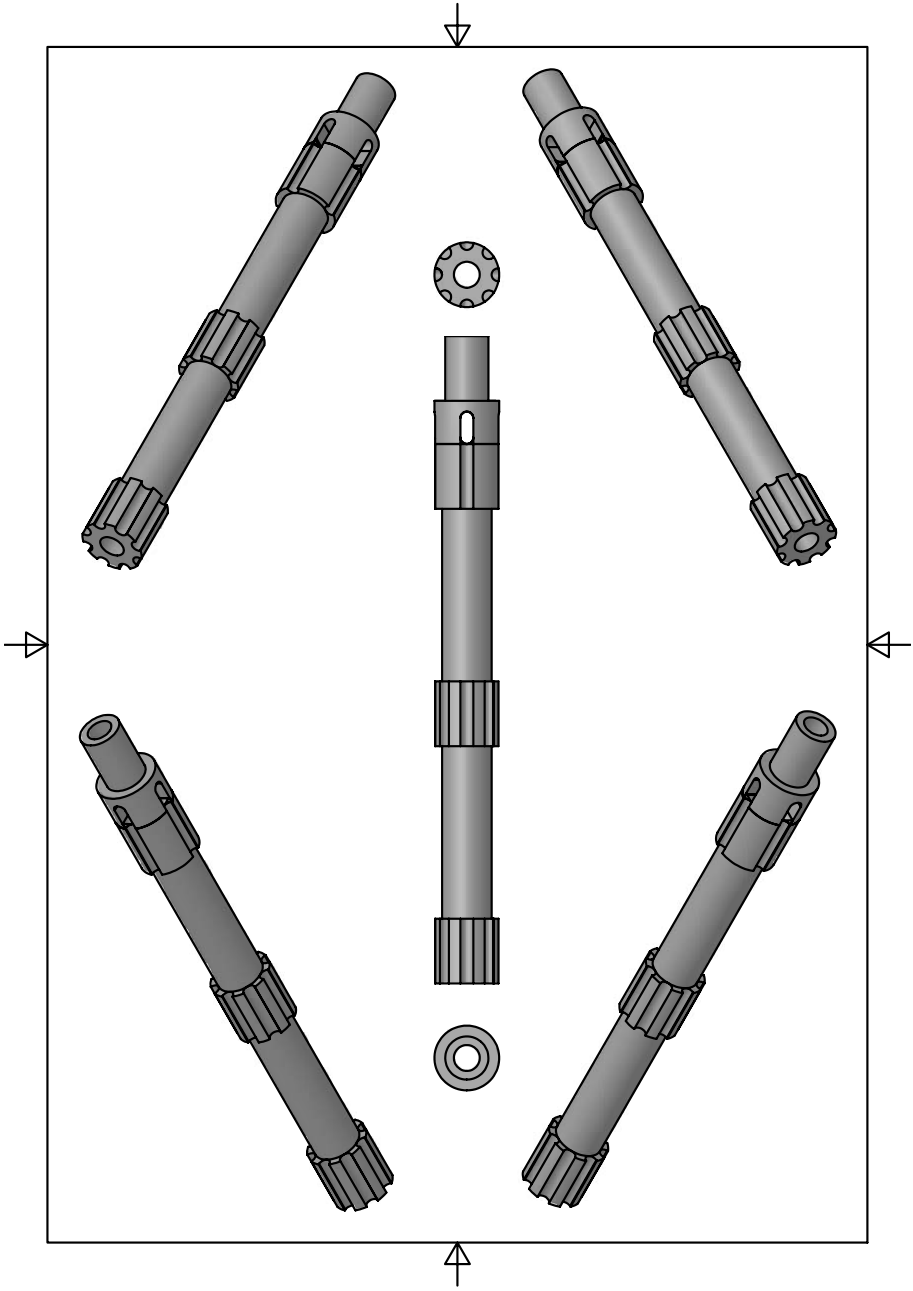

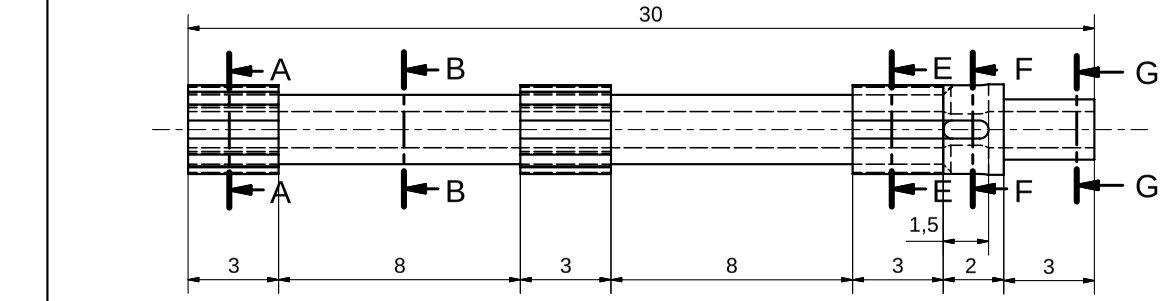

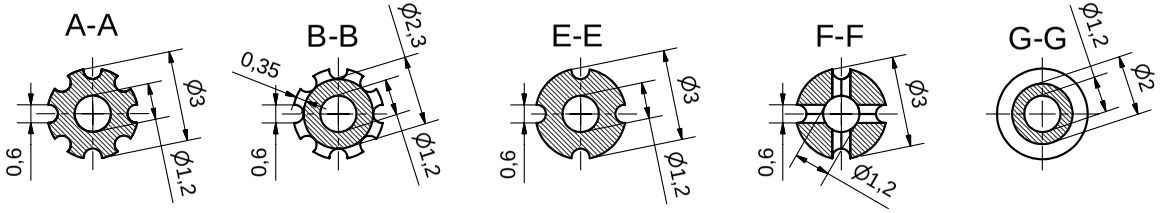

Designed by	Checked by	Approved by	Date		Date	
Raphaël Imer	Bernard Scanio	Urs Staufer	10.06.2004	IMT	07.06.2004	

Material	PEEK	Stabilization stage		
Quantity	1			
Scale	7:1	Balloon holder	Edition v.4	Sheet 1 / 1

Appendix B

Indentation stage

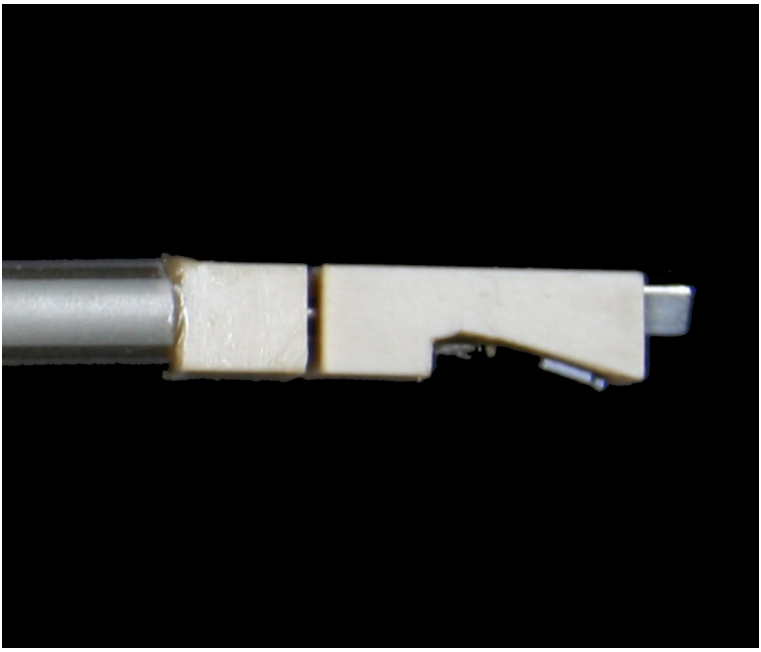

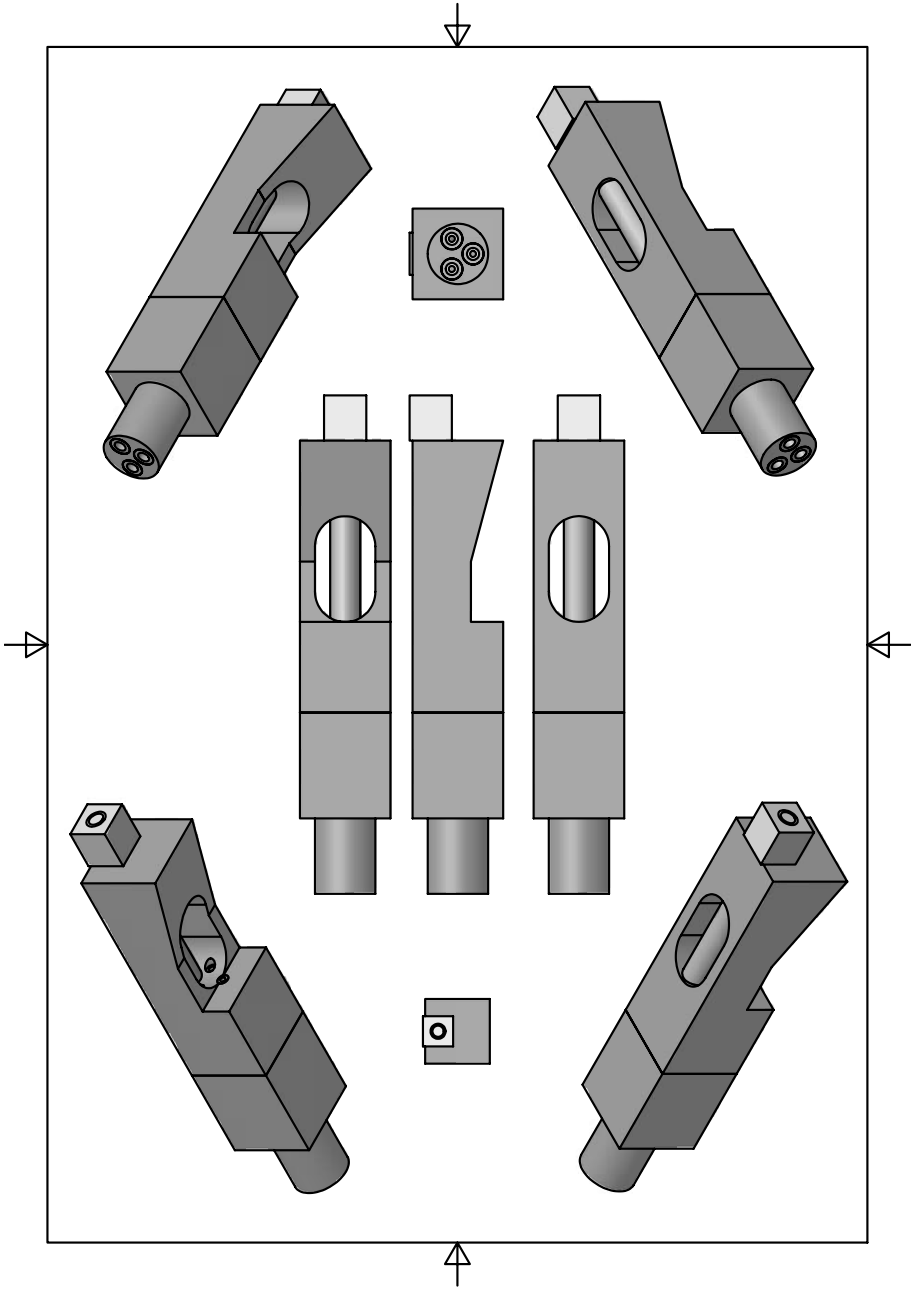

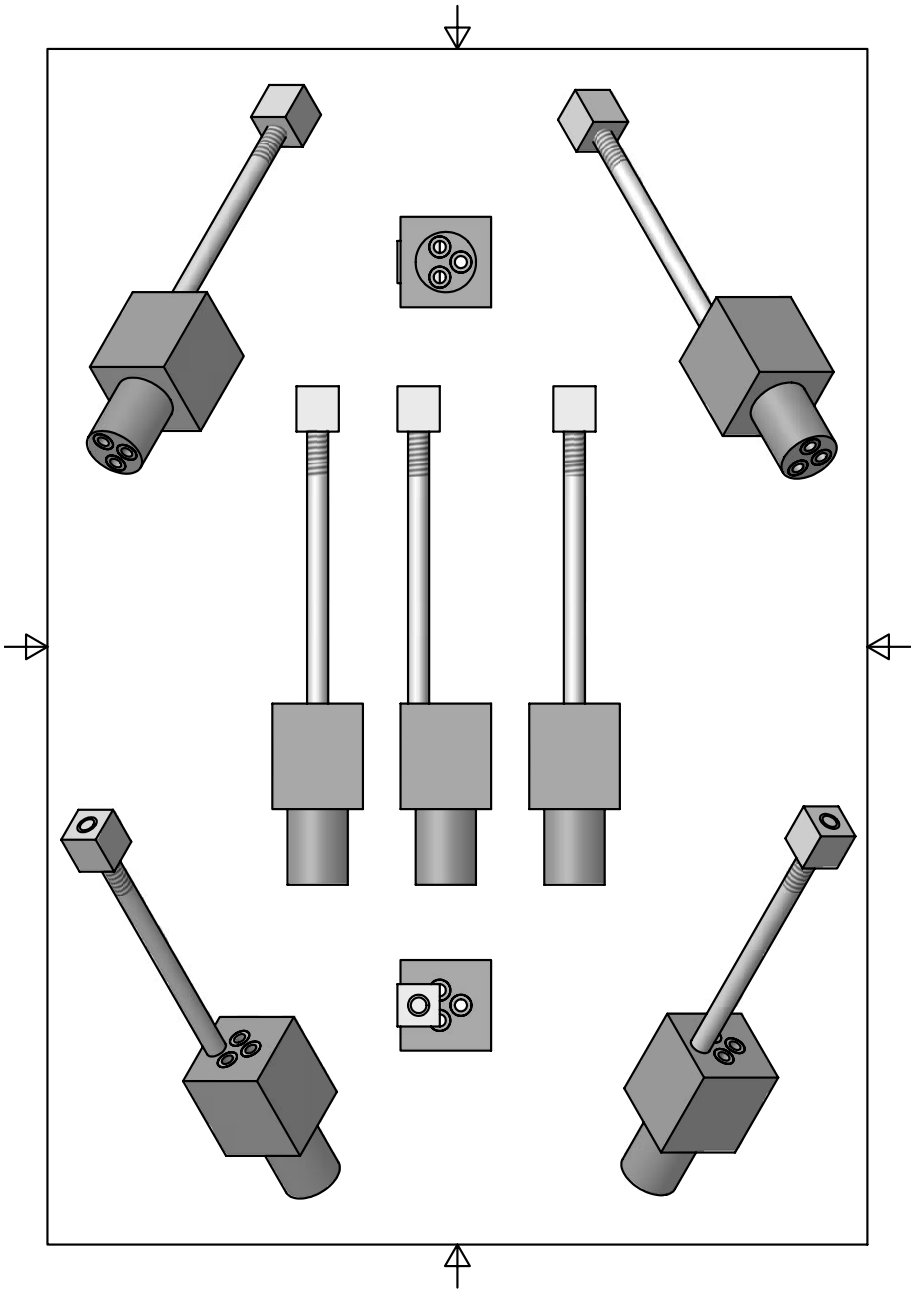

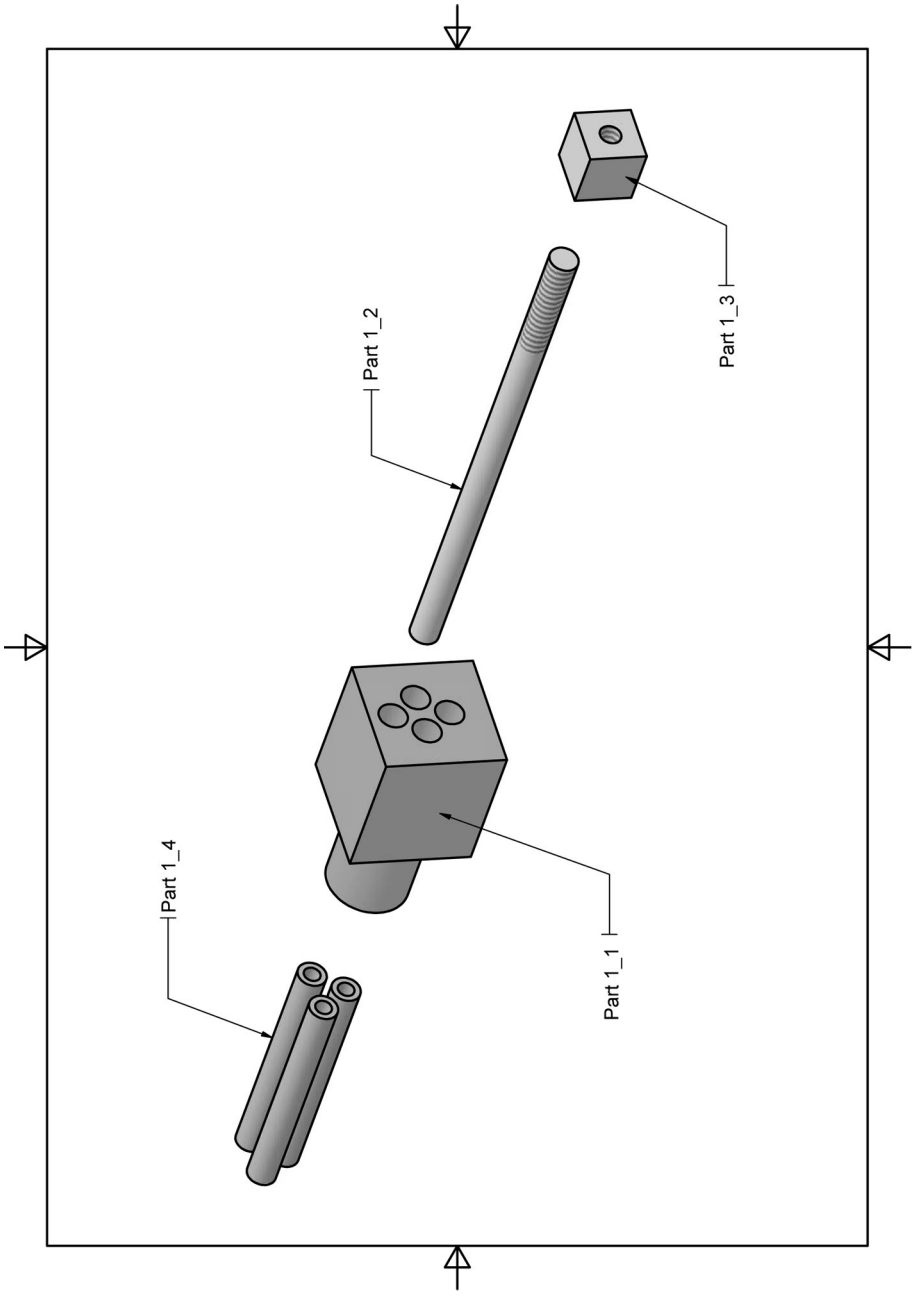
Part 1_3
Part 1_2
Part 1_4
Part 1_1

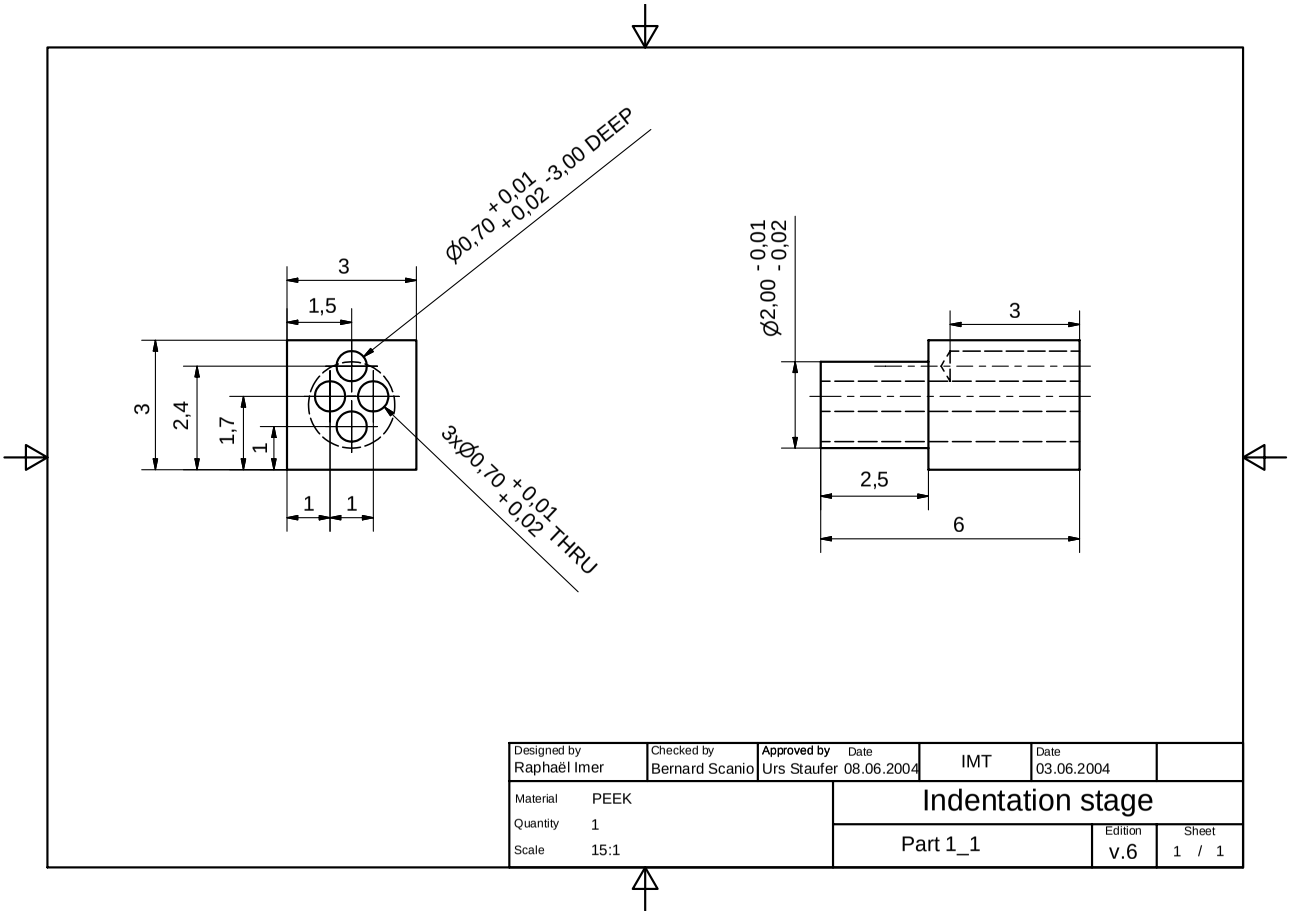

Designed by Raphaël Imer	Checked by Bernard Scanio	Approved by Urs Staufer Date 08.06.2004	IMT	Date 03.06.2004	
Material PEEK Quantity 1 Scale 15:1	Indentation stage				
	Part 1_1		Edition v.6	Sheet 1 / 1	

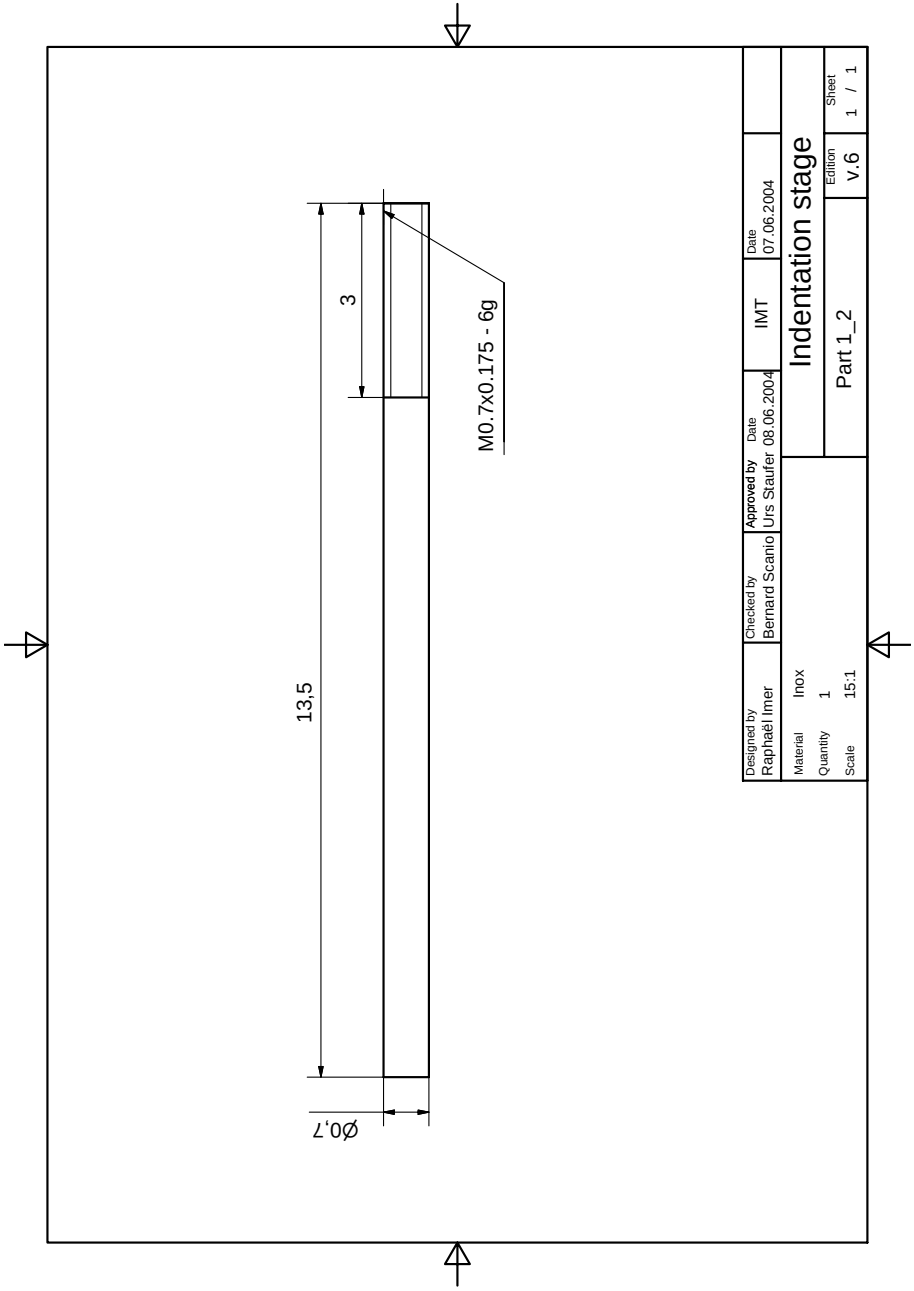
13,5
3
M0.7x0.175 - 6g
Ø0,7
Designed by
Raphaël Imer
Checked by
Bernard Scanio
Approved by
Urs Staufer
Date
08.06.2004
IMT
Date
07.06.2004
Material
Inox
Quantity
1
Scale
15:1
Indentation stage
Part 1_2
Edition
v.6
Sheet
1 / 1

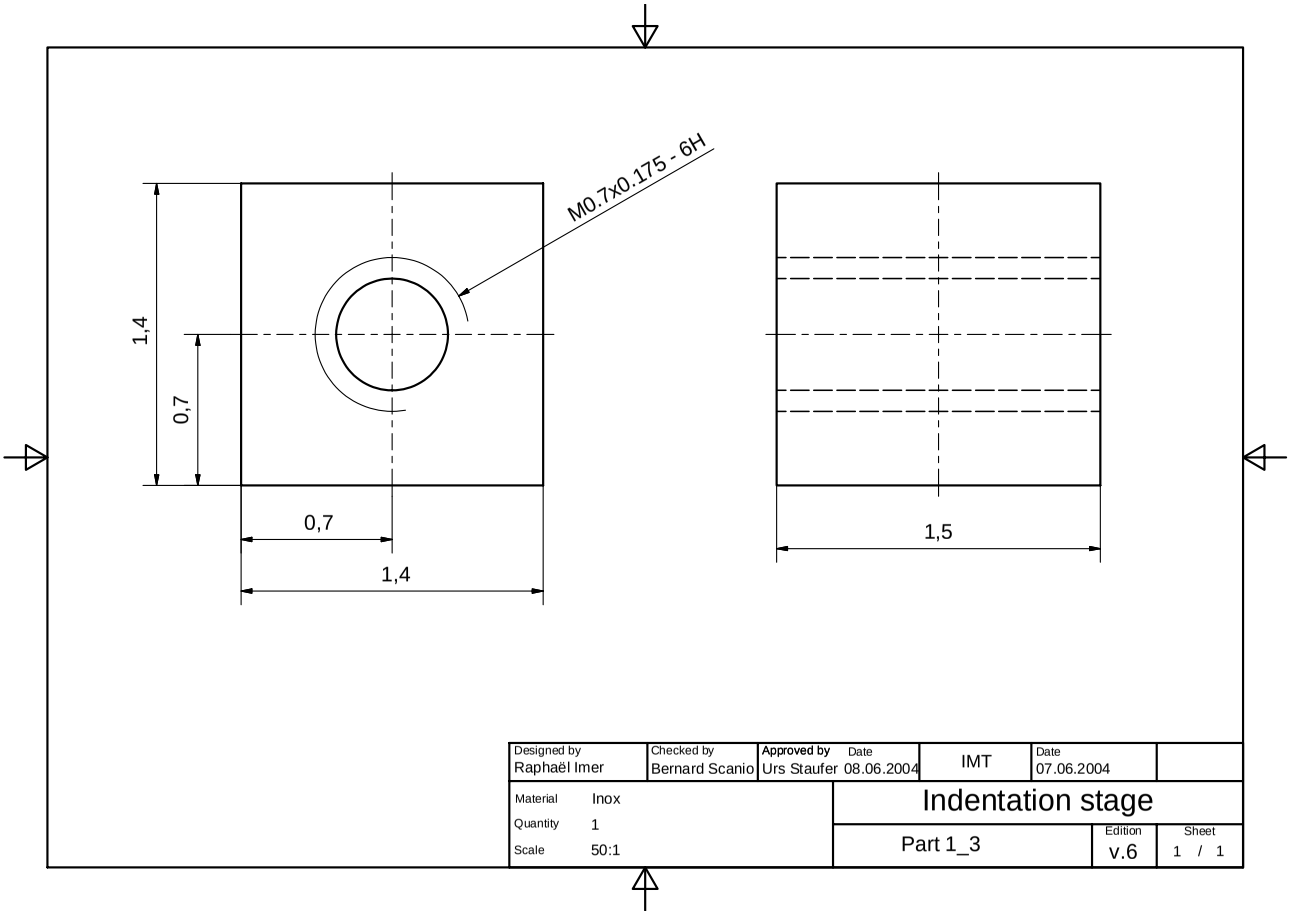

Designed by	Checked by	Approved by	Date		Date	
Raphaël Imer	Bernard Scanio	Urs Staufer	08.06.2004	IMT	07.06.2004	

Material	Inox	Indentation stage		
Quantity	1			
Scale	50:1	Part 1_3	Edition v.6	Sheet 1 / 1

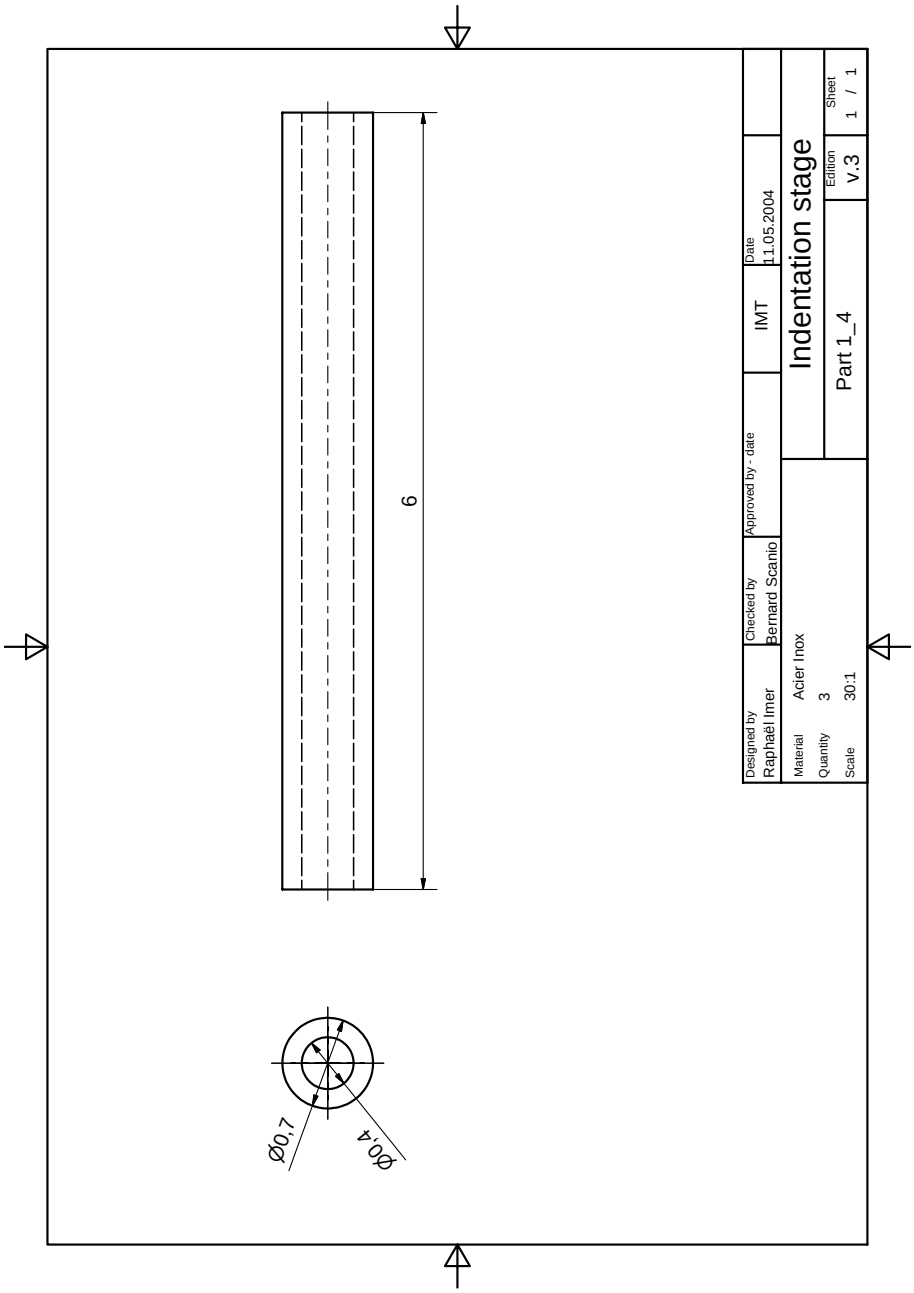
6
Ø0,7
Ø0,4
Designed by
Raphaël Imer
Checked by
Bernard Scanio
Approved by - date
IMT
Date
11.05.2004
Material
Acier Inox
Quantity
3
Scale
30:1
Indentation stage
Part 1_4
Edition
v.3
Sheet
1 / 1

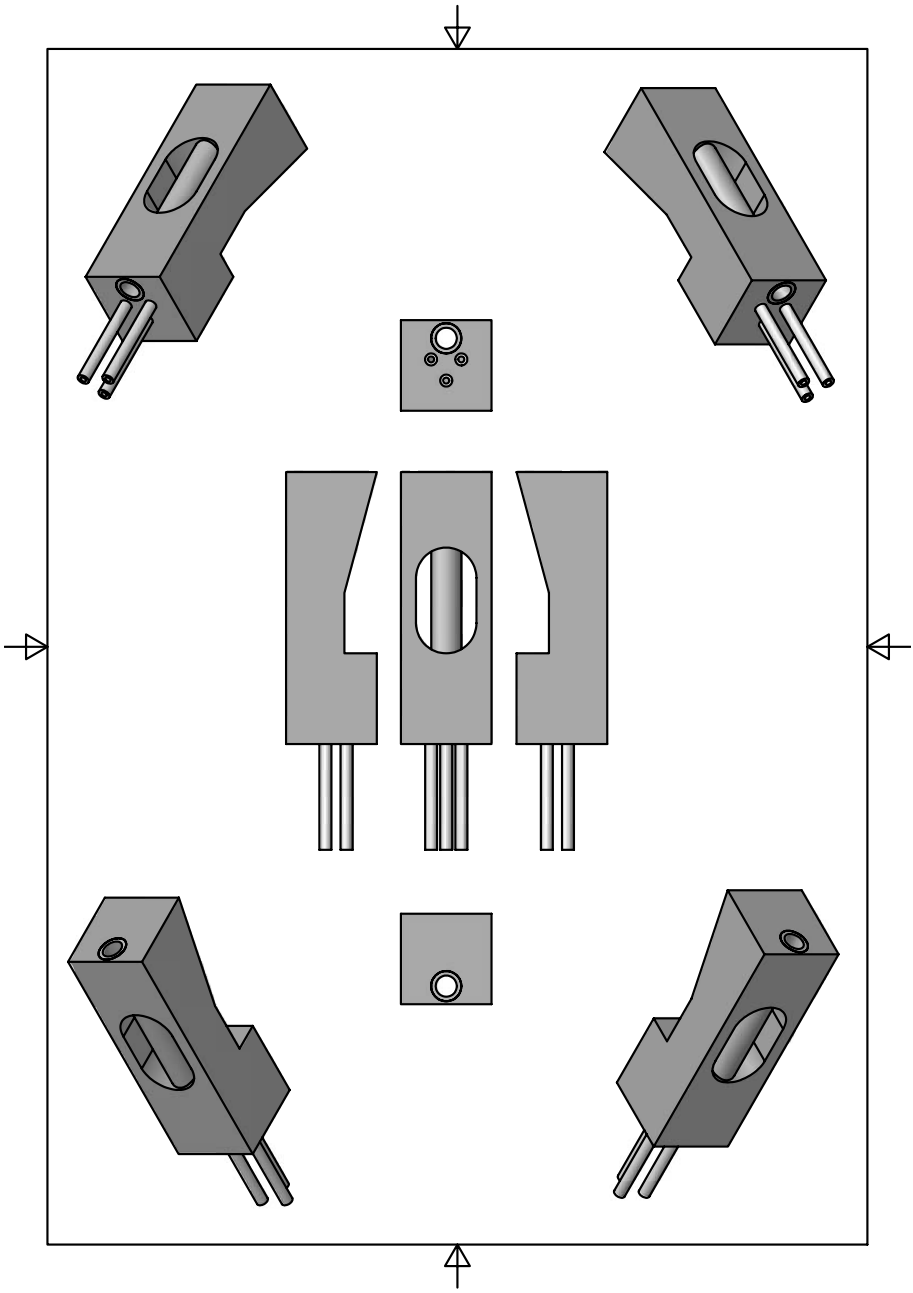

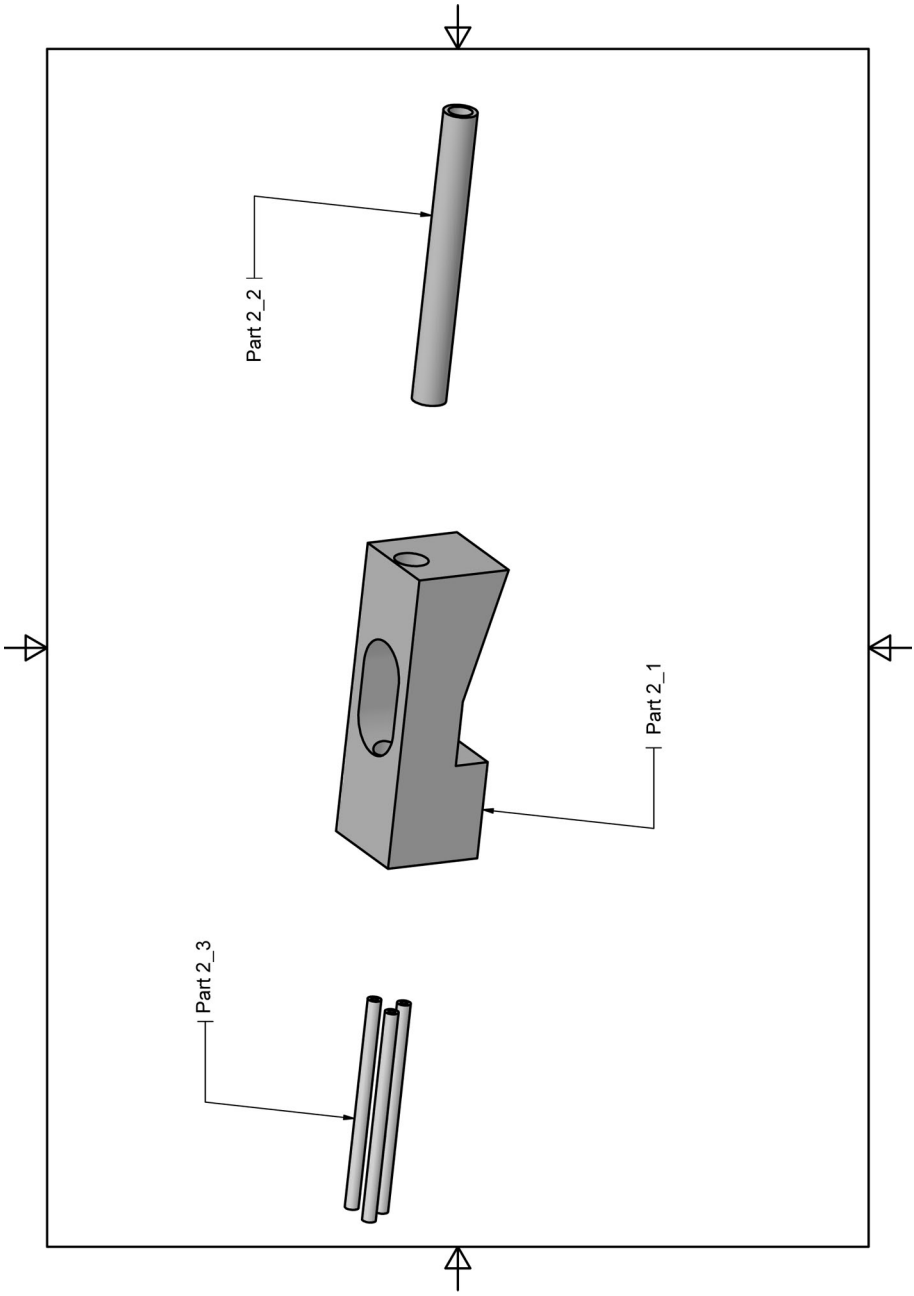
Part 2_2
Part 2_1
Part 2_3

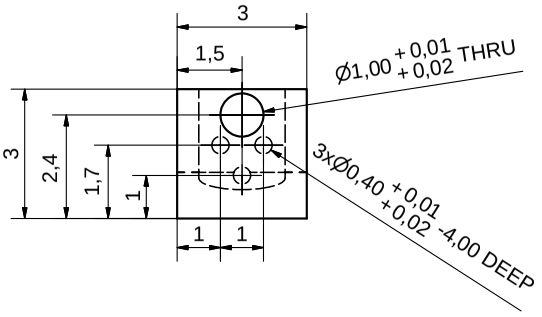

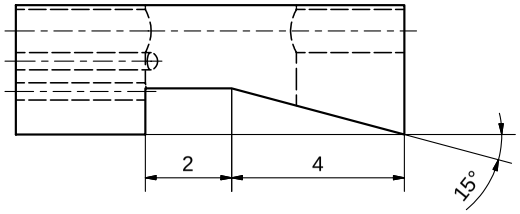

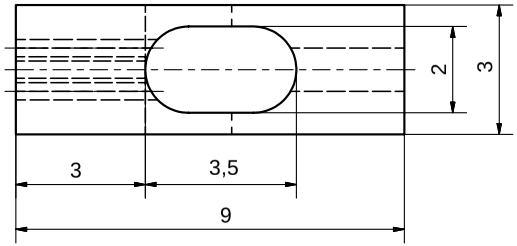

Designed by: Raphaël Imer	Checked by: Bernard Scanio	Approved by: Urs Staufer	Date: 08.06.2004	IMT	Date: 03.06.2004
Material: PEEK		Indentation stage			
Quantity: 1		Part 2_1		Edition: v.6	Sheet: 1 / 1
Scale: 10:1					

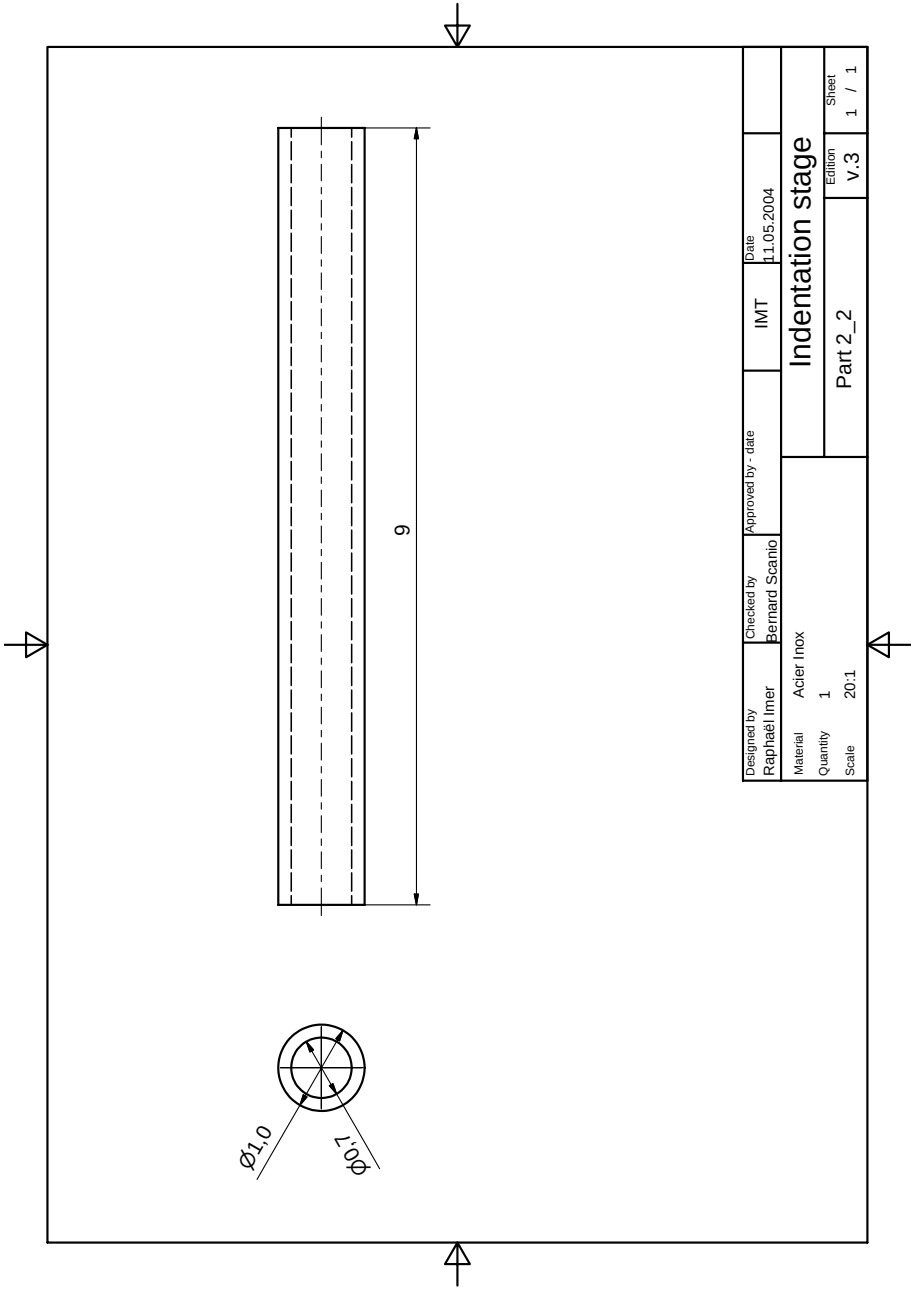
9
Ø1,0
1,0Ø
Designed by
Raphaël Imer
Checked by
Bernard Scanio
Approved by - date
IMT
Date
11.05.2004
Indentation stage
Material
Acier Inox
Quantity
1
Scale
20:1
Part 2_2
Edition
v.3
Sheet
1 / 1

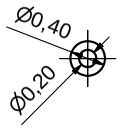

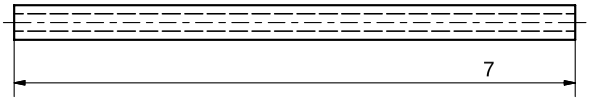

Designed by	Checked by	Approved by - date		Date	
Raphaël Imer	Bernard Scanio		IMT	11.05.2004	

Material	Acier Inox	Indentation stage		
Quantity	3			
Scale	20:1	Part 2_3	Edition v.3	Sheet 1 / 1

Appendix C

SFA handle

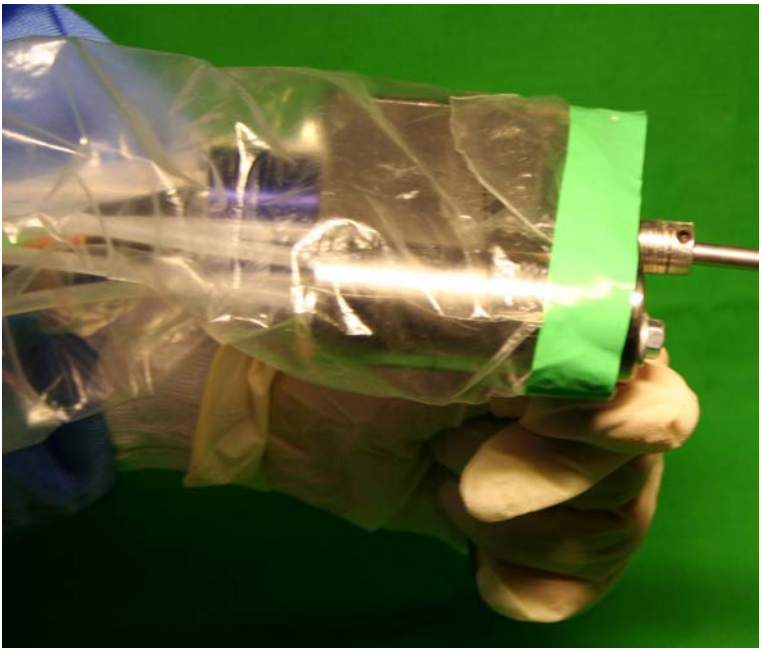

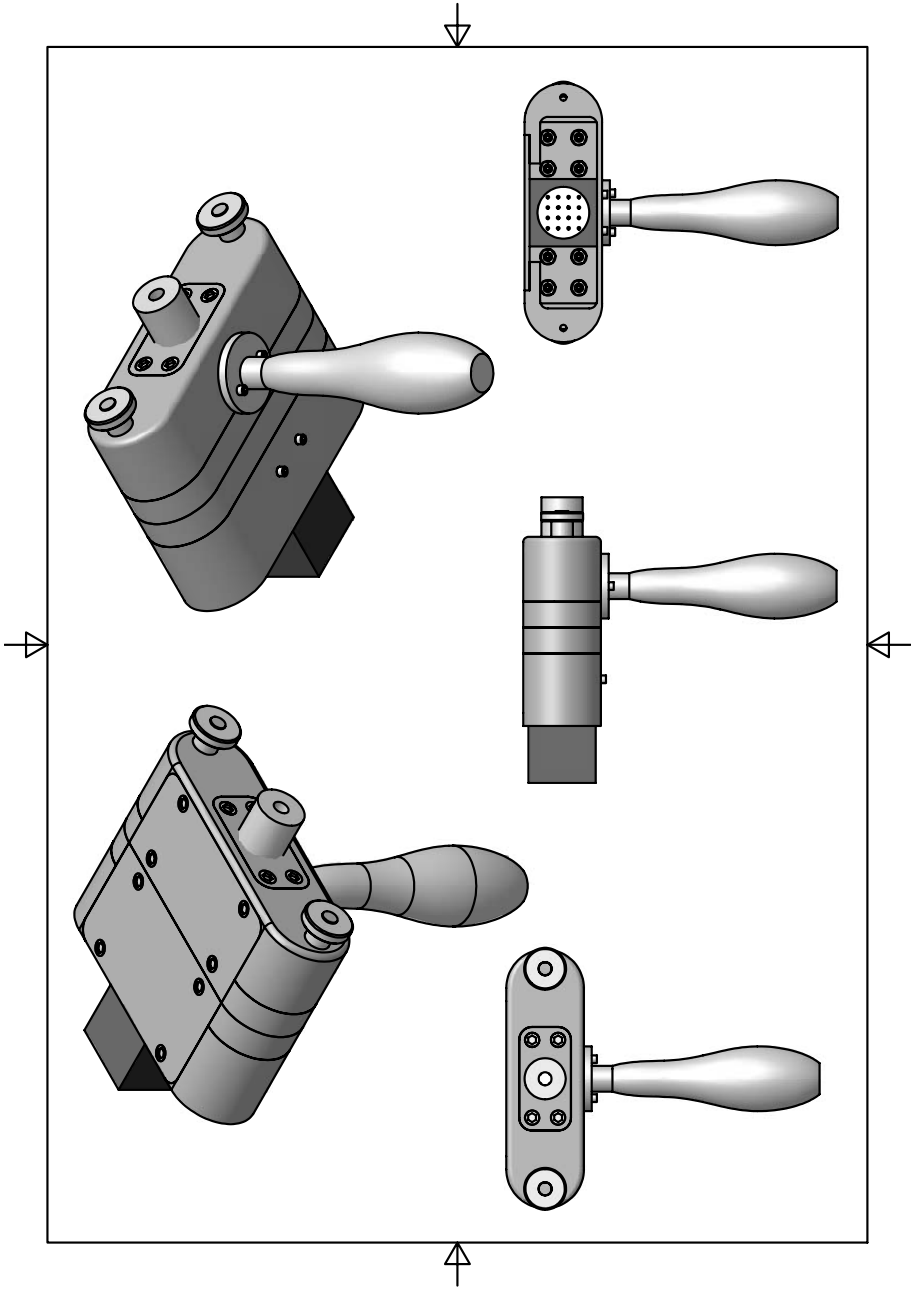

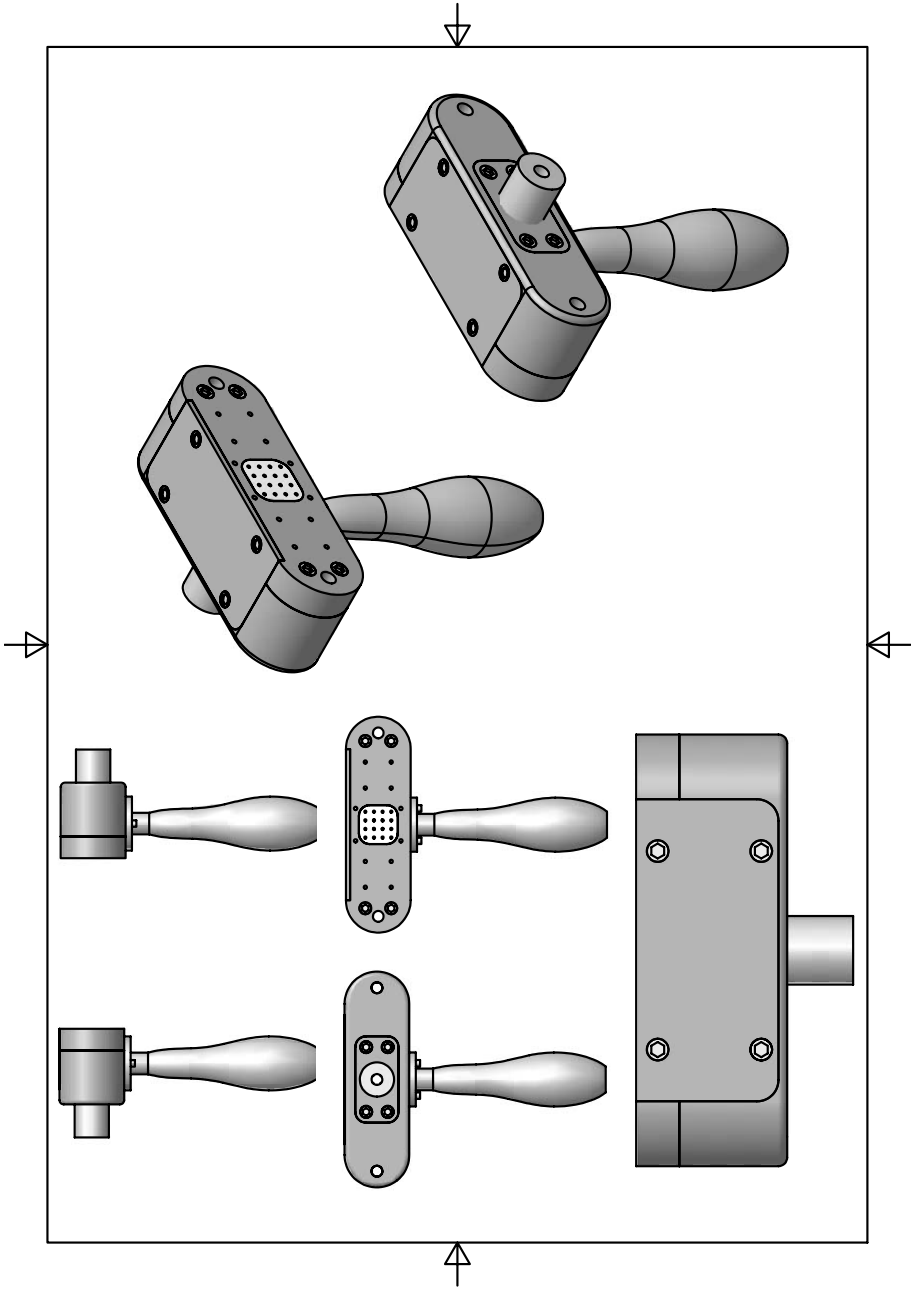

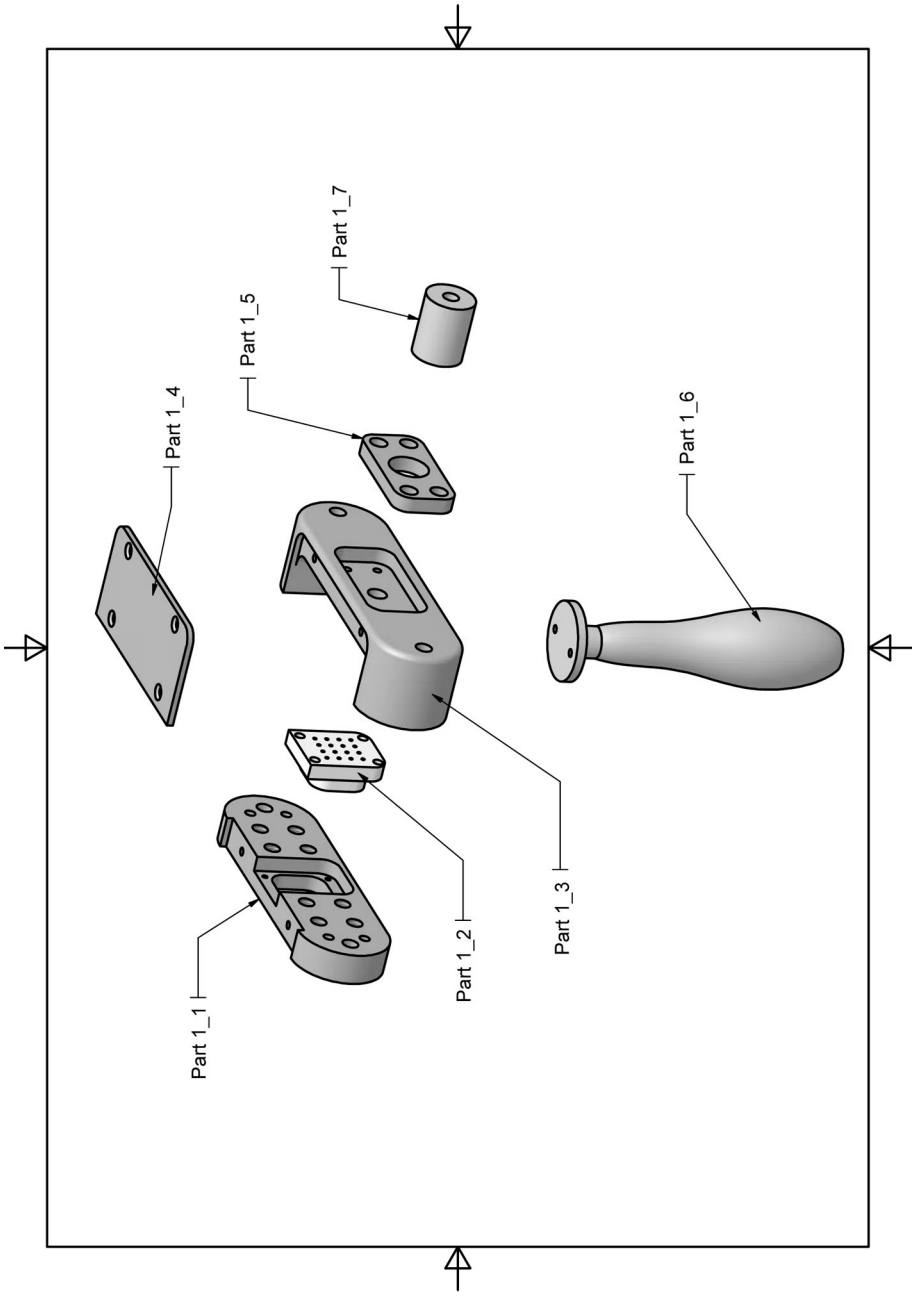
Part 1_7
Part 1_5
Part 1_4
Part 1_6
Part 1_3
Part 1_2
Part 1_1

2xØ2,50 -8,00 DEEP
M3x0,5 - 6H
2xØ5,00 H7 THRU
4xØ3,20 THRU
⌴ Ø5,50 ↧ 3,10
8xØ5,00 -8,00 DEEP
M6x1 - 6H
4xM2x0.4 - 6H
R5
R5
R15
21
18
6
6
100
70,0 +0,1 +0,2
22,0 +0,1 +0,2
18,0 +0,1 +0,2
42,50 ± 0,01
42,50 ± 0,01
7,5
17
29
38,75
23
Ø1,5
10
5
13
26,0 +0,1 +0,2
30
Designed by
Raphaël Imer
Checked by
Bernard Scanio
Approved by - date
IMT
Date
04.12.2006
SFA handle
part1_1
Edition
1
Sheet
1 / 1
Material
Stainless Steel, 440C
Quantity
1
Scale
1.5:1

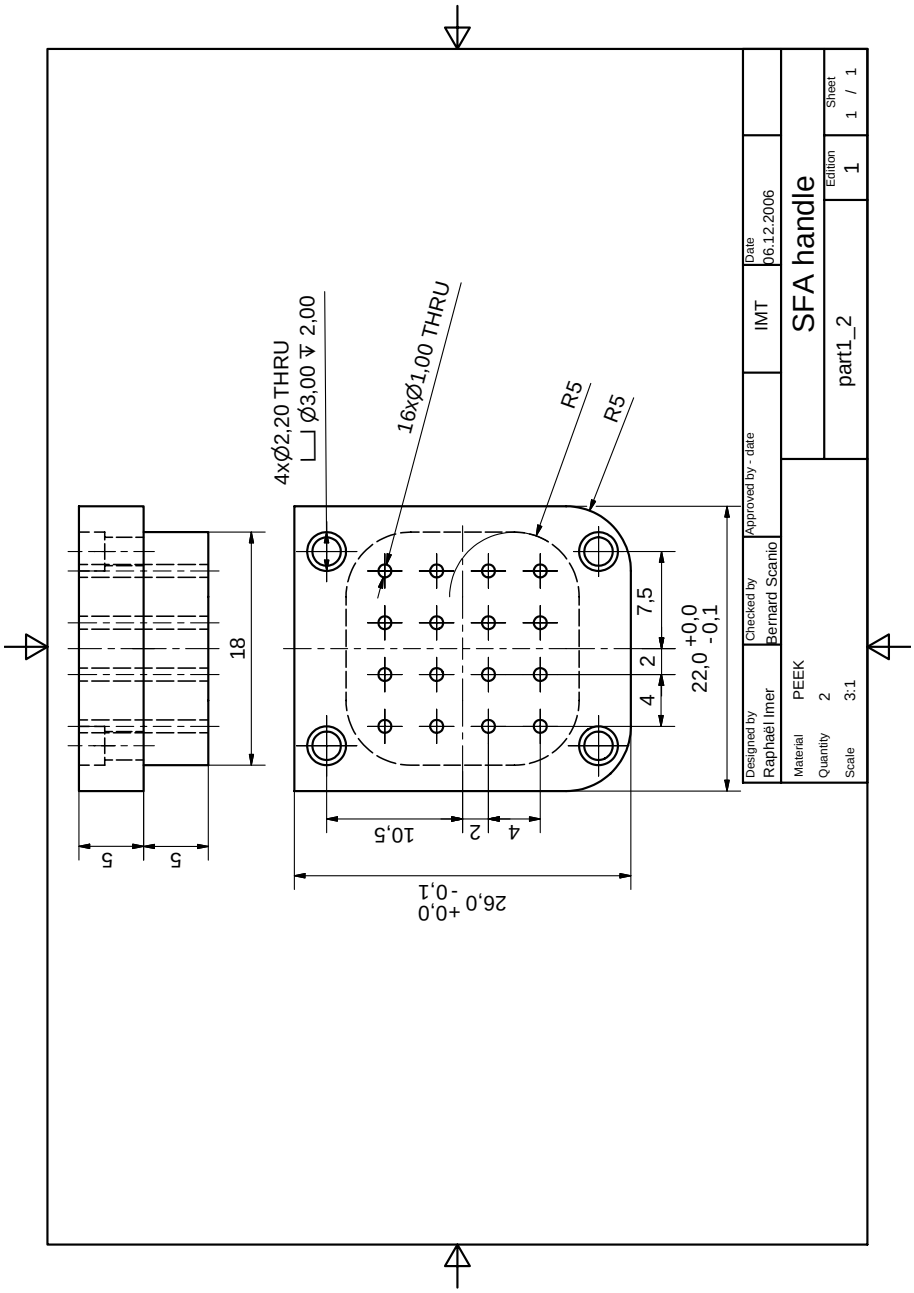
4xØ2,20 THRU
⌴ Ø3,00 ↧ 2,00
16xØ1,00 THRU
R5
R5
7,5
2
4
22,0 +0,0 -0,1
10,5
2
4
26,0 +0,0 -0,1
18
5
5
Designed by
Raphaël Imer
Checked by
Bernard Scanio
Approved by - date
IMT
Date
06.12.2006
SFA handle
part1_2
Edition
1
Sheet
1 / 1
Material
PEEK
Quanity
2
Scale
3:1

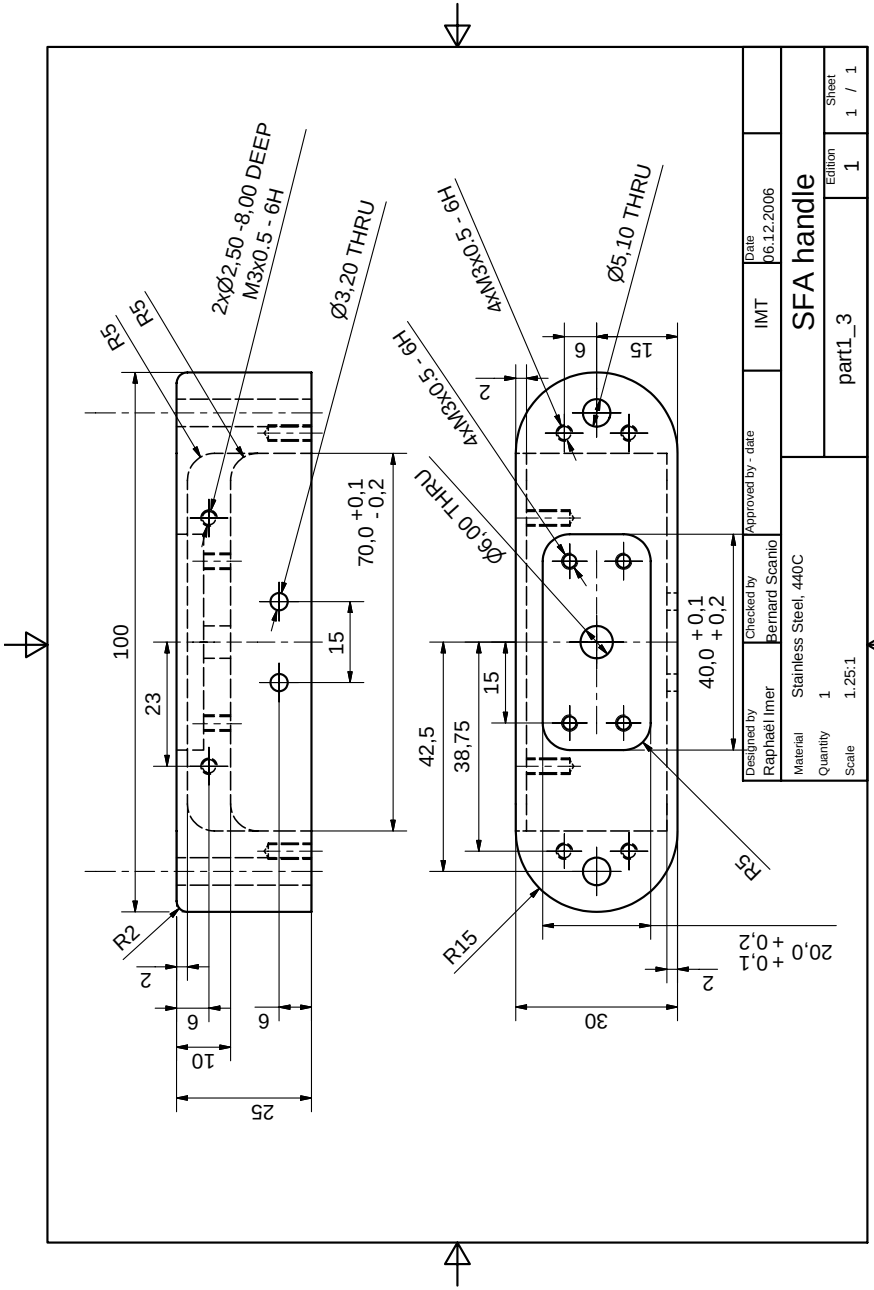
2xØ2,50 -8,00 DEEP
M3x0.5 - 6H
Ø3,20 THRU
R5
R5
R2
100
23
15
70,0 +0,1 -0,2
2
6
6
10
25
4xM3x0.5 - 6H
4xM3x0.5 - 6H
Ø6,00 THRU
Ø5,10 THRU
R5
R15
42,5
38,75
15
40,0 +0,1 +0,2
6
15
2
30
20,0 +0,1 +0,2
Designed by
Raphaël Imer
Checked by
Bernard Scanio
Approved by - date
IMT
Date
06.12.2006
SFA handle
part1_3
Edition
1
Sheet
1 / 1
Material
Stainless Steel, 440C
Quantity
1
Scale
1.25:1

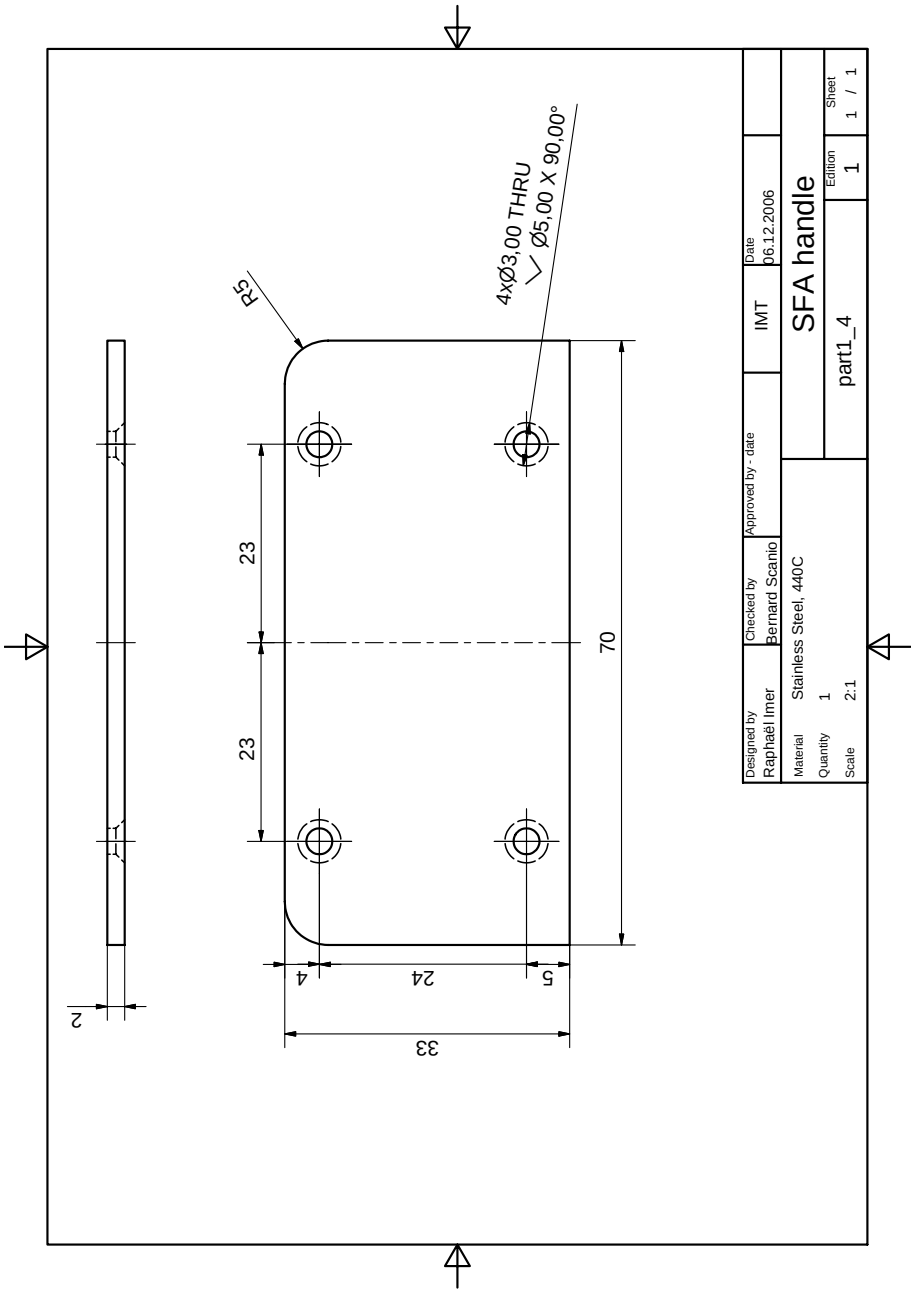
4xØ3,00 THRU
Ø5,00 X 90,00°
R5
23
23
70
2
4
24
5
33
Designed by
Raphaël Imer
Checked by
Bernard Scanio
Approved by - date
IMT
Date
06.12.2006
SFA handle
part1_4
Edition
1
Sheet
1 / 1
Material
Stainless Steel, 440C
Quantity
1
Scale
2:1

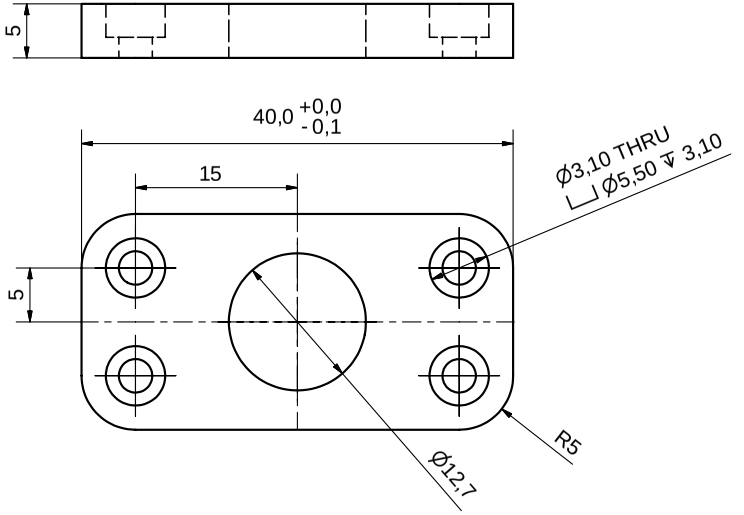

Designed by	Checked by	Approved by - date		Date	
Raphaël Imer	Bernard Scanio		IMT	06.12.2006	

Material	Stainless Steel, 440C	SFA handle		
Quantity	1	part1_5	Edition 1	Sheet 1 / 1
Scale	2.5:1			

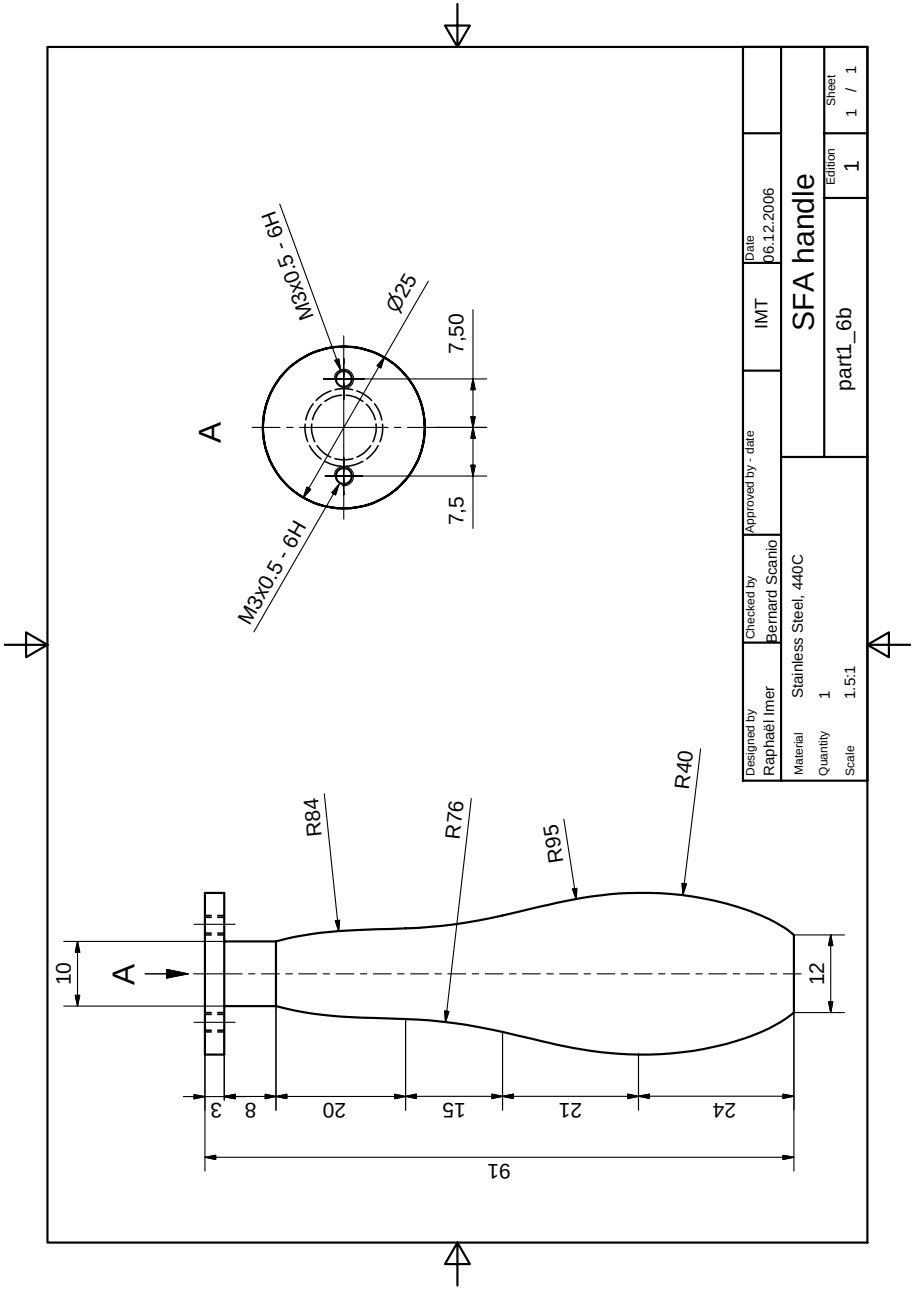
A
M3x0.5 - 6H
Ø25
7,50
7,5
M3x0.5 - 6H
A
10
R84
R76
R95
R40
12
3
8
20
15
21
24
91
Designed by
Raphaël Imer
Checked by
Bernard Scanio
Approved by - date
IMT
Date
06.12.2006
SFA handle
Material
Stainless Steel, 440C
Quantity
1
Scale
1.5:1
part1_6b
Edition
1
Sheet
1 / 1

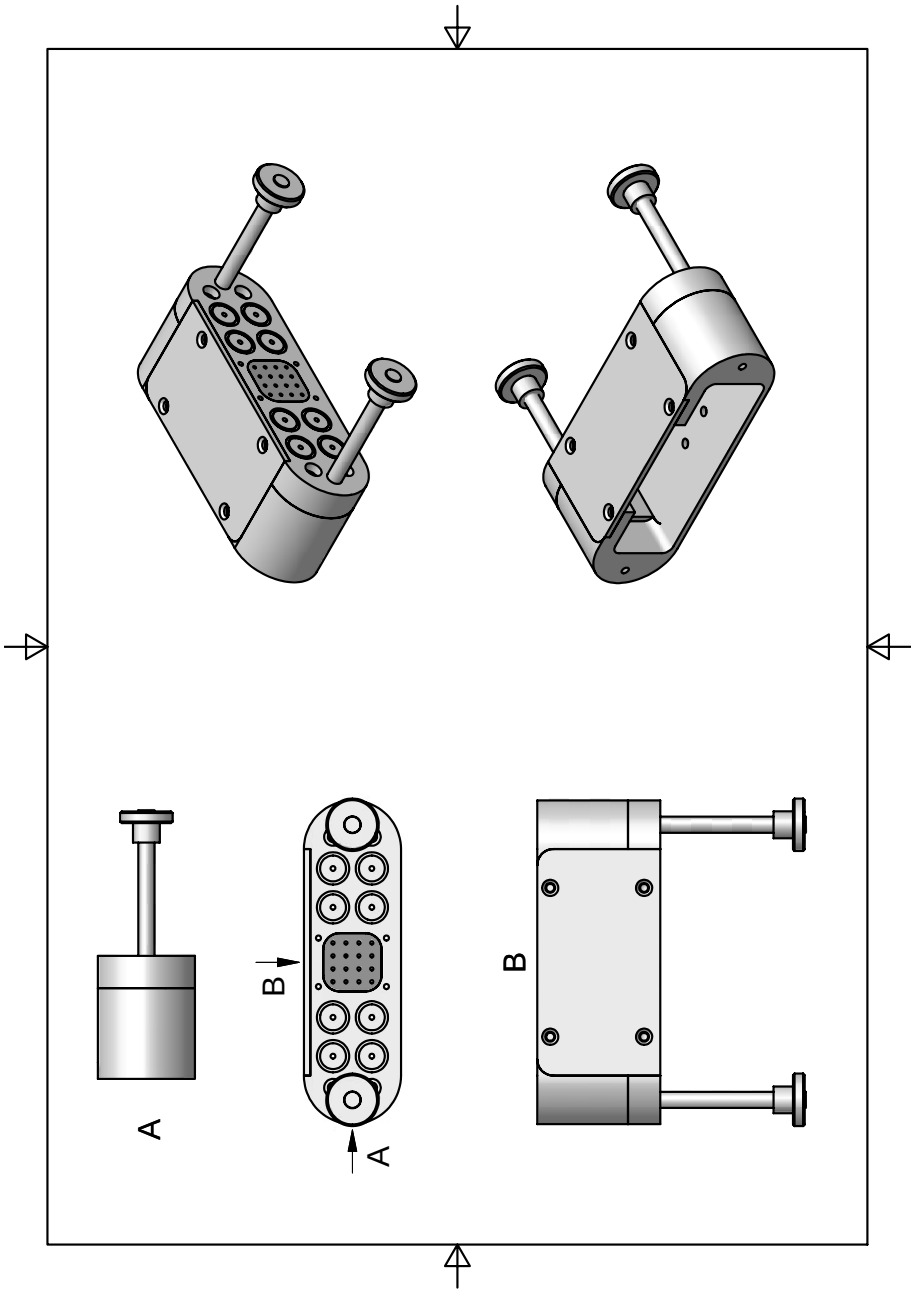
A
B
A
B

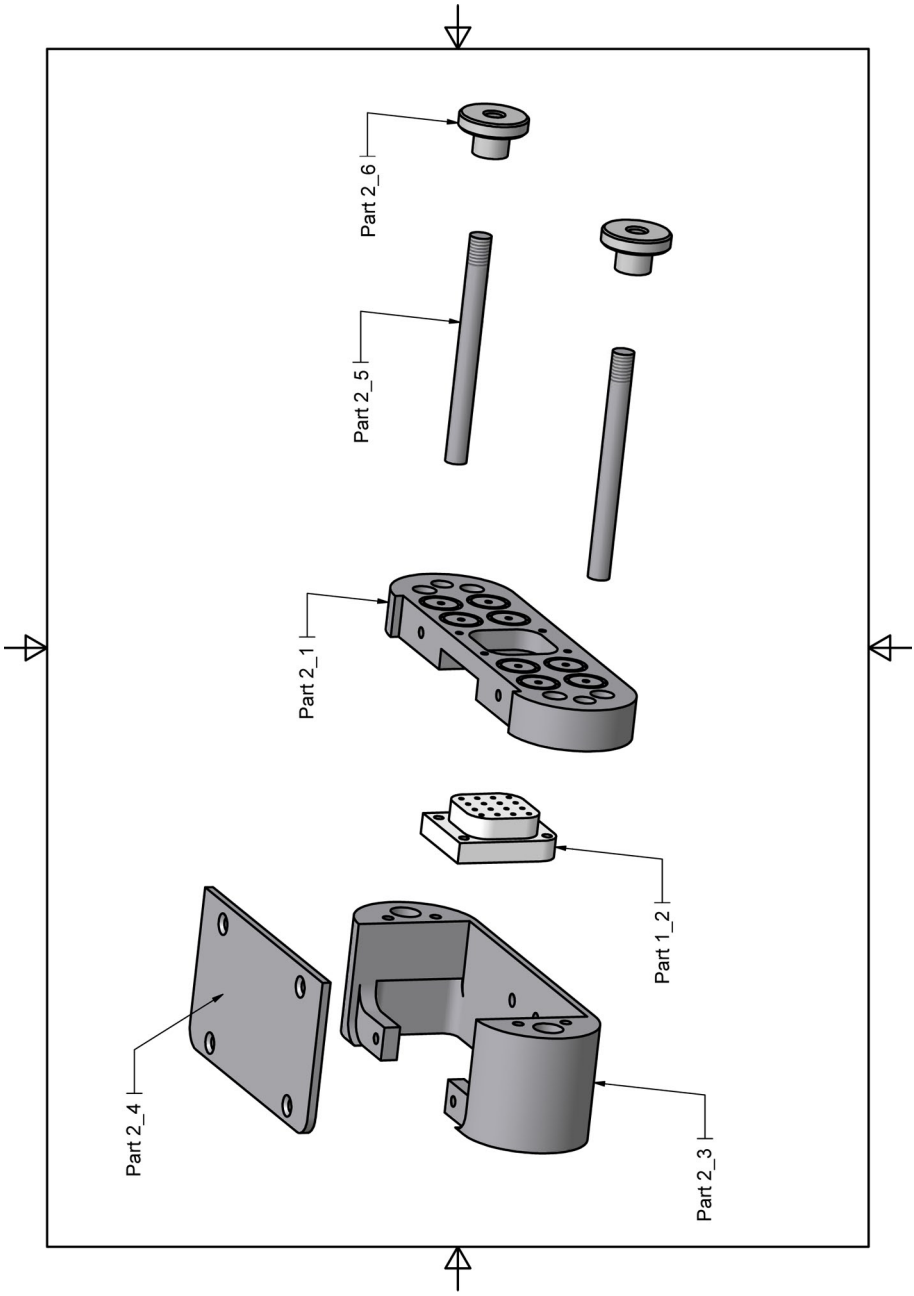
Part 2_6
Part 2_5
Part 2_1
Part 1_2
Part 2_4
Part 2_3

2xØ2,50 -8,00 DEEP
M3x0.5 - 6H
0,7
2xØ5,00 P7 THRU
4xØ3,20 THRU
⌴ Ø5,50 ↧ 3,10
8xØ5,00 -8,00 DEEP
M6x1 - 6H
21
6
6
Ø10
Ø8
R5
R5
4xM2x0.4 - 6H
18,0 +0,1 +0,2
70,0 +0,1 +0,2
22,0 +0,1 +0,2
100
23
Ø1,5
5
10
7,5
17
29
38,75
42,50 ± 0,01
42,50 ± 0,01
13
26
30
18,0 +0,1 -0,2
R15
Designed by
Raphaël Imer
Checked by
Bernard Scanio
Approved by - date
IMT
Date
06.12.2006
SFA handle
part2_1
Edition
1
Sheet
1 / 1
Material
Stainless Steel, 440C
Quantity
1
Scale
1.5:1

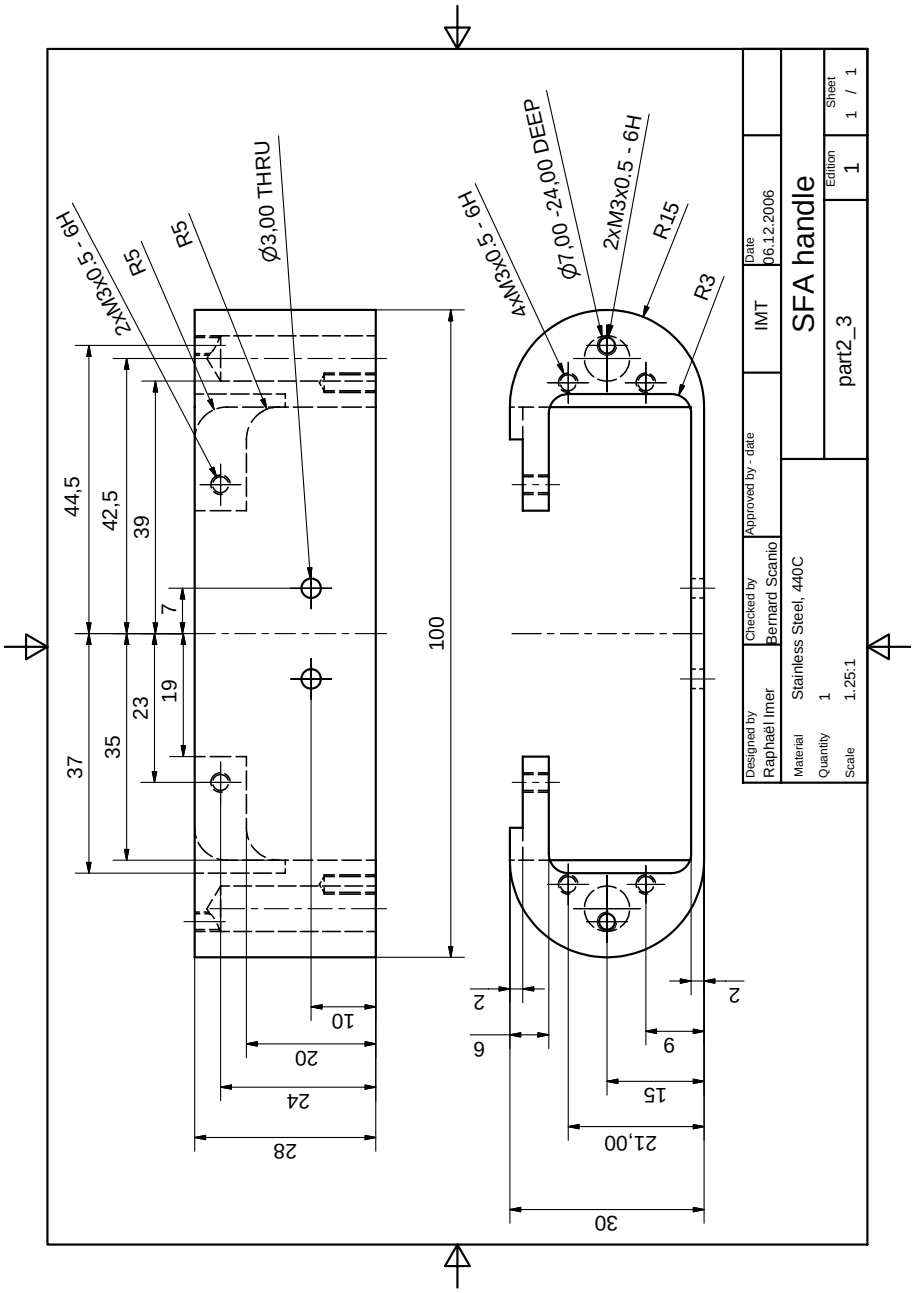
2xM3x0.5 - 6H
R5
R5
Ø3,00 THRU
4xM3x0.5 - 6H
Ø7,00 -24,00 DEEP
2xM3x0.5 - 6H
R15
R3
44,5
42,5
39
7
37
35
23
19
100
10
20
24
28
2
6
9
15
21,00
30
2
Designed by
Raphaël Imer
Checked by
Bernard Scanio
Approved by - date
IMT
Date
06.12.2006
SFA handle
Material
Stainless Steel, 440C
Quantity
1
Scale
1.25:1
part2_3
Edition
1
Sheet
1 / 1

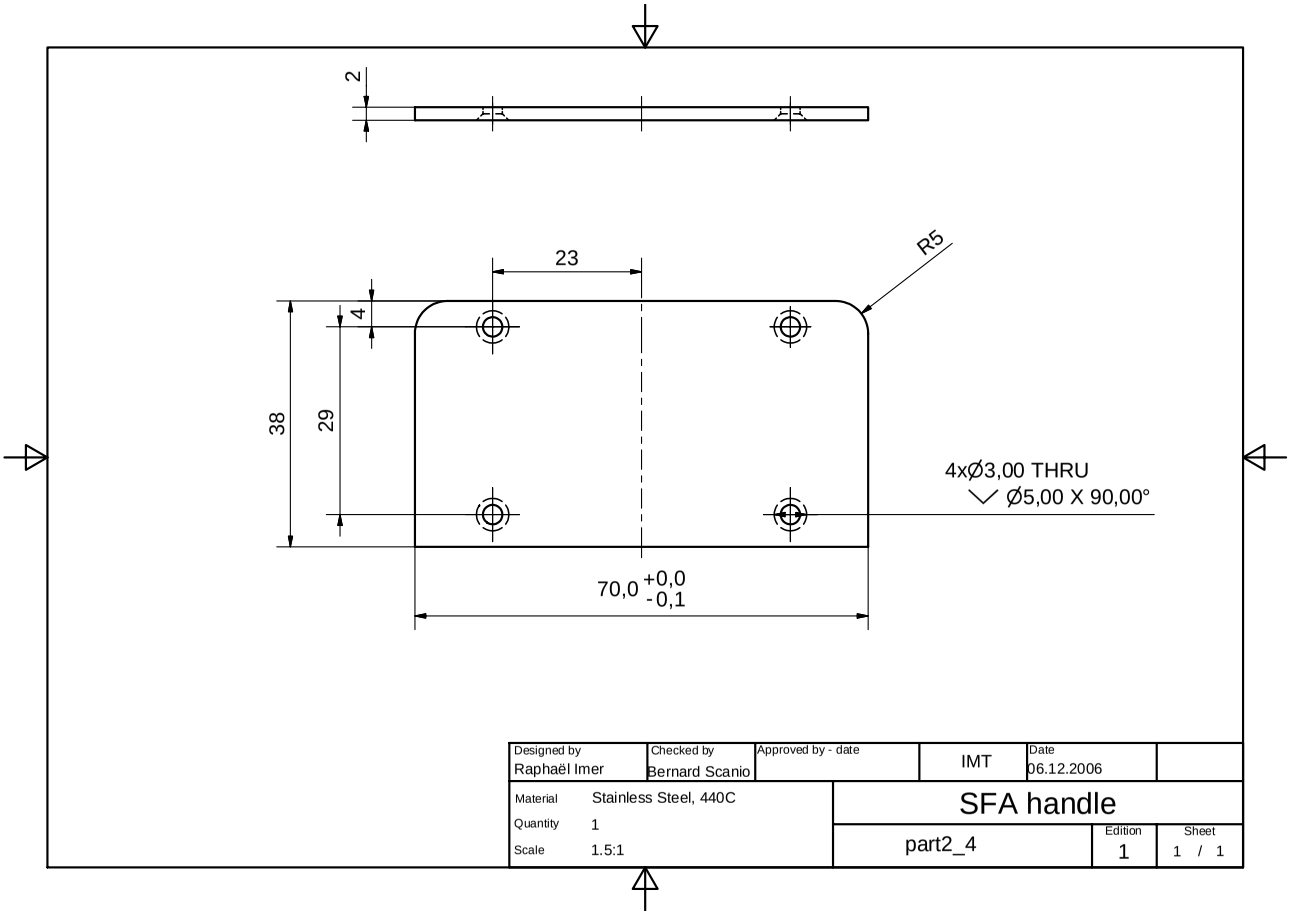

Designed by: Raphaël Imer	Checked by: Bernard Scanio	Approved by - date:	IMT	Date: 06.12.2006	
Material: Stainless Steel, 440C Quantity: 1 Scale: 1.5:1		SFA handle			
		part2_4		Edition: 1	Sheet: 1 / 1

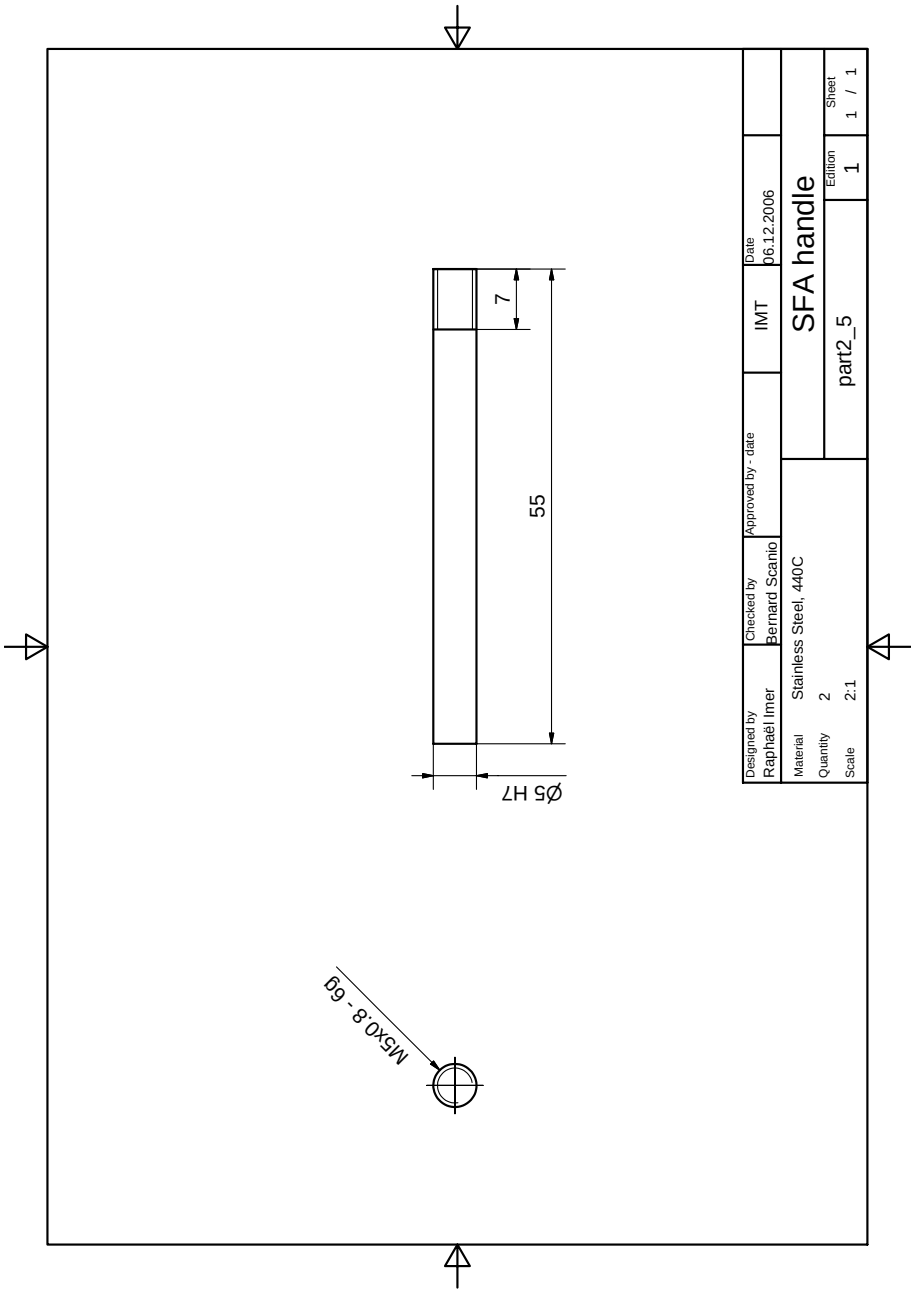
7
55
Ø5 H7
M5x0.8 - 6g
Designed by
Raphaël Imer
Checked by
Bernard Scanio
Approved by - date
IMT
Date
06.12.2006
SFA handle
Material
Stainless Steel, 440C
Quantity
2
Scale
2:1
part2_5
Edition
1
Sheet
1 / 1

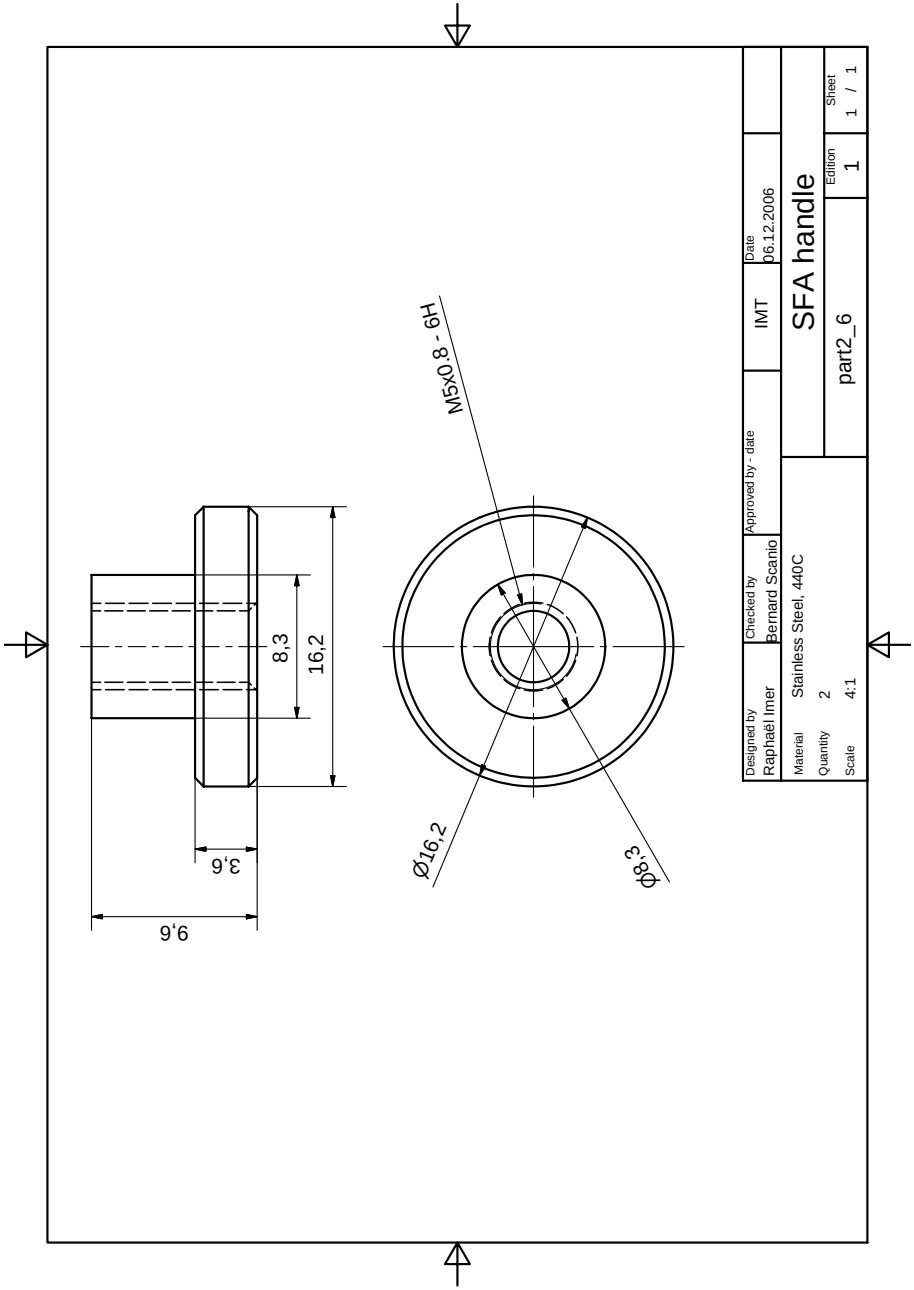
M5x0.8 - 6H
Ø16,2
Ø8,3
8,3
16,2
3,6
9,6
Designed by
Raphaël Imer
Checked by
Bernard Scanio
Approved by - date
IMT
Date
06.12.2006
SFA handle
part2_6
Edition
1
Sheet
1 / 1
Material
Stainless Steel, 440C
Quantity
2
Scale
4:1

Appendix D

Syringe-pusher

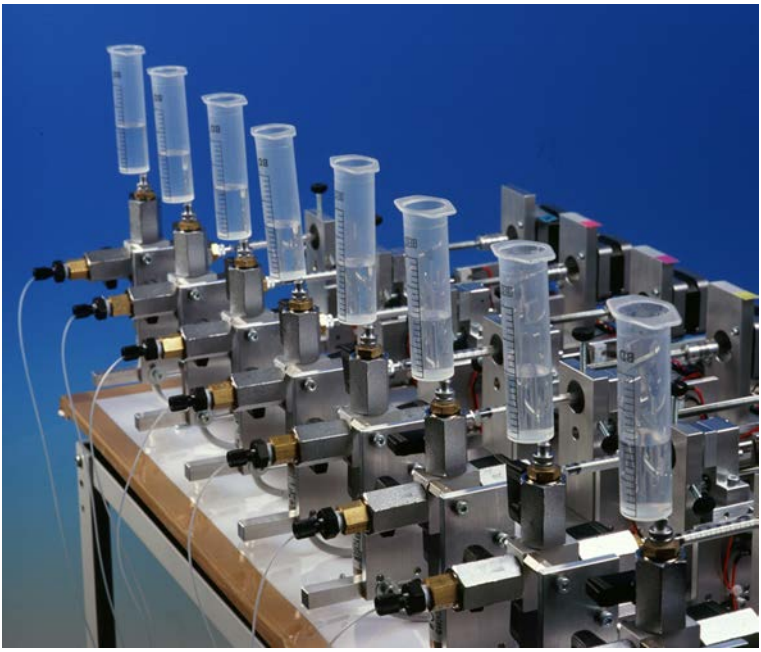

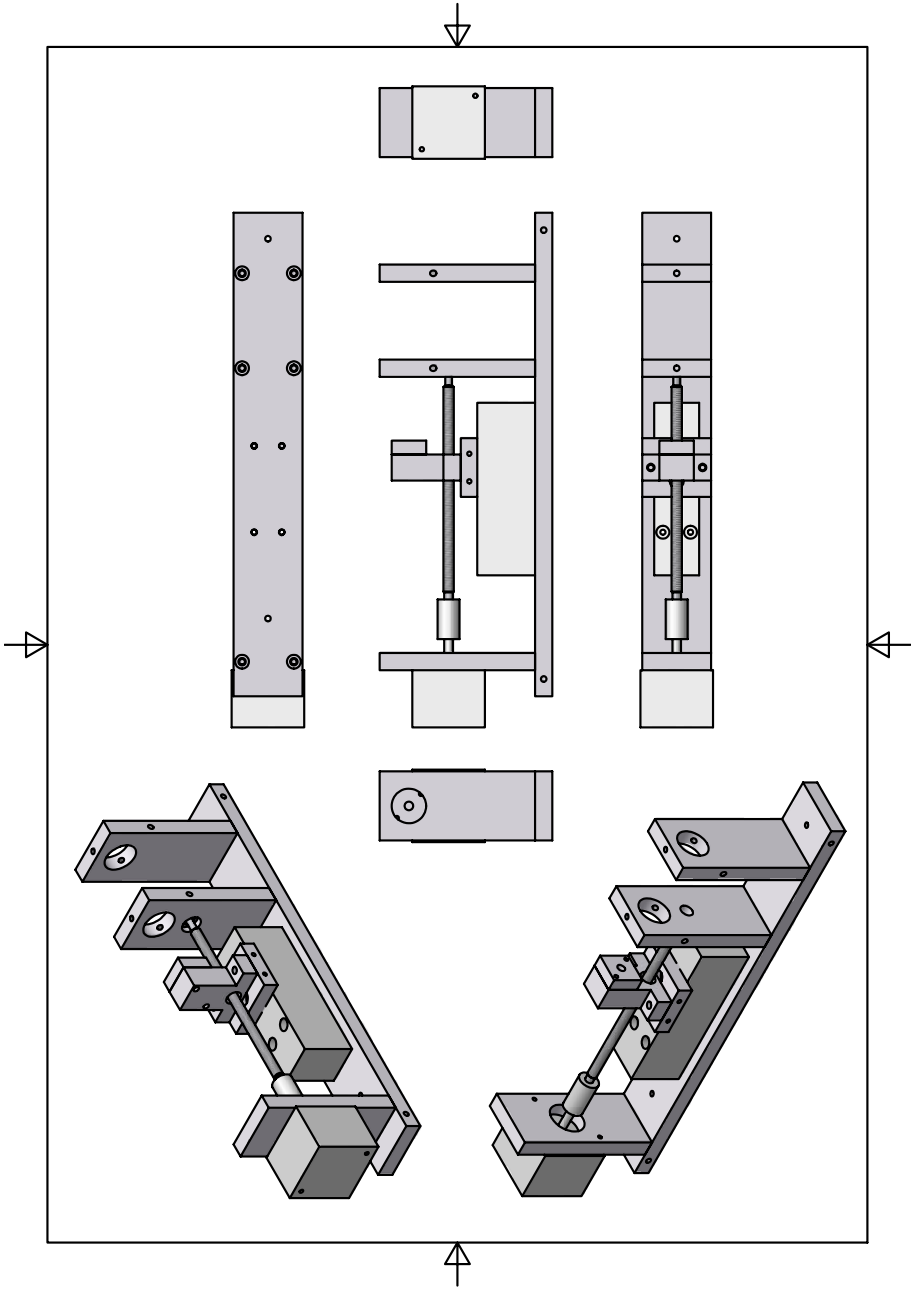

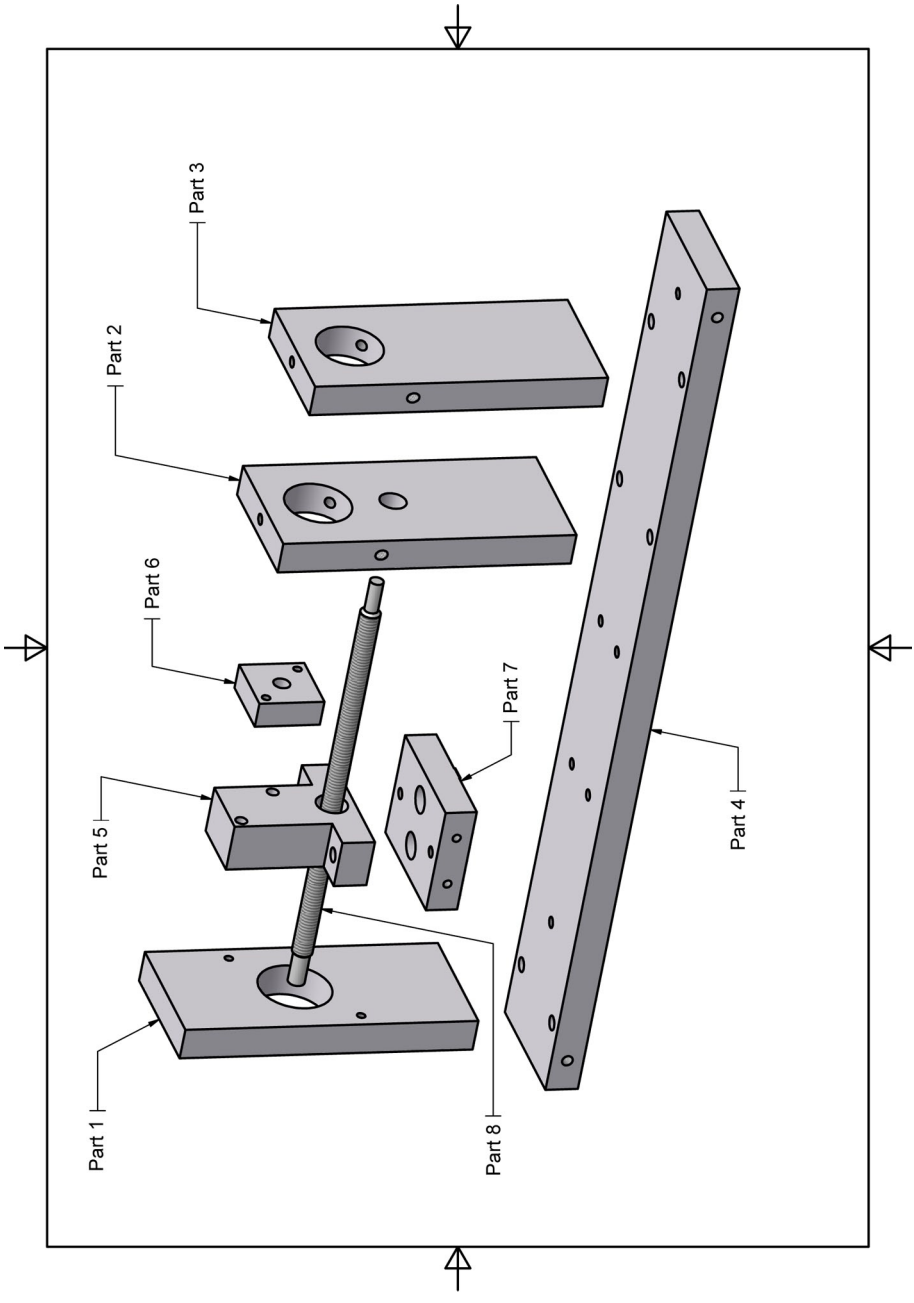
Part 3
Part 2
Part 6
Part 7
Part 5
Part 4
Part 1
Part 8

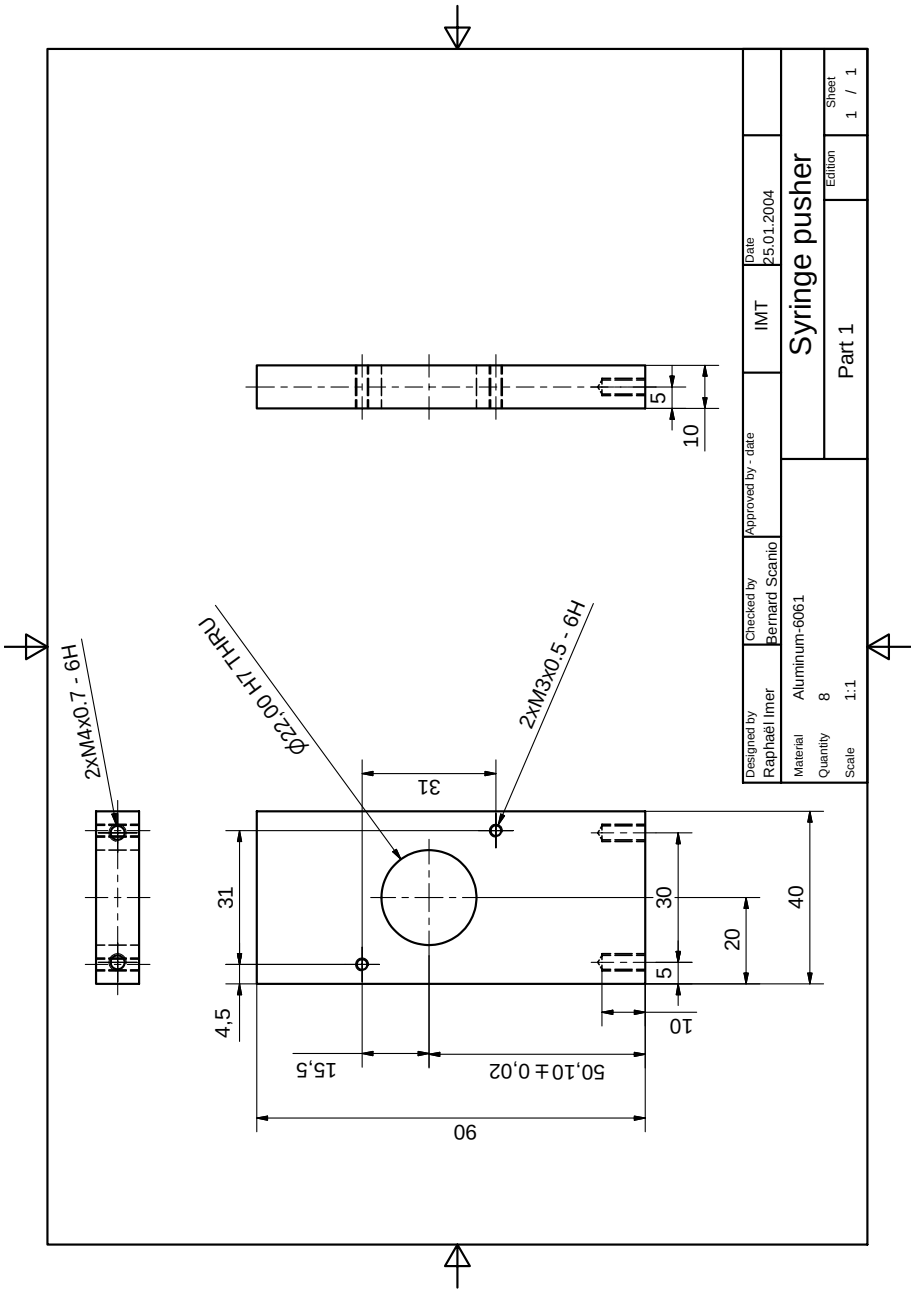
2xM4x0.7 - 6H
Ø22.00 H7 THRU
2xM3x0.5 - 6H
31
31
4,5
15,5
50,10 ± 0,02
90
5
30
40
20
10
5
10
Designed by
Raphaël Imer
Checked by
Bernard Scanio
Approved by - date
IMT
Date
25.01.2004
Material
Aluminum-6061
Quantity
8
Scale
1:1
Syringe pusher
Part 1
Edition
Sheet
1 / 1

3xM4x0.7 - H6
2xM4x0.7 - 6H
Ø20,00 THRU
30°
Ø8,00 THRU
⌴ Ø12,00 K7 ↧ 4,00
40
20
30
5
10
50,10 ± 0,02
73,1
90
10
5
Designed by
Raphaël Imer
Checked by
Bernard Scanio
Approved by - date
IMT
Date
27.01.2004
Material
Aluminum-6061
Quantity
8
Scale
1:1
Syringe pusher
Part 2
Edition
Sheet
1 / 1

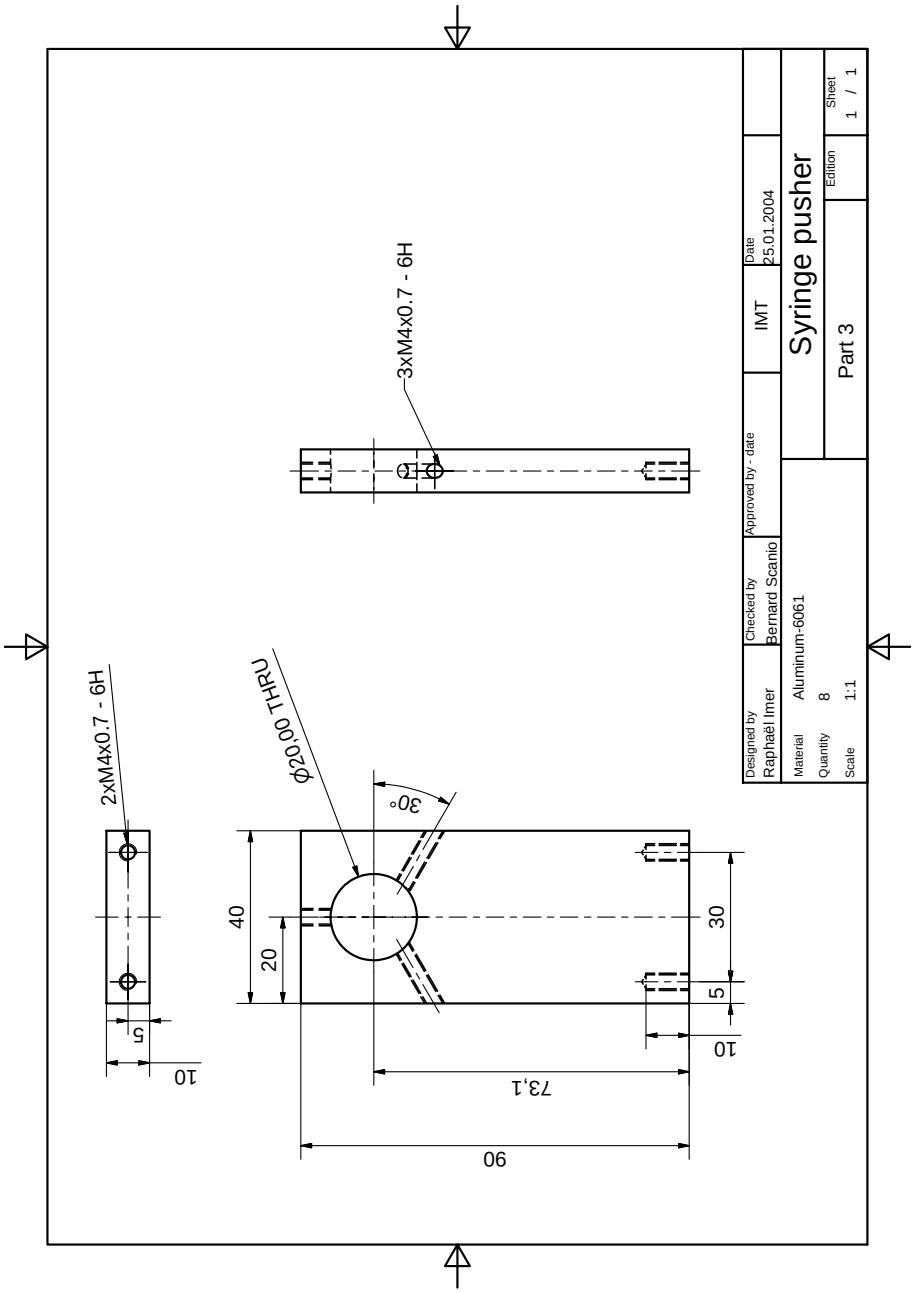
3xM4x0.7 - 6H
2xM4x0.7 - 6H
ϕ20.00 THRU
30°
40
20
30
5
10
73,1
90
10
5
Designed by
Raphaël Imer
Checked by
Bernard Scanio
Approved by - date
IMT
Date
25.01.2004
Material
Aluminum-6061
Quantity
8
Scale
1:1
Syringe pusher
Part 3
Edition
Sheet
1 / 1

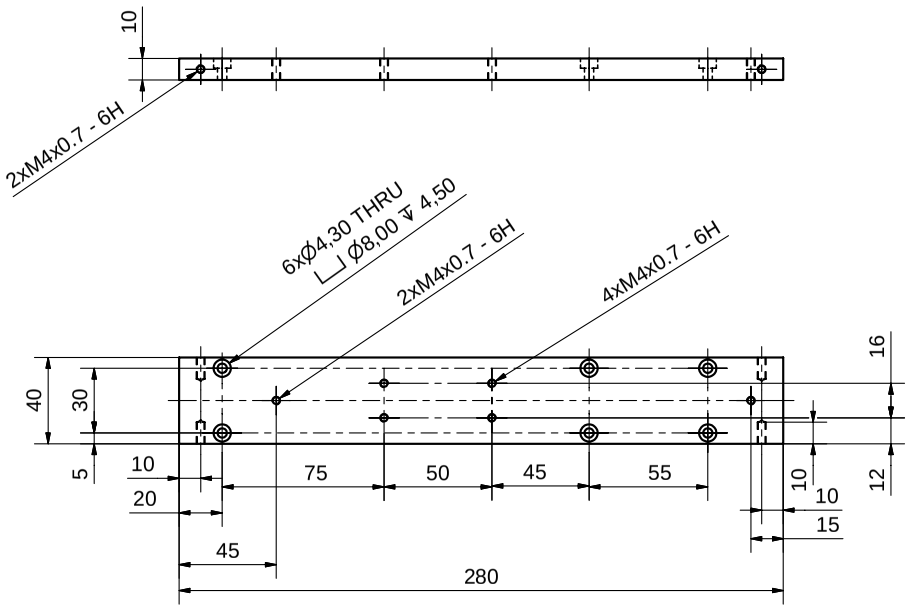

Designed by: Raphaël Imer	Checked by: Bernard Scanio	Approved by: Date	IMT	Date: 26.01.2004	
Material: Aluminium Quantity: 8 Scale: 1:2	Syringe pusher				
	Part 4		Edition: 2	Sheet: 1 / 1	

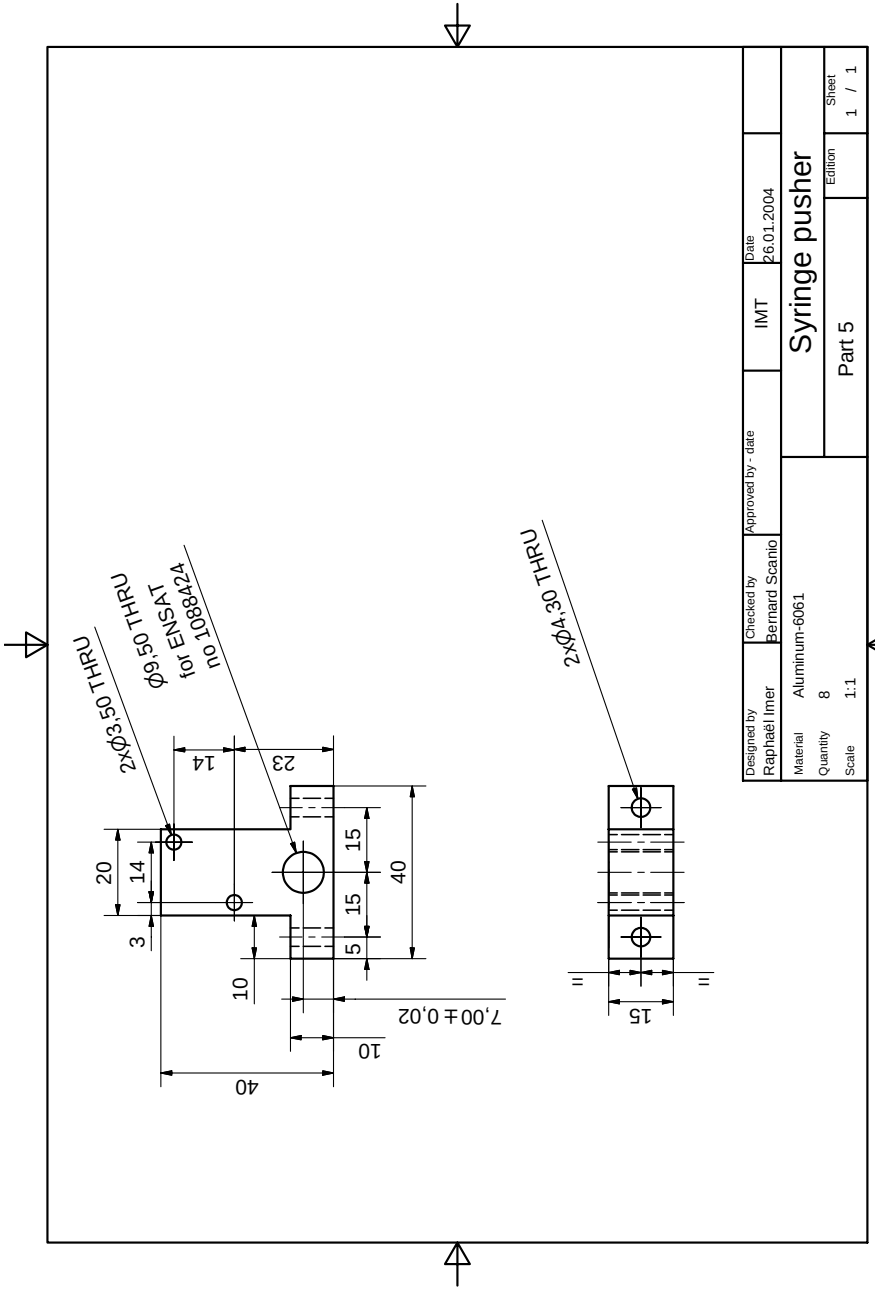
2xΦ3,50 THRU
Φ9,50 THRU
for ENSAT
no 1088424
2xΦ4,30 THRU
14
23
20
14
3
15
15
5
40
10
40
10
7,00± 0,02
15
Designed by
Raphaël Imer
Checked by
Bernard Scanio
Approved by - date
IMT
Date
26.01.2004
Material
Aluminum-6061
Quantity
8
Scale
1:1
Syringe pusher
Part 5
Edition
Sheet
1 / 1

118°
Ø11
1,5
8
Ø5
2XM3X0.5 - 6H
3
14
3
14
10
20
10
20
Designed by
Raphaël Imer
Checked by
Bernard Scanio
Approved by - date
IMT
Date
26.01.2004
Material
Aluminum-6061
Quantity
8
Scale
3:1
Syringe pusher
Part 6
Edition
Sheet
1 / 1

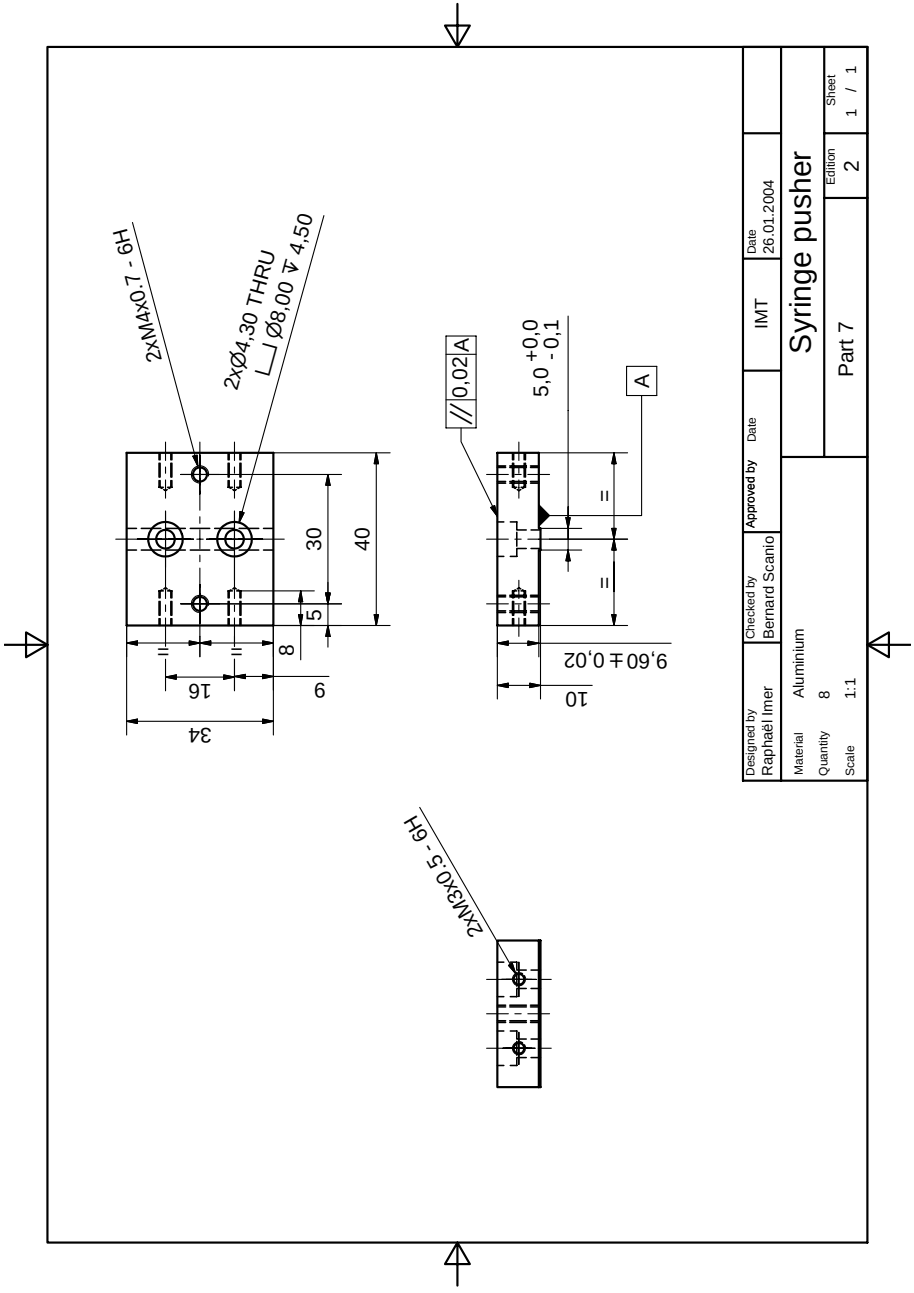
2xM4x0,7 - 6H
2xØ4,30 THRU
Ø8,00 ↧ 4,50
34
16
9
8
5
30
40
// 0,02 A
5,0 +0,0 -0,1
A
9,60 ± 0,02
10
2xM3x0,5 - 6H
Designed by
Raphaël Imer
Checked by
Bernard Scanio
Approved by
Date
IMT
Date
26.01.2004
Material
Aluminium
Quantity
8
Scale
1:1
Syringe pusher
Part 7
Edition
2
Sheet
1 / 1

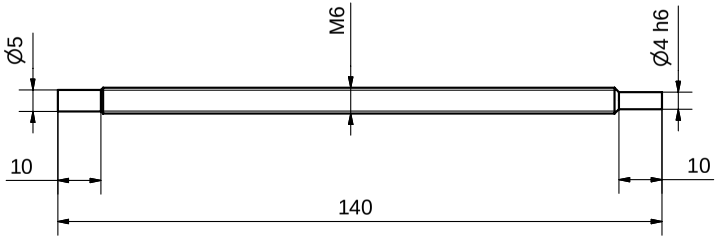

Designed by: Raphaël Imer	Checked by: Bernard Scanio	Approved by - date:	IMT	Date: 29.01.2004	
Material: Steel, Mild Quantity: 8 Scale: 1:2			Syringe pusher		
			Part 8	Edition:	Sheet: 1 / 1

Acknowledgments

First of all, I would like to thanks Prof. Nico de Rooij for giving me the opportunity to join his research group.

I'm particulary grateful to my advisor Prof. Urs Staufer for his advises, his unlimited patience and his constant encouragement. His enthusiasm about this project gives me, day after day, inspiration and motivation.

I wish to thank Prof. Ueli Aebi and Dr. Martin Stolz from the University of Basel and Dr. Riccardo Gottardi from the University of Genova for introducing me to the fascinating world of cartilage. I wish also to thank Dr. N. Friederich for his constant disponibilty to answer my medical questions. I will never forget the day spend in your operating room to learn how arthroscopic instruments must be used. I wish to thank Prof. A.U.D. Daniels and Dr. D. Wirz from the laboratory for orthopedic biomechanics of the University of Basel for the fruitful collaboration and the many interesting discussions.

I am especially grateful to Bernard Scanio for his assistance throughout this work. Many thanks for all these days, nights and weekend spend to correct my technical drawings and to help me building the first SFA prototypes.

Special thank go to my semester student Mathieu Gaillard that build the first version of the sofware used for controlling the syringe's pushers.

I would like to deeply thank Laure Aeschimann which introduce me to the IMT cleanroom and which help me to capture and glue bloody micrometer beads at the end of our AFM cantilevers.
I also would like to thank all members of the SAMLAB for their help in the lab and for the pleasant working atmosphere. Special thanks goes to the member of the Nanotools group, Terunobu Akiyama, Sebastian Gautsch, Laure Aeschimann, Maurizio Gullo, Kaspar Suter, Anpan Han, Daniel Parrat, Dara Bayat, Friedjof Heuck, Thomas Hug, Schahrazede Mouaziz and Gregor Schuermann.

I also acknowledge Mireille Leboeuf and Massoud Dadras for their availability and useful discussions around the microscopes, Peter van der Wal who was always available to answer my questions about chemistry, Sylvian Pochon for making the most impossible wire bonding of the world, and all the other members of the COMLAB technical staf, Edith Millotte, Nicole Hegelbach, Sabina Jenny, Gianni Mondin, Pierre-André Clerc, Giovanni Bergonzi, Stéphane Ischer, Sylvain Jeanneret, Eduardo Santoli, José Vaquera for their help during my rare appearance in the clean room.

A very special thanks goes to the best office colleagues of the world, Quyên Pham Phoung, Kaspar Suter and Jerôme Courbat, your madness was a daily pleasure.

My gratitude also goes to Roman Schwendtmayer for the time given to read and correct the English of this manuscript.

I would like to thank all the survivors of page 1.12, Olivier Scherler, Thomas Overstolz, Johann Richard, Stephan Beer and Charlotte Lambelet for their friendship. I hope we will never forget what an OTA 11 is!

I deeply thank my wife for her support, her comprehension and her love. Thank you Ling for giving me Sophie and Alexandre, the two most beautyfull gifts that I could dream.

Finally, I express my gratitude to my parents and to my sister who always supported me always showed interest for my work.

This work wouldn't have been possible without the financial support of the SNF NCCR Nano scale science.

Acronyms

2D two-dimensional

3D three-dimensional

AAOS American Academy of Orthopedic Surgeons

ABS Acrylonitrile butadiene styrene

ACI Autologous chondrocyte implantation

ACL anterior cruciate ligament

AFM atomic force microscope

APCVD atmospheric pressure chemical vapor deposition

BHF buffered hydrofluoric

BRL Buffalo rat liver

CS chondroitin sulfate

DI deionized

ECM extracellular matrix

GAG glycosaminoglycan

HA hyaluronan

ICR instant center of rotation

ICRS International Cartilage Repair Society

IT AFM indentation-type atomic force microscopy

KOH potassium hydroxide

KOOS knee injury and osteoarthritis outcome score

KS keratan sulfate

LCL lateral collateral ligament

LPCVD low pressure chemical vapor deposition

MCL medial collateral ligament

MRI Magnetic resonance imaging

NSAID Nonsteroidal anti-inflammatory drug

OA osteoarthritis

OATS osteochondral autograft transfer system

PBS Phosphate Buffered Saline

PCL posterior cruciate ligament

PEEK polyetheretherketone

PET polyethylene terephthalate

PG Proteoglycan

PCB printed circuit board

PVC polyvinyl chloride

PZT lead zirconate titanate

RMS root mean square

SEM scanning electron microscope

SFA scanning force arthroscope

SFM scanning force microscope

SNR signal-to-noise ratio

TEM transmission electron microscope

UV ultraviolet

Publications

Refereed articles

R. Imer, T. Akiyama, N.F. de Rooij, M. Stolz, U. Aebi, R. Kilger, N.F. Friederich, D. Wirz, A.U. Daniels and U. Staufer. *In Situ Measurements of Human Articular Cartilage Stiffness By Means of a Scanning Force Microscope*, Journal of Physics : Conference Series (2007) **61** 467-471.

U. Staufer, T. Akiyama, M.R. Gullo, A. Han, R. Imer, N.F. de Rooij, U. Aebi, A. Engel, P.L.T.M. Frederix, M. Stolz, N.F. Friederich and D. Wirz. *Micro and nanosystems for biology and medicine*, Microelectronic Engineering (2007) **84** 1681-1684.

R. Imer, T. Akiyama, N.F. de Rooij, M. Stolz, U. Aebi, N.F. Friederich, U. Koenig, D. Wirz, A.U. Daniels and U. Staufer. *Development of Atomic Force Microscope for Arthroscopic Knee Cartilage*, Japanese Journal of Applied Physique (2006) **45 3B** 2319-2323.

M. Stolz, R. Imer, U. Staufer and U. Aebi. *Development of an Arthroscopic Atomic Force Microscope*, Bioworld (2003) **4** 1-4.

Patent

U. Staufer and R. Imer. *Device for Stabilising and/or positioning a medical tool in a body cavity*, US patent application, US 2006/0111739 A1.

Oral presentation

R. Imer, T. Akiyama, N. F. de Rooij, M. Stolz, U. Aebi, R. Kilger, N.F. Friederich, D. Wirz, A.U. Daniels and U. Staufer. *Development of an arthroscopic Scanning Force Microscope for in situ knee cartilage inspection.* Summerschool: Highlights in Microtechnology 2007, Neuchâtel, Switzerland, Jul. (2007).

R. Imer, T. Akiyama, N. F. de Rooij, M. Stolz, U. Aebi, R. Kilger, N.F. Friederich, D. Wirz, A.U. Daniels and U. Staufer. *In situ stiffness measurements of human articular cartilage.* International Conference on Nanoscience and Technology (ICN&T) 2006, Basel, Switzerland, Aug. (2006).

R. Imer, R. Gottardi, R. Raiteri, R. Kilger, L. Aeschimann, V. Cardinali, U. König, N. Friederich, U. Staufer, M. Stolz and U. Aebi. *Towards early detection of osteoarthritis: Assessing human articular cartilage by scanning force microscopy.* European Orthopaedic Research Society 16th Annual Meeting, Bologna, Italy, Jun. (2006).

R. Imer T. Akiyama, N.F. de Rooij, M. Stolz, U. Aebi, R. Kilger, N.F. Friederich, D. Wirz, A.U. Daniels and U. Staufer. *Development of an arthroscopic Scanning Force Microscope for in situ knee cartilage inspection.* International Cartilage Repair Society (ICRS) 6th Symposium, San Diego, USA, Jan. (2006).

R. Imer T. Akiyama, N.F. de Rooij, M. Stolz, U. Aebi, U. König, N.F. Friederich, D. Wirz, A.U. Daniels and U. Staufer. *Scanning Force Endoscope*. Invited talk, 13th International Conference on Scanning Tunneling Microscopy (STM'05), Sapporo, Japan, Jul. (2005).

R. Imer T. Akiyama, N.F. de Rooij, M. Stolz, U. Aebi, N.F. Friederich, D. Wirz, A.U. Daniels and U. Staufer. *Scanning Force Endoscope.* Seeing at nanoscale II (VEECO), Grenoble, France, Oct. (2004).

R. Imer T. Akiyama, N.F. de Rooij, M. Stolz, U. Aebi, A. Wild, P. Hunziker and U. Staufer. *Scanning Force Endoscope.* Swiss Physical Society Annual Meeting (SPS04), Neuchâtel, Switzerland, Mar. (2004).

R. Imer T. Akiyama, N.F. de Rooij, M. Stolz, U. Aebi, A. Wild, P. Hunziker and U. Staufer. *Scanning Force Endoscope.* National Centrer of Competence in Research (NCCR) in Nanoscale Science Workshop, Pontresina, Switzerland, Sep. (2002).

Posters

R. Imer, T. Akiyama, N. F. de Rooij, Stolz, U. Aebi, N. F. Friederich, R. Gottardi, R. Raiteri, D. Wirz, A. U. Daniels and U. Staufer. *Development of a scanning force arthroscope for in situ inspection of knee cartilage.* NanoEurope 2006, St-Gallen, Switzerland, Sep. (2006).

R. Imer T. Akiyama, N.F. de Rooij, M. Stolz, U. Aebi, R. Kilger, N.F. Friederich, D. Wirz, A.U. Daniels and U. Staufer. *Scanning Force Endoscope.* 7th CMI-Comlab day, Lausanne, Switzerland, Mai. (2006).

R. Imer T. Akiyama, N.F. de Rooij, M. Stolz, U. Aebi, R. Kilger, N.F. Friederich, D. Wirz, A.U. Daniels and U. Staufer. *Scanning Force Arthroscope.* 13th International Conference on Scanning Tunneling Microscopy

Spectroscopy and Annual Review Meeting of the National Centrer of Competence in Research (NCCR) in Nanoscale Science, Gwatt (Thun), Switzerland, Oct. (2005).

R. Imer T. Akiyama, N.F. de Rooij, M. Stolz, U. Aebi, N.F. Friederich, D. Wirz, A.U. Daniels and U. Staufer. *Scanning Force Endoscope.* Biosurf IV, Lausanne, Switzerland, sep. (2005).

R. Imer T. Akiyama, N.F. de Rooij, M. Stolz, U. Aebi, N.F. Friederich and U. Staufer. *Scanning Force Endoscope.* 6th CMI-Comlab day, Lausanne, Switzerland, Mai. (2005).

R. Imer T. Akiyama , N.F. de Rooij, M. Stolz, U. Aebi and U. Staufer. *Scanning Force Endoscope.* Scanning Probe Microscopies and Organic Materials, Bielefeld, Germany, Sep. (2004).

R. Imer T. Akiyama, N.F. de Rooij, M. Stolz, U. Aebi, P. Hunziker and U. Staufer. *Scanning Force Endoscope.* 5th CMI-Comlab day, Lausanne, Switzerland, Mai. (2004).

R. Imer T. Akiyama, N.F. de Rooij, M. Stolz, U. Aebi, A. Wild, P. Hunziker and U. Staufer. *Scanning Force Endoscope.* Medicluster 04, Neuchâtel, Switzerland, Mar. (2004).

R. Imer T. Akiyama, N.F. de Rooij, M. Stolz, U. Aebi, A. Wild, P. Hunziker and U. Staufer. *3D Model of a knee.* Annual Review Meeting of the National Centrer of Competence in Research (NCCR) in Nanoscale Science, Basel, Switzerland, Mai. (2003).

R. Imer T. Akiyama, N.F. de Rooij, M. Stolz, U. Aebi, A. Wild, P. Hunziker and U. Staufer. *Scanning Force Endoscope.* SNF Review Pannel, Basel, Switzerland, Mai. (2003).

List of Figures

List of Tables